8-2022

Impacts of the Changing Pacific on North American Drought, Atmospheric Rivers, and Explosive Cyclones

Jacob Stuivenvolt-Allen
Utah State University

Recommended Citation

IMPACTS OF THE CHANGING PACIFIC ON NORTH AMERICAN DROUGHT,

ATMOSPHERIC RIVERS, AND EXPLOSIVE CYCLONES

by

Jacob Stuivenvolt-Allen

A dissertation submitted in partial fulfillment
of the requirements for the degree

of

DOCTOR OF PHILOSOPHY

in

Climate Science

Approved:

_____   _____
Shih-Yu Simon Wang, Ph.D.   Yoshimitsu Chikamoto, Ph.D.
Major Professor   Committee Member

_____   _____
Wei Zhang, Ph.D.   Emily Becker, Ph.D.
Committee Member   Committee Member

_____   _____
Jin-ho Yoon, Ph.D.   D. Richard Cutler, Ph.D.
Committee Member   Vice Provost of Graduate Studies

UTAH STATE UNIVERSITY
Logan, Utah

2022

ABSTRACT

Impacts of the Changing Pacific on North American Drought, Atmospheric Rivers, and

Explosive Cyclones

by

Jacob Stuivenvolt-Allen, Doctor of Philosophy

Utah State University, 2022

Major Professor: Dr. Shih-Yu Simon Wang
Department: Plants, Soils, and Climate

While drought, atmospheric rivers (ARs) and explosive cyclones are disparate weather and climate events that impact separate regions of the United States, this research similarly evaluates the role of large-scale climate variability in influencing their temporal variability. Our results show that the tropical and north Pacific Ocean drive year-to-year variations in the occurrence of each event. Through shifting teleconnection patterns associated with the tropical Pacific and a rapid emergence of decadal variability in the north Pacific, low-frequency oceanic and atmospheric circulation are more clearly influencing the seasonal accumulation of each impactful event.

This dissertation is split into three manuscripts and five chapters. Following an introduction of this research in Chapter 1, Chapter 2 focuses on the growing relationship between Pacific climate variability and the frequency of explosive cyclogenesis along the

east coast of North America. Transitioning to the west coast, Chapter 3 provides a long-

term perspective on the year-to-year fluctuations in atmospheric rivers that impact

Northern California, showing that these storms can strongly influence multi-year wet and

dry periods in the region. Finally, Chapter 4 continues to focus on hydroclimate

variability and outlines the emerging role of decadal variability in driving multi-year,

pan-western droughts in the United States. As summarized in Chapter 5, the results of

this dissertation generally show that Pacific climate variability has become more

important for these impactful weather and climate extremes.

(158 pages)

PUBLIC ABSTRACT

Impacts of the Changing Pacific on North American Drought, Atmospheric Rivers, and

Explosive Cyclones

Jacob Stuivenvolt-Allen

The impacts of specific weather events can vary greatly from year to year. Much of these impacts depend heavily on the frequency of impactful weather which is constrained by the state of the climate system each year. This research focuses largely on the impacts that climate oscillations from year-to-year or even from decade-to-decade have on the frequency of impactful weather. There are numerous examples of impactful weather that impact North America, but this work focuses on drought in the western United States, atmospheric rivers in Northern California and rapidly developing winter storms along the east coast. While seemingly disparate events, there is much overlap in the mechanisms by which variations in the ocean and atmosphere can impact the frequency of these impactful events. Most of these mechanisms involve the tropical Pacific Ocean, which acts as a major driving force for the state of the atmosphere over North America and the resulting frequency of weather extremes.

ACKNOWLEDGMENTS

I am extremely thankfully for the guidance and trust of my major advisor, Dr. Shih-Yu Simon Wang. His energy and enthusiasm around science has always been contagious and extremely motivating for me. Simon's lessons have extended far beyond the classroom and the scientific process, and I feel that I am a better communicator, collaborator, and leader because of his teaching.

The rest of my committee has been instrumental in my research and understanding of climate. Dr. Yoshimitsu Chikamoto has kept his door open to me and I always leave his office with an improved figure, a testable hypothesis, or a better grasp of a complicated idea. The countless hours in his office were truly invaluable. The arrival of Dr. Wei Zhang during my last year was reinvigorating due to the enthusiasm he brings to research and teaching, and the novel methods he applies to climate science. Finally, I am extremely thankful to Dr. Emily Becker and Dr. Jin-ho Yoon for their "teleconnections". I'm an avid reader of the ENSO blog and look-up to Dr. Becker's dedication to effective communication and cultivation of true expertise. Concerning Dr. Yoon, keeping up with his publications has greatly improved my understanding of global climate models and methods.

My life-partner, Vanessa Sigman, has been the source of my stability and happiness for 7 years and her unflinching support has built the foundation that I work on each day. Vanessa has constantly reminded me about and invited me to take part in the most fulfilling aspects of life that can be obscured by publications and approaching deadlines.

This work would not have been possible without my parents' dedication to learning, growth and education. John and Mandy Stuivenvolt-Allen have sacrificed a lot to pave the road that I walk, and I think of them every day that I continue forward with my dream career. Lieren and Lexie Stuivenvolt-Allen have provided far reaching support and my time with them during the last four years was always restorative and revitalizing.

Finally, I'd like to thank the staff in the Plants, Soils and Climate department, Keren Williams, Lorie Fajardo, Lorie Staples, and Jeanette Norton for their services and the friends that have made these four years an absolute pleasure.

Jacob Stuivenvolt-Allen

CONTENTS

LIST OF TABLES

LIST OF FIGURES

ACRONYMS

AR	Atmospheric rivers
CESM	Community earth system model
COBE	Centennial observation-based climate
ENSO	El Niño Southern Oscillation
EOF	Empirical orthogonal function
EGR	Eady growth rate
EP-NP	East Pacific-North Pacific
ERA5	European reanalysis 5
eqPAC	Equatorial Pacific
GLOB	Global oceans
GPCC	Global Precipitation Climatology Centre
NAO	North Atlantic Oscillation
NCAR	National Center for Atmospheric Research
NCEP	National Centers for Environmental Prediction
NOAA	National Oceanic and Atmospheric Administration
MSLP	Mean sea level pressure
NAWD	North American Winter Dipole
NPGO	North Pacific Gyre Oscillation
NPO	North Pacific Oscillation
PDO	Pacific Decadal Oscillation
PNA	Pacific-North American Pattern
SST	Sea surface temperature

WAF	Wave-activity flux
U250	250 hPa zonal wind
US	United States
Z250	250 hPa geopotential height
Z500	500 hPa geopotential height

CHAPTER 1
GENERAL INTRODUCTION

1.1   General Motivation and Chapter Outline

There are many examples of severe weather that have impacts on North America, but specific events in the last four years have motivated the following analysis of east coast explosive cyclones, atmospheric rivers in Northern California, and drought in the entire western half of the United States (discussed in individual chapters). While largely distinct events, the following research will similarly analyze the impact of large-scale climate variability on the spatial and temporal variability of drought, atmospheric rivers (ARs) and explosive cyclones. Rather than identifying the background conditions that led to a single extreme, this work provides mechanisms for which background states can influence the seasonal potential of impactful weather events. There are two motivations for this:

1. Understanding the seasonal drivers of integrated weather events can improve outlooks and prediction for specific events (McKinnon et al., 2016; Mundhenk et al., 2018; Vecchi et al., 2014),

2. Amidst a non-stationary climate, the background conditions which predicate impactful weather may also be changing and climate adaptation may benefit from realizing these non-stationarities (Cole & Cook, 1998; Coopersmith et al., 2014; Soulard et al., 2019; Trenberth, 1990).

Due to these motivations, this introduction will discuss the relevant forcing mechanisms for North American climate anomalies and climate change. Broadly, these mechanisms can be grouped into tropical and extratropical climate variability internal to the system, and external forcings like anthropogenic climate change.

First, we will discuss tropical climate variability and its far-reaching impacts to North American weather and climate. Section 1.2 will first highlight the canonical impacts of El Niño Southern Oscillation (ENSO) and then describe more recent developments in non-canonical tropical teleconnections. Section 1.3 will then shift focus to the northern latitudes and introduce modes of atmospheric variability that heavily impact North American climate and are largely independent of the tropics. Section 1.4 will focus on non-stationarity in the climate system as evidenced by an externally forced component, anthropogenic climate change, and an internally forced example like the Pacific climate shift in the mid 1970s. While the focus of this dissertation is climate variability, some results highlight that shifts in the climate mean state and in northern hemisphere winter circulation may be changing the expression of climate variability. For background on mean-state circulation in the Northern Hemisphere, section 1.5 will review stationary waves in a changing climate. Finally, an outline of the dissertation will be provided in section 1.6.

1.2   From the tropics to North America

The far stretching impacts of tropical ocean variability were initially observed almost 100 years ago (Walker, 1925), as statistical relationships between observations of temperature, pressure, and precipitation between the tropics and North America. Since the first observations of these teleconnections, the role of the tropics in driving subseasonal-to-multidecadal variations in North American weather and climate has been elucidated with many theoretical, statistical (Ropelewski & Halpert, 1986), and dynamic tools (Held et al., 1989; B. J. Hoskins & Karoly, 1981; Sardeshmukh & Hoskins, 1988; Trenberth et al., 1998). Tropical teleconnection research has focused heavily on the

dominant mode of global climate variability, El Niño Southern Oscillation (ENSO).

ENSO is characterized by three states in the eastern and central tropical Pacific: El Niño

conditions which feature anomalously warm sea surface temperatures (SST), La Niña

defined by anomalously cool conditions, and ENSO neutral conditions with temperature

ranges and thermocline depths which are close to climatological values. Each of these

states has been linked to atmospheric circulation anomalies (Leathers et al., 1991;

Wallace & Gutzler, 1981), "typical" temperature and precipitation patterns (Ropelewski

& Halpert, 1986), altered probabilities of weather extremes, and impacts on biological

and socio-economic systems (Changnon, 1999, p. 199; Hansen et al., 1998; Kilduff et al.,

2015).

The tropical ocean's primary impact on the atmosphere is through changes to

tropical convection and upper-level divergence. Anomalously warm SSTs enhance

overlying precipitation and convection, shifting the zonal heating distribution in the

tropics due to latent heat release in rising, moist air. As a response, the Hadley circulation

can be intensified and result in enhanced divergence at the subsiding branch of the

Hadley cell – acting as a Rossby wave source which initiates an extratropical atmospheric

response in the mean westerly flow (Kilduff et al., 2015). An important complexity for

understanding the impacts of tropical heating on North American weather and climate is

understanding the immense variance possible from similar tropical heating anomalies.

While the location and intensity of the tropical heating anomaly impacts the wavelength

and great circle path of the extratropical wave (B. J. Hoskins & Karoly, 1981; Trenberth

et al., 1998), the greatest sources of heterogeneity in the extratropical atmospheric and

oceanic response to tropical heating are associated with zonal asymmetries in the mean

state climate (Held et al., 2002; B. J. Hoskins & Ambrizzi, 1993; B. J. Hoskins & Karoly, 1981), transient disturbances which can alter Rossby wave propagation (Held et al., 1989), and nonlinear feedbacks (Sardeshmukh & Hoskins, 1988). Additionally, the more recent understanding of ENSO diversity has identified different types of ENSO associated with different North American impacts (Liang et al., 2014, 2015). As a result, North American responses to ENSO forcing can be large but quite variable from case to case.

An emerging tropical source for North American weather and climate extremes appears to be in the western Tropical Pacific. Teng and Branstator (Teng & Branstator, 2017) have shown that the ridges which induce prolonged California droughts are more consistently influenced by SSTs in the western and central tropical Pacific rather than ENSO. Similar findings were presented by Schulte and Lee (Schulte & Lee, 2017) who discovered that shifts in the tropical Pacific climate variability resulted in an emergence of a wave-train of alternating atmospheric circulation anomalies over North America characterized by the East Pacific-North Pacific pattern in winter. This pattern has become more strongly related to wintertime North American precipitation and temperature in the recent decades – highlighting that non-stationarity in the climate system can result in shifting significance of teleconnections. The wave-train pattern associated with the EP-NP bears a resemblance to the North American Winter Dipole (NAWD), which features opposing circulation anomalies over the western and eastern halves of North America (Singh et al., 2016; S.-Y. Wang et al., 2014; S.-Y. Wang et al., 2015). The NAWD has also been linked to anomalous SSTs in the western tropical Pacific. Aside from seasonal temperature and precipitation, these teleconnections are not directly associated with

ENSO forcing can result in enhanced weather extremes as well. In California, the NAWD strongly influenced the 2012-2016 drought and even facilitated the rapid reversal to excessively wet conditions the following year with enhanced AR activity and flooding (S.-Y. Wang et al., 2017).

Along with the tropical Pacific, the tropical Indian and Atlantic Oceans also exert influences on North American atmospheric circulation, affecting the frequency and magnitude of drought, wildfire, and agricultural yield (Chikamoto et al., 2020). Largely through tropical interactions associated with alterations of the Walker Circulation (Chikamoto et al., 2016; Johnson et al., 2020; McGregor et al., 2014), these inter-basin interactions can synchronize with or oppose the tropical forcing from another basin to result in distinct extratropical impacts. While inter-basin interactions are important for understanding the entire picture of large-scale climate variability, they will not be a focus of this work.

1.3   Impacts of the Extratropical Climate

The tropics greatly influence seasonal-to-decadal states of the Northern Hemisphere climate, however, elements of seasonal-to-decadal climate in North America are largely independent of tropical forcing. Examples include the North Pacific Oscillation (Linkin & Nigam, 2008; Rogers, 1981) and the North Atlantic Oscillation (Barnston & Livezey, 1987), which are thought to be generally driven by stochastic, internal atmospheric variability. Both the NPO and the NAO are characterized by meridional dipoles of opposing sign pressure anomalies that occur respectively in the North Pacific and North Atlantic basins. In analyzing the energetics of these modes of variability, Kim et al. (2021) identified that these patterns comprise meridional dipoles due to the conversion of

potential energy in both the zonal and meridional directions at jet exit regions. Due to the tilted southwest to northeast climatological temperature gradient along the western boundary currents, the eddy heat flux across the tilted temperature gradient can reinforce and maintain the north-south circulation anomalies. This differs from tropically induced teleconnections, which typically display arching wave-train pattern which are dominated by zonal eddy heat flux (Kim et al., 2021).

These intrinsic extratropical modes, the NPO and NAO, are extremely important for winter climate in North America. Linkin and Nigam (Linkin & Nigam, 2008) identified the NPO to be as influential for North American winter hydroclimate as the Pacific North American (PNA) pattern and ENSO variability. Extreme climate events have been tied to the NPO, with Baxter and Nigam identifying the NPO as a fundamental driver of the anomalously cold winter in 2013-2014 for the central and eastern US and a leading contributor to North American winter climate variability after 1980 (Baxter & Nigam, 2015). Finally, the NAO also impacts eastern US temperature variability, but research has focused extensively on the role that the strengthened jet stream associated with the NAO can have on shifts in the storm track and major extratropical cyclones, which will be discussed more extensively in Chapter 2 (Chartrand & Pausata, 2020; Gómara et al., 2016; Pinto et al., 2009; Trigo, 2006).

While the formation of the NPO is not associated with tropical variability, they can in turn impact tropical climate by altering sub-tropical atmospheric and ocean circulation. A well-known example is the Seasonal Footprinting Mechanism (Alexander et al., 2010; Vimont et al., 2001, 2003) in which NPO driven SST anomalies in the north Pacific contribute to the formation of ENSO the following year. This example highlights that

climate forcings are not just directed away from the tropics; these regions interact non-linearly and the climate that we experience is often an amalgamation of their mutual and entangled influence.

The arctic is another source of North American climate variability with increasing attention paid to the potential for the loss of arctic sea ice to influence winter climate and weather extremes (Cohen et al., 2014, 2020; Jaiser et al., 2012; Mori et al., 2019). Current theories posit that a reduced meridional temperature gradient from the more rapid warming of the arctic in comparison to the rest of the globe may result in a weaker and wavier jet stream. Sea ice loss has also been linked sudden stratospheric warming events (Overland et al., 2011; Zhang et al., 2020), but large uncertainty and other theories behind mid-latitude extremes and cooling trends exist (Cohen et al., 2020; McCusker et al., 2016; Screen & Simmonds, 2013; Sun et al., 2016). Our work will not focus on Arctic influences as the role of the tropical and Pacific oceans were found to be the most important.

1.4   Anthropogenic and Internal Non-Stationarity

A common theme of the research in this dissertation is the role of non-stationarity in shifting or changing the relationships between weather and climate extremes and large-scale climate variability. The major source of non-stationarity in today's climate is associated with anthropogenic climate change and climate studies have focused extensively on the observed shifts in the mean climate as these are more robust in model projections. However, our understanding of changes to climate variability from anthropogenic forcing is lacking (Thornton et al., 2014).

Studies of ENSO in future scenarios have been more common and some consensus is emerging regarding the spatial and temporal changes to ENSO in a warming climate. In general, the IPCC Sixth Assessment Report has concluded that it is "very likely that the ENSO rainfall variability is projected to be amplified by the second half of the 21st century" (Cai et al., 2014; Power et al., 2013). Impacts of strengthened ENSO teleconnections have already been observed in flooding events in the Great Plains (Liang et al., 2014; S.-Y. Wang et al., 2015), though multidecadal variance in the strength of ENSO teleconnections has also been established (Cai et al., 2010; Chowdary et al., 2014; McCabe & Dettinger, 1999) and potentially obscures long-term trends. As discussed previously, much of the heterogeneity in North American responses to ENSO comes from extratropical processes, so there is still great uncertainty regarding the impact that changing tropical teleconnections will have on North America. Due to these uncertainties and inadequacies in model simulations of future climate variability, the following work largely focuses on observed climate variability.

Climate shifts can also occur somewhat independent of external forcing. In the mid-1970s, sea surface temperatures (SST) in the central North Pacific rapidly cooled in conjunction with an emergence of warm sea SSTs wrapping around the north, east (along the west coast of North America), and south side of this cold SST anomaly. This state change was associated with large impacts on Salmon production (Mantua et al., 1997), high-frequency precipitation and runoff regimes (Coopersmith et al., 2014), low-frequency variability in the Upper Colorado River Basin (Hidalgo & Dracup, 2003; Nowak et al., 2012), and increased storminess and heat in Alaska (Hartmann & Wendler, 2005). Most work describes this state change as a product of internal oceanic and

atmospheric variability. Primarily through warming in the tropical Pacific which forced a

deepened Aleutian Low and its associated North Pacific SST changes, the PDO index

rapidly transitioned from a persistent cool phase to a warm phase (Graham et al., 1994;

Miller et al., 1994; Trenberth, 1990; Yeh et al., 2011). While most research has described

this shift as a product of internal variability related to the tropics and stochastic North

Pacific atmosphere, Meehl et al. (2009) found that some aspect of the cool-warm phase

transition in the PDO may have exacerbated by anthropogenic forcing – again

highlighting the entangled nature of the forcings for North American climate variability.

1.5   Stationary waves and mean-state climate

Some findings from this dissertation will be related to changing circulation

regimes and patterns in Northern Hemisphere winter climate. Understanding how or why

these changes occurred requires understanding the forcing mechanisms responsible for

mean-state circulation. Much literature has been devoted to understanding why mean-

state atmospheric circulation is zonally asymmetric. These zonal asymmetries are

referred to as stationary waves or stationary eddies, and they are partly responsible for

many distinct climate features (like the relative aridity of the western United States when

compared to the east even though these regions are at the same latitude). I will briefly

summarize the natural components involved in stationary waves and how these

components work in unison to create asymmetries in general circulation. These mean-

state features dictate the parameters of climate variability and the expression of

phenomena like ENSO. Finally, I will highlight our current (albeit limited) understanding

of how stationary waves and wintertime circulation may be impacted by anthropogenic

climate change.

Linear models using quasi-geostrophic assumptions have been used to model general circulation since the work of Charney and Eliassen (1949) and Smargorinsky (1953). From these works, it was found that the orientation of land masses was important for mid-latitude circulation and that incorporating the impacts of continental land masses into a weather forecast of upper-level geopotential height improved the accuracy. Specifically, major orographic features like the Tibetan plateau and the Rocky Mountains are fundamental towards understanding the prominent stationary waves over North America, Europe, and Asia (Chang, 2009; DeWeaver, 1995; Nigam et al., 1988; Son et al., 2009; Wills & Schneider, 2018). Smagorinsky further elucidated the impact of global heating distributions on large-scale atmospheric circulation, showing that asymmetries in heating play a role in the asymmetries in mid-latitude circulation. The heterogenous temperatures of the global oceans including warm western boundary currents, and the distribution of latent heat release in response to deep convection are the most crucial for driving asymmetries in mid-latitude circulation (Held 2002, Chang 2009, Chen and Trenberth 1987).

Some disagreement exists on the relative importance of orographically forced stationary waves when compared to thermal forcings. Valdes and Hoskins (1991) found that including nonlinear interactions between orographic and thermal forcings led to the suggestion that global heating is the most important driver of observed stationary waves. The importance of heating is supported by other research (Chang, 2009; Held et al., 2002), but Held and Ting (1990) demonstrated that responses to orography and heating in models can be heavily impacted by the strength of low-level winds in the model and may account for some of the discrepancies in the dominant forcing (Nigam et al., 1988).

Momentum transients associated with storm track activity also play a role in general circulation (Chang, 2009; Held et al., 2002; Held & Ting, 1990; Valdes & Hoskins, 1991). Earlier studies largely considered transients to act as a damping force for stationary waves, acting to reduce zonal asymmetries in circulation, though many of the seminal works either omitted the impact of transients or represented these transients in "crude" ways (Held 2002, Chang 2009). There has been a focus on how stationary waves impact transient disturbances and the distributions of storm tracks in the Northern Hemisphere (Branstator, 1995; Son et al., 2009; Tamarin & Kaspi, 2017), but the non-linear interactions between transients and stationary eddies are less understood. Recent research has highlighted that transients may play a different role in orographically forced and thermally forced stationary waves – further complexifying the relationship between high-frequency and low-frequency eddies (Wills et al., 2019; Wills & Schneider, 2018).

To quantitatively model stationary waves and account for non-linearities, idealized global climate models (GCMs) have been more recently deployed to describe stationary waves and the impact of anthropogenic climate change on mid-latitude circulation. GCMs provide the best estimate of stationary waves in a changing climate, but limitations and uncertainties remain. Specifically, extratropical circulation in GCMs is sensitive to horizontal resolution and parameterized orographic gravity wave drag (Niekerk et al., 2017; Sigmond et al., 2007). However, CMIP and other GCM projects have provided valuable insight into how climate change and natural fluctuations in climate may alter stationary waves and mean state circulation.

With the use of GCMs, maintenance mechanisms for stationary waves have been proposed by White et al. (2021). Using the atmospheric model in the Community Earth

System Model Version 2, the author's find that the signal of orographic forcing on stationary waves is most prominent in the stratosphere. They hypothesize that gravity waves resulting from the interaction of mid-latitude flow with orography propagate vertically into the stratosphere and act to slow down the climatological wind at this level. A slower stratospheric flow permits for increased wave dispersion into the stratosphere (Charney & Drazin, 1961), allowing both orographic and thermal forcings to have a larger impact of the upper-level flow. This positive feedback between decelerated stratospheric winds and increased wave dispersion into the stratosphere is the proposed maintenance mechanism for stationary waves. The concluded importance of orography in these findings suggest that previous studies employing idealized stationary wave models may be overestimating the relative importance of land-sea contrast and diabatic heating towards stationary wave maintenance and that complex GCMs with the ability to simulate the response of climatological winds (rather than prescribed climatological winds) are crucial towards developing more precise knowledge about our stationary climate (Garfinkel et al., 2020; White et al., 2021; Wills et al., 2019).

GCMs have also shown that the changing climate may have a different influence on stationary waves forced by heating, orography, and transient components. For example, as arctic amplification leads to a decreased meridional temperature gradient, a larger meridional wind (stationary wave) would be necessary to balance both stationary waves forced by orography and diabatic heating (Cook & Held, 1988; Held et al., 2002; B. J. Hoskins & Karoly, 1981; B. Hoskins & Woollings, 2015). Held and Ting (1990)

report that low-level wind speed is inversely proportional to the amplitude of heating induced stationary waves while orographically forced waves are proportional to the speed of wind over terrain (Chen & Trenberth, 1988; Ringler & Cook, 1997; Valdes & Hoskins, 1991). As low-level winds associated with general circulation are expected to shift poleward in a warming world, impacts are expected on stationary wave amplitude and phase (relative positioning in the northern hemisphere), though great uncertainty persists.

1.6   Outline

The previous sections have highlighted that North American climate is influenced by an array of entangled processes, and the following chapters will seek to slightly disentangle the role of the ocean and atmosphere in driving interannual variability of impactful weather. Chapter 2 will investigate the role of the Pacific in facilitating winters with more frequent cases of explosive cyclogenesis along the east coast of North America. This chapter describes the non-stationary relationship between these extreme weather events and up-stream forcings traced to the tropical Pacific. Chapter 3 will shift the spatial domain to the west coast of North America and show a more consistent relationship between Pacific climate variability, AR frequency, and wet-dry cycles in Northern California. Importantly, the main conclusions of this chapter are related to Pacific decadal variability, low-frequency oscillations in the Pacific Ocean and atmosphere which drastically impact hydroclimate in the western United States. Chapter 4 will continue to focus on decadal hydroclimate variability to show that these decadal cycles associated with the Pacific have become more important for pan-western drought, precipitation, and river discharge. Finally, chapter 5 will briefly highlight the general conclusions from this dissertation.

REFERENCES

Alexander, M. A., Vimont, D. J., Chang, P., & Scott, J. D. (2010). The Impact of Extratropical Atmospheric Variability on ENSO: Testing the Seasonal Footprinting Mechanism Using Coupled Model Experiments. Journal of Climate, 23(11), 2885–2901. https://doi.org/10.1175/2010JCLI3205.1

Barnston, A. G., & Livezey, R. E. (1987). Classification, Seasonality and Persistence of Low-Frequency Atmospheric Circulation Patterns. Monthly Weather Review, 115(6), 1083–1126. https://doi.org/10.1175/1520-0493(1987)115<1083:CSAPOL>2.0.CO;2

Baxter, S., & Nigam, S. (2015). Key Role of the North Pacific Oscillation–West Pacific Pattern in Generating the Extreme 2013/14 North American Winter. Journal of Climate, 28(20), 8109–8117. https://doi.org/10.1175/JCLI-D-14-00726.1

Branstator, G. (1995). Organization of Storm Track Anomalies by Recurring Low-Frequency Circulation Anomalies. Journal of the Atmospheric Sciences, 52(2), 207–226. https://doi.org/10.1175/1520-0469(1995)052<0207:OOSTAB>2.0.CO;2

Cai, W., Borlace, S., Lengaigne, M., van Rensch, P., Collins, M., Vecchi, G., Timmermann, A., Santoso, A., McPhaden, M. J., Wu, L., England, M. H., Wang, G., Guilyardi, E., & Jin, F.-F. (2014). Increasing frequency of extreme El Niño events due to greenhouse warming. Nature Climate Change, 4(2), 111–116. https://doi.org/10.1038/nclimate2100

Cai, W., Rensch, P. van, Cowan, T., & Sullivan, A. (2010). Asymmetry in ENSO Teleconnection with Regional Rainfall, Its Multidecadal Variability, and Impact. Journal of Climate, 23(18), 4944–4955. https://doi.org/10.1175/2010JCLI3501.1

Chang, E. K. M. (2009). Diabatic and Orographic Forcing of Northern Winter Stationary Waves and Storm Tracks. Journal of Climate, 22(3), 670–688. https://doi.org/10.1175/2008JCLI2403.1

Changnon, S. A. (1999). Impacts of 1997–98 EI Niño–Generated Weather in the United States. Bulletin of the American Meteorological Society, 80(9), 1819–1828. https://doi.org/10.1175/1520-0477(1999)080<1819:IOENOG>2.0.CO;2

Charney, J. G., & Drazin, P. G. (1961). Propagation of planetary-scale disturbances from the lower into the upper atmosphere. Journal of Geophysical Research (1896-1977), 66(1), 83–109. https://doi.org/10.1029/JZ066i001p00083

Chartrand, J., & Pausata, F. S. R. (2020). Impacts of the North Atlantic Oscillation on winter precipitations and storm track variability in southeast Canada and the northeast United States. Weather and Climate Dynamics, 1(2), 731–744. https://doi.org/10.5194/wcd-1-731-2020

Chen, S.-C., & Trenberth, K. E. (1988). Forced Planetary Waves in the Northern Hemisphere Winter: Wave-Coupled Orographic and Thermal Forcings. Journal of the Atmospheric Sciences, 45(4), 682–704. https://doi.org/10.1175/1520-0469(1988)045<0682:FPWITN>2.0.CO;2

Chikamoto, Y., Mochizuki, T., Timmermann, A., Kimoto, M., & Watanabe, M. (2016). Potential tropical Atlantic impacts on Pacific decadal climate trends. Geophysical Research Letters, 43(13), 7143–7151. https://doi.org/10.1002/2016GL069544

Chikamoto, Y., Wang, S.-Y. S., Yost, M., Yocom, L., & Gillies, R. R. (2020). Colorado River water supply is predictable on multi-year timescales owing to long-term ocean memory. Communications Earth & Environment, 1(1), 1–11. https://doi.org/10.1038/s43247-020-00027-0

Chowdary, J. S., Parekh, A., Gnanaseelan, C., & Sreenivas, P. (2014). Inter-decadal modulation of ENSO teleconnections to the Indian Ocean in a coupled model: Special emphasis on decay phase of El Niño. Global and Planetary Change, 112, 33–40. https://doi.org/10.1016/j.gloplacha.2013.11.003

Cohen, J., Screen, J. A., Furtado, J. C., Barlow, M., Whittleston, D., Coumou, D., Francis, J., Dethloff, K., Entekhabi, D., Overland, J., & Jones, J. (2014). Recent Arctic amplification and extreme mid-latitude weather. Nature Geoscience, 7(9), 627–637. https://doi.org/10.1038/ngeo2234

Cohen, J., Zhang, X., Francis, J., Jung, T., Kwok, R., Overland, J., Ballinger, T. J., Bhatt, U. S., Chen, H. W., Coumou, D., Feldstein, S., Gu, H., Handorf, D., Henderson, G., Ionita, M., Kretschmer, M., Laliberte, F., Lee, S., Linderholm, H. W., … Yoon, J. (2020). Divergent consensuses on Arctic amplification influence on midlatitude severe winter weather. Nature Climate Change, 10(1), 20–29. https://doi.org/10.1038/s41558-019-0662-y

Cole, J. E., & Cook, E. R. (1998). The changing relationship between ENSO variability and moisture balance in the continental United States. Geophysical Research Letters, 25(24), 4529–4532. https://doi.org/10.1029/1998GL900145

Cook, K. H., & Held, I. M. (1988). Stationary Waves of the Ice Age Climate. Journal of Climate, 1(8), 807–819. https://doi.org/10.1175/1520-0442(1988)001<0807:SWOTIA>2.0.CO;2

Coopersmith, E. J., Minsker, B. S., & Sivapalan, M. (2014). Patterns of regional hydroclimatic shifts: An analysis of changing hydrologic regimes. Water Resources Research, 50(3), 1960–1983. https://doi.org/10.1002/2012WR013320

DeWeaver, E. (1995). Influence of mountain ranges on the mid-latitude atmospheric response to El Niiio events. 3.

Garfinkel, C. I., White, I., Gerber, E. P., Jucker, M., & Erez, M. (2020). The Building Blocks of Northern Hemisphere Wintertime Stationary Waves. Journal of Climate, 33(13), 5611–5633. https://doi.org/10.1175/JCLI-D-19-0181.1

Gómara, I., Rodríguez-Fonseca, B., Zurita-Gotor, P., Ulbrich, S., & Pinto, J. G. (2016). Abrupt transitions in the NAO control of explosive North Atlantic cyclone development. Climate Dynamics, 47(9), 3091–3111. https://doi.org/10.1007/s00382-016-3015-9

Graham, N. E., Barnett, T. P., Wilde, R., Ponater, M., & Schubert, S. (1994). On the Roles of Tropical and Midlatitude SSTs in Forcing Interannual to Interdecadal Variability in the Winter Northern Hemisphere Circulation. Journal of Climate,

7(9), 1416–1441. https://doi.org/10.1175/1520-0442(1994)007<1416:OTROTA>2.0.CO;2

Hansen, J. W., Hodges, A. W., & Jones, J. W. (1998). ENSO Influences on Agriculture in the Southeastern United States. Journal of Climate, 11(3), 404–411. https://doi.org/10.1175/1520-0442(1998)011<0404:EIOAIT>2.0.CO;2

Hartmann, B., & Wendler, G. (2005). The Significance of the 1976 Pacific Climate Shift in the Climatology of Alaska. Journal of Climate, 18(22), 4824–4839. https://doi.org/10.1175/JCLI3532.1

Held, I. M., Lyons, S. W., & Nigam, S. (1989). Transients and the Extratropical Response to El Niño. Journal of the Atmospheric Sciences, 46(1), 163–174. https://doi.org/10.1175/1520-0469(1989)046<0163:TATERT>2.0.CO;2

Held, I. M., & Ting, M. (1990). Orographic versus Thermal Forcing of Stationary Waves: The Importance of the Mean Low-Level Wind. Journal of the Atmospheric Sciences, 47(4), 495–500. https://doi.org/10.1175/1520-0469(1990)047<0495:OVTFOS>2.0.CO;2

Held, I. M., Ting, M., & Wang, H. (2002). Northern Winter Stationary Waves: Theory and Modeling. Journal of Climate, 15(16), 2125–2144. https://doi.org/10.1175/1520-0442(2002)015<2125:NWSWTA>2.0.CO;2

Hidalgo, H. G., & Dracup, J. A. (2003). ENSO and PDO Effects on Hydroclimatic Variations of the Upper Colorado River Basin. Journal of Hydrometeorology, 4(1), 5–23. https://doi.org/10.1175/1525-7541(2003)004<0005:EAPEOH>2.0.CO;2

Hoskins, B. J., & Ambrizzi, T. (1993). Rossby Wave Propagation on a Realistic Longitudinally Varying Flow. Journal of the Atmospheric Sciences, 50(12), 1661–1671. https://doi.org/10.1175/1520-0469(1993)050<1661:RWPOAR>2.0.CO;2

Hoskins, B. J., & Karoly, D. J. (1981). The Steady Linear Response of a Spherical Atmosphere to Thermal and Orographic Forcing. Journal of the Atmospheric Sciences, 38(6), 1179–1196. https://doi.org/10.1175/1520-0469(1981)038<1179:TSLROA>2.0.CO;2

Hoskins, B., & Woollings, T. (2015). Persistent Extratropical Regimes and Climate Extremes. Current Climate Change Reports, 1(3), 115–124. https://doi.org/10.1007/s40641-015-0020-8

Jaiser, R., Dethloff, K., Handorf, D., Rinke, A., & Cohen, J. (2012). Impact of sea ice cover changes on the Northern Hemisphere atmospheric winter circulation. Tellus A: Dynamic Meteorology and Oceanography, 64(1), 11595. https://doi.org/10.3402/tellusa.v64i0.11595

Johnson, Z. F., Chikamoto, Y., Wang, S.-Y. S., McPhaden, M. J., & Mochizuki, T. (2020). Pacific decadal oscillation remotely forced by the equatorial Pacific and the Atlantic Oceans. Climate Dynamics, 55(3), 789–811. https://doi.org/10.1007/s00382-020-05295-2

Kilduff, D. P., Di Lorenzo, E., Botsford, L. W., & Teo, S. L. H. (2015). Changing central Pacific El Niños reduce stability of North American salmon survival rates. Proceedings of the National Academy of Sciences, 112(35), 10962–10966. https://doi.org/10.1073/pnas.1503190112

Kim, M., Yoo, C., Sung, M.-K., & Lee, S. (2021). Classification of Wintertime Atmospheric Teleconnection Patterns in the Northern Hemisphere. Journal of Climate, 34(5), 1847–1861. https://doi.org/10.1175/JCLI-D-20-0339.1

Leathers, D. J., Yarnal, B., & Palecki, M. A. (1991). The Pacific/North American Teleconnection Pattern and United States Climate. Part I: Regional Temperature and Precipitation Associations. Journal of Climate, 4(5), 517–528. https://doi.org/10.1175/1520-0442(1991)004<0517:TPATPA>2.0.CO;2

Liang, Y.-C., Lo, M.-H., & Yu, J.-Y. (2014). Asymmetric responses of land hydroclimatology to two types of El Niño in the Mississippi River Basin. Geophysical Research Letters, 41(2), 582–588. https://doi.org/10.1002/2013GL058828

Liang, Y.-C., Yu, J.-Y., Lo, M.-H., & Wang, C. (2015). The changing influence of El Niño on the Great Plains low-level jet. Atmospheric Science Letters, 16(4), 512–517. https://doi.org/10.1002/asl.590

Linkin, M. E., & Nigam, S. (2008). The North Pacific Oscillation–West Pacific Teleconnection Pattern: Mature-Phase Structure and Winter Impacts. Journal of Climate, 21(9), 1979–1997. https://doi.org/10.1175/2007JCLI2048.1

Mantua, N. J., Hare, S. R., Zhang, Y., Wallace, J. M., & Francis, R. C. (1997). A Pacific Interdecadal Climate Oscillation with Impacts on Salmon Production*. Bulletin of the American Meteorological Society, 78(6), 1069–1080. https://doi.org/10.1175/1520-0477(1997)078<1069:APICOW>2.0.CO;2

McCabe, G. J., & Dettinger, M. D. (1999). Decadal variations in the strength of ENSO teleconnections with precipitation in the western United States. International Journal of Climatology, 19(13), 1399–1410. https://doi.org/10.1002/(SICI)1097-0088(19991115)19:13<1399::AID-JOC457>3.0.CO;2-A

McCusker, K. E., Fyfe, J. C., & Sigmond, M. (2016). Twenty-five winters of unexpected Eurasian cooling unlikely due to Arctic sea-ice loss. Nature Geoscience, 9(11), 838–842. https://doi.org/10.1038/ngeo2820

McGregor, S., Timmermann, A., Stuecker, M. F., England, M. H., Merrifield, M., Jin, F.-F., & Chikamoto, Y. (2014). Recent Walker circulation strengthening and Pacific cooling amplified by Atlantic warming. Nature Climate Change, 4(10), 888–892. https://doi.org/10.1038/nclimate2330

McKinnon, K. A., Rhines, A., Tingley, M. P., & Huybers, P. (2016). Long-lead predictions of eastern United States hot days from Pacific sea surface temperatures. Nature Geoscience, 9(5), 389–394. https://doi.org/10.1038/ngeo2687

Meehl, G. A., Hu, A., & Santer, B. D. (2009). The Mid-1970s Climate Shift in the Pacific and the Relative Roles of Forced versus Inherent Decadal Variability. Journal of Climate, 22(3), 780–792. https://doi.org/10.1175/2008JCLI2552.1

Miller, A. J., Cayan, D. R., Barnett, T. P., Graham, N. E., & Oberhuber, J. M. (1994). The 1976-77 Climate Shift of the Pacific Ocean. Oceanography, 7(1), 21–26.

Mori, M., Kosaka, Y., Watanabe, M., Nakamura, H., & Kimoto, M. (2019). A reconciled estimate of the influence of Arctic sea-ice loss on recent Eurasian cooling. Nature Climate Change, 9(2), 123–129. https://doi.org/10.1038/s41558-018-0379-3

Mundhenk, B. D., Barnes, E. A., Maloney, E. D., & Baggett, C. F. (2018). Skillful empirical subseasonal prediction of landfalling atmospheric river activity using the Madden–Julian oscillation and quasi-biennial oscillation. Npj Climate and Atmospheric Science, 1(1), 1–7. https://doi.org/10.1038/s41612-017-0008-2

Niekerk, A. van, Scinocca, J. F., & Shepherd, T. G. (2017). The Modulation of Stationary Waves, and Their Response to Climate Change, by Parameterized Orographic Drag. Journal of the Atmospheric Sciences, 74(8), 2557–2574. https://doi.org/10.1175/JAS-D-17-0085.1

Nigam, S., Held, I. M., & Lyons, S. W. (1988). Linear Simulation of the Stationary Eddies in a GCM. Part II: The "Mountain" Model. Journal of the Atmospheric Sciences, 45(9), 1433–1452. https://doi.org/10.1175/1520-0469(1988)045<1433:LSOTSE>2.0.CO;2

Nowak, K., Hoerling, M., Rajagopalan, B., & Zagona, E. (2012). Colorado River Basin Hydroclimatic Variability. Journal of Climate, 25(12), 4389–4403. https://doi.org/10.1175/JCLI-D-11-00406.1

Overland, J. E., Wood, K. R., & Wang, M. (2011). Warm Arctic—cold continents: Climate impacts of the newly open Arctic Sea. Polar Research, 30(1), 15787. https://doi.org/10.3402/polar.v30i0.15787

Pinto, J. G., Zacharias, S., Fink, A. H., Leckebusch, G. C., & Ulbrich, U. (2009). Factors contributing to the development of extreme North Atlantic cyclones and their relationship with the NAO. Climate Dynamics, 32(5), 711–737. https://doi.org/10.1007/s00382-008-0396-4

Power, S., Delage, F., Chung, C., Kociuba, G., & Keay, K. (2013). Robust twenty-first-century projections of El Niño and related precipitation variability. Nature, 502(7472), 541–545. https://doi.org/10.1038/nature12580

Ringler, T. D., & Cook, K. H. (1997). Factors Controlling Nonlinearity in Mechanically Forced Stationary Waves over Orography. Journal of the Atmospheric Sciences, 54(22), 2612–2629. https://doi.org/10.1175/1520-0469(1997)054<2612:FCNIMF>2.0.CO;2

Rogers, J. C. (1981). The North Pacific Oscillation. Journal of Climatology, 1(1), 39–57. https://doi.org/10.1002/joc.3370010106

Ropelewski, C. F., & Halpert, M. S. (1986). North American Precipitation and Temperature Patterns Associated with the El Niño/Southern Oscillation (ENSO).

Monthly Weather Review, 114(12), 2352–2362. https://doi.org/10.1175/1520-0493(1986)114<2352:NAPATP>2.0.CO;2

Sardeshmukh, P. D., & Hoskins, B. J. (1988). The Generation of Global Rotational Flow by Steady Idealized Tropical Divergence. Journal of the Atmospheric Sciences, 45(7), 1228–1251. https://doi.org/10.1175/1520-0469(1988)045<1228:TGOGRF>2.0.CO;2

Schulte, J. A., & Lee, S. (2017). Strengthening North Pacific Influences on United States Temperature Variability. Scientific Reports, 7(1). https://doi.org/10.1038/s41598-017-00175-y

Screen, J. A., & Simmonds, I. (2013). Exploring links between Arctic amplification and mid-latitude weather. Geophysical Research Letters, 40(5), 959–964. https://doi.org/10.1002/grl.50174

Sigmond, M., Kushner, P. J., & Scinocca, J. F. (2007). Discriminating robust and non-robust atmospheric circulation responses to global warming. Journal of Geophysical Research: Atmospheres, 112(D20). https://doi.org/10.1029/2006JD008270

Simon Wang, S.-Y., Huang, W.-R., Hsu, H.-H., & Gillies, R. R. (2015). Role of the strengthened El Niño teleconnection in the May 2015 floods over the southern Great Plains. Geophysical Research Letters, 42(19), 8140–8146. https://doi.org/10.1002/2015GL065211

Singh, D., Swain, D. L., Mankin, J. S., Horton, D. E., Thomas, L. N., Rajaratnam, B., & Diffenbaugh, N. S. (2016). Recent amplification of the North American winter temperature dipole. Journal of Geophysical Research: Atmospheres, 121(17), 9911–9928. https://doi.org/10.1002/2016JD025116

Son, S.-W., Ting, M., & Polvani, L. M. (2009). The Effect of Topography on Storm-Track Intensity in a Relatively Simple General Circulation Model. Journal of the Atmospheric Sciences, 66(2), 393–411. https://doi.org/10.1175/2008JAS2742.1

Soulard, N., Lin, H., & Yu, B. (2019). The changing relationship between ENSO and its extratropical response patterns. Scientific Reports, 9(1), 6507. https://doi.org/10.1038/s41598-019-42922-3

Sun, L., Perlwitz, J., & Hoerling, M. (2016). What caused the recent "Warm Arctic, Cold Continents" trend pattern in winter temperatures? Geophysical Research Letters, 43(10), 5345–5352. https://doi.org/10.1002/2016GL069024

Tamarin, T., & Kaspi, Y. (2017). Mechanisms Controlling the Downstream Poleward Deflection of Midlatitude Storm Tracks. Journal of the Atmospheric Sciences, 74(2), 553–572. https://doi.org/10.1175/JAS-D-16-0122.1

Teng, H., & Branstator, G. (2017). Causes of Extreme Ridges That Induce California Droughts. Journal of Climate, 30(4), 1477–1492. https://doi.org/10.1175/JCLI-D-16-0524.1

Thornton, P. K., Ericksen, P. J., Herrero, M., & Challinor, A. J. (2014). Climate variability and vulnerability to climate change: A review. Global Change Biology, 20(11), 3313–3328. https://doi.org/10.1111/gcb.12581

Trenberth, K. E. (1990). Recent Observed Interdecadal Climate Changes in the Northern Hemisphere. Bulletin of the American Meteorological Society, 71(7), 988–993. https://doi.org/10.1175/1520-0477(1990)071<0988:ROICCI>2.0.CO;2

Trenberth, K. E., Branstator, G. W., Karoly, D., Kumar, A., Lau, N.-C., & Ropelewski, C. (1998). Progress during TOGA in understanding and modeling global teleconnections associated with tropical sea surface temperatures. Journal of Geophysical Research: Oceans, 103(C7), 14291–14324. https://doi.org/10.1029/97JC01444

Trigo, I. F. (2006). Climatology and interannual variability of storm-tracks in the Euro-Atlantic sector: A comparison between ERA-40 and NCEP/NCAR reanalyses. Climate Dynamics, 26(2), 127–143.

Valdes, P. J., & Hoskins, B. J. (1991). Nonlinear Orographically Forced Planetary Waves. Journal of the Atmospheric Sciences, 48(18), 2089–2106. https://doi.org/10.1175/1520-0469(1991)048<2089:NOFPW>2.0.CO;2

Vecchi, G. A., Delworth, T., Gudgel, R., Kapnick, S., Rosati, A., Wittenberg, A. T., Zeng, F., Anderson, W., Balaji, V., Dixon, K., Jia, L., Kim, H.-S., Krishnamurthy, L., Msadek, R., Stern, W. F., Underwood, S. D., Villarini, G., Yang, X., & Zhang, S. (2014). On the Seasonal Forecasting of Regional Tropical Cyclone Activity. Journal of Climate, 27(21), 7994–8016. https://doi.org/10.1175/JCLI-D-14-00158.1

Vimont, D. J., Battisti, D. S., & Hirst, A. C. (2001). Footprinting: A seasonal connection between the tropics and mid-latitudes. Geophysical Research Letters, 28(20), 3923–3926. https://doi.org/10.1029/2001GL013435

Vimont, D. J., Wallace, J. M., & Battisti, D. S. (2003). The Seasonal Footprinting Mechanism in the Pacific: Implications for ENSO. Journal of Climate, 16(16), 2668–2675. https://doi.org/10.1175/1520-0442(2003)016<2668:TSFMIT>2.0.CO;2

Walker, G. T. (1925). CORRELATION IN SEASONAL VARIATIONS OF WEATHER—A FURTHER STUDY OF WORLD WEATHER. Monthly Weather Review, 53(6), 252–254. https://doi.org/10.1175/1520-0493(1925)53<252:CISVOW>2.0.CO;2

Wallace, J. M., & Gutzler, D. S. (1981). Teleconnections in the Geopotential Height Field during the Northern Hemisphere Winter. Monthly Weather Review, 109(4), 784–812. https://doi.org/10.1175/1520-0493(1981)109<0784:TITGHF>2.0.CO;2

Wang, S.-Y., Hipps, L., Gillies, R. R., & Yoon, J.-H. (2014). Probable causes of the abnormal ridge accompanying the 2013–2014 California drought: ENSO precursor and anthropogenic warming footprint. Geophysical Research Letters, 41(9), 3220–3226. https://doi.org/10.1002/2014GL059748

Wang, S.-Y. S., Huang, W.-R., & Yoon, J.-H. (2015). The North American winter 'dipole' and extremes activity: A CMIP5 assessment. Atmospheric Science Letters, 16(3), 338–345. https://doi.org/10.1002/asl2.565

Wang, S.-Y. S., Yoon, J.-H., Becker, E., & Gillies, R. (2017). California from drought to deluge. Nature Climate Change, 7, 465–468. https://doi.org/10.1038/nclimate3330

White, R. H., Wallace, J. M., & Battisti, D. S. (2021). Revisiting the Role of Mountains in the Northern Hemisphere Winter Atmospheric Circulation. Journal of the Atmospheric Sciences, 78(7), 2221–2235. https://doi.org/10.1175/JAS-D-20-0300.1

Wills, R. C. J., & Schneider, T. (2018). Mechanisms Setting the Strength of Orographic Rossby Waves across a Wide Range of Climates in a Moist Idealized GCM. Journal of Climate, 31(18), 7679–7700. https://doi.org/10.1175/JCLI-D-17-0700.1

Wills, R. C. J., White, R. H., & Levine, X. J. (2019). Northern Hemisphere Stationary Waves in a Changing Climate. Current Climate Change Reports, 5(4), 372–389. https://doi.org/10.1007/s40641-019-00147-6

Yeh, S.-W., Kang, Y.-J., Noh, Y., & Miller, A. J. (2011). The North Pacific Climate Transitions of the Winters of 1976/77 and 1988/89. Journal of Climate, 24(4), 1170–1183. https://doi.org/10.1175/2010JCLI3325.1

Zhang, P., Wu, Y., Chen, G., & Yu, Y. (2020). North American cold events following sudden stratospheric warming in the presence of low Barents-Kara Sea sea ice. Environmental Research Letters, 15(12), 124017. https://doi.org/10.1088/1748-9326/abc215

CHAPTER 2

GROWING PACIFIC LINKAGE WITH WESTERN NORTH ATLANTIC
EXPLOSIVE CYCLOGENESIS

2.1   Abstract

Explosive cyclones (ECs), defined as developing extratropical cyclones that experience pressure drops of at least 24 hPa in 24 hours, are impactful weather events which occur along highly populated coastal regions in the eastern United States. These storms occur due to a combination of atmospheric and surface processes, such as jet stream intensification and latent heat release at the ocean surface. Even though previous literature has elucidated the role of these processes in EC formation, the sources of interannual variability that impact seasonal EC frequency are not well known. To analyze the sources of interannual variability, we track cases of ECs and dissect them into two spatial groups: those that formed near the east coast of North America (coastal) and those in the North Central Atlantic (high latitude). The frequency of high-latitude ECs is strongly correlated with the North Atlantic Oscillation, a well-known feature, whereas coastal EC frequency exhibits a growing relationship with an atmospheric wave- train emanating from the North Pacific in the last 30 years. This wave-train pattern of alternating high-and-low pressure resulted in heightened upper-level divergence and baroclinic instability along the east coast of North America. Using a coupled model experiment, we show that the tropical Pacific Ocean is the main driver of this atmospheric wave train and the subsequent enhancement seasonal baroclinic instability in the North Atlantic.

2.2   Introduction

Explosive cyclones (ECs) in the North Atlantic have long been a subject of meteorological interest, largely because their complex atmospheric processes were difficult to forecast and they often result in high impact weather for the eastern coast of the United States (Bosart, 1981; Sanders, 1986; Sanders & Gyakum, 1980; Silberberg & Bosart, 1982). One impactful example is winter storm Grayson (January 3-5, 2018) which resulted in 22 deaths and approximately $1.1 billion in economic costs (LeComte, 2019). Defined as extratropical cyclones which experience a minimum surface pressure drop of 24 hPa over a 24-hour period, ECs are caused by synoptic and mesoscale interactions that result in enhanced baroclinic instability. The dynamic and thermodynamic mechanisms of explosive cyclogenesis have studied extensively, but limited records of high-fidelity data for tracking and analyzing ECs has hindered studies of interannual EC variability.

To understand how ECs may vary on interannual timescales, it is important to consider the interannual variability of the synoptic and mesoscale processes that can result in rapid cyclogenesis. In the early analyses by Sanders and Gyakum (1980) and in subsequent studies, ECs were commonly studied over warm ocean currents, like the Gulf Stream, where atmospheric and boundary-layer instability is enhanced due to latent heat release (Gall, 1976; Gyakum, 1983; Konrad & Colucci, 1988; Kuwano-Yoshida & Asuma, 2008; Minobe et al., 2008; Rudeva & Gulev, 2011; Sanders & Davis, 1988; Whitaker & Davis, 1994). Other cyclogenesis processes include baroclinicity driven by strong atmospheric temperature contrasts (Bosart, 1981; Bosart & Lin, 1984), the upper-level jet-stream and storm track (Colucci, 1985; Macdonald & Reiter, 1988; Rogers & Bosart, 1986; Ulbrich et al., 2001), and upper level divergence from enhanced upward

motion (Bosart & Lin, 1984; Pinto et al., 2009; Uccellini, 1990; Uccellini & Johnson, 1979). These processes will be broadly referred to as cyclogenesis mechanisms.

Due to the spatial heterogeneity of cyclogenesis mechanisms in the North Atlantic (C.-C. Wang & Rogers, 2001), it is important to analyze how the sources of interannual variability may vary within the North Atlantic. Specifically, this study focuses on teleconnection patterns that impact EC frequency. For example, the North Atlantic Oscillation (NAO), characterized by a meridional dipole of alternating pressure anomalies in the North Pacific, has been shown to strengthen and shift the jet stream to the north in the positive phase, displacing ECs further to the north as well (Gómara et al., 2016). However, many highly impactful ECs like winter storm Grayson form at lower latitudes along the East Coast of the United States and are unlikely to be associated with the high-latitude atmospheric changes induced by the NAO (LeComte, 2019). Additionally, Pinto et al. (2009) highlighted two epicenters for extreme cyclogenesis: one adjacent to the east coast of the United States and another east of the southern tip of Greenland (see their Figure 4c). The teleconnections which impact interannual variability in ECs for these two regions likely differ due to the geographical separation of these two cyclogenesis epicenters.

The NAO has been the focus for literature relating interannual climate variability with EC frequency and intensity. A positive NAO results in more frequent high-latitude cyclogenesis cases (Gómara et al., 2016; Pinto et al., 2009). However, analyses of potential up-stream forcing mechanisms for North Atlantic cyclogenesis mechanisms have not been extended to explosive cyclogenesis (Schemm et al., 2018). Especially for lower-latitude ECs which form along the east coast of North America, different

teleconnections may impact cyclogenesis mechanisms than in the high-latitudes of the

North Atlantic. Of primary interest are atmospheric teleconnections which can induce an

anomalous wave-train pattern over North America, a feature which is often associated

with severe winter weather. One increasingly important example is the Eastern Pacific–

North Pacific pattern (EP-NP), which has been increasingly linked to extreme winter

temperatures and weather in eastern North America (Schulte & Lee, 2017). While the

EP-NP pattern is most prominent during the spring, summer, or fall season, it has

amplified in the recent decades during the winter (Schulte & Lee, 2017). This

amplification, which has been associated with pronounced ridging events over western

North America and deepened seasonal troughs over the eastern part of the

continent(Schulte & Lee, 2017; Wang et al., 2014; Wang et al., 2017), may potentially

impact upper-level circulation features relevant for ECs along the southeast coast of

North America. The Pacific North American (PNA) pattern can also facilitate negative

pressure anomalies over the Southeast United States that may impact seasonal

baroclinicity and cyclogenesis mechanisms (Wettstein & Wallace, 2010).

Many of the atmospheric teleconnection patterns that span North America during the

winter season are linked to the tropical Pacific Ocean, such as El Niño Southern

Oscillation (ENSO) (Branstator, 2014; Ciasto et al., 2016; May & Bengtsson, 1998).

Anomalous tropical heating and convection can form arcing patterns of alternating

pressure anomalies through stationary Rossby wave propagation in the westerly mid-

latitude flow (Held et al., 2002; Hoskins & Ambrizzi, 1993; Hoskins & Karoly, 1981).

These large-scale alterations to the mid-latitude flow, combined with the impact of

transient troughs and ridges (Held et al., 1989; May & Bengtsson, 1998), shift regions of

baroclinicity in the North Atlantic (Schemm et al., 2018). Given this relationship, we

expect that the frequency of ECs in the North Atlantic is somewhat dependent on tropical

Pacific climate variability.

Our objectives are to identify the sources of interannual variability associated with

EC frequency in the North Atlantic and to determine the role of Pacific forcing in

modulating EC frequency. After the methods in section two, section three documents the

relationship between seasonal atmospheric circulation features and EC frequency for low-

latitude coastal and high-latitude ECs (defined explicitly in methods). As the results for

high-latitude ECs are largely supportive of other literature, we focus on coastal ECs and

their associated cyclogenesis mechanisms which exhibit a growing relationship with an

atmospheric wave-train of alternating pressure anomalies that branches out from the

tropical Pacific. Finally, the impacts of Pacific climate variability from sections three and

four are examined with the fully coupled Community Earth System Model (CESM) in

section five.

2.3   Methods

2.3.1   EC definition and Tracking

Tracking explosive cyclogenesis is attainable through automated detection

techniques in reanalysis data and has been performed in multiple studies (Allen et al.,

2010a; Gómara et al., 2016; Kuwano-Yoshida & Asuma, 2008; Reale et al., 2019).

Automated tracking requires a strict definition of an EC, of which the normalized

deepening rate of central pressure (NDR) is commonly used (Sanders & Gyakum, 1980).

The NDR is defined as follows:

$$(1) \qquad \text{NDR} = \frac{\Delta p}{24} \frac{\sin(60)}{|\sin\theta|},$$

where Δp is the change in central MSLP within the cyclone and θ is the latitudinal

position of the EC. The NDR determines the raw change in mean sea level pressure

(MSLP) relative to 60° latitude, to account for the negative pressure tendency from the

tropics to the poles. An explosive event would result in a value equal to or greater than

one, which is defined as one Bergeron.

Tracking is performed in ERA5 global reanalysis (Hersbach et al., 2020), at six-

hourly data at a 0.25° resolution from 1950 through 2020. The 1950-1978 period of the

data has been released as a preliminary back-extension, so tracking in this data is

compared with tracking output from the National Centers for Environmental Prediction

Reanalysis 1 (NCEP R1) at 2.5° resolution (Kalnay et al., 1996) and the Japanese 55-year

Reanalysis project at 1.25° resolution (Ebita et al., 2011). EC tracking is done for the

Northern hemisphere's cool season, November through March, which has been identified

as the most common season for ECs in the North Atlantic (Allen et al., 2010a). Following

Hodges and Hoskins (2002), a Fourier transform is applied to the global MSLP field at

each six-hour time step to remove large scale planetary waves (wavenumber 1-5). The

minimum value in this filtered field is identified for the domain of 90°W – 0°W and 20°N

to 60°N, and the raw MSLP value is documented within 2.5° from the filtered MSLP

value (T0). Subsequently, the tracking steps back one time step (six hours) to identify the

location and intensity of minimum MSLP that occurred within 7.5° of the location of T0,

to ensure that the tracking is only picking up locally relevant features. This distance

(7.5°) was chosen as it was manually verified to accurately track the same system while

eliminating the chance of a "jump" in the tracking to a low-pressure center far away. The

minimum MSLP within this smaller domain is retained (T-1), along with the latitude and

longitude, and the tracking continues to iteratively step back and retain the location and value of minimum MSLP relative to the location of minimum MSLP from the time step six hours ahead. This continues until we have reached 24 hours before T0. The pressure difference in 24 hours is recorded and the latitudinal position of each point is used to calculate the NDR for a 24-hour period. If the NDR is greater than or equal to 1 Bergeron, the latitude, longitude, MSLP and date of each minimum MSLP point are retained from 24 hours before T0. Subsequently, the tracking algorithm goes forward in time to analyze the progression of the mature EC 24 hours ahead of T0 and well beyond the initial search domain. We manually checked to ensure that these methods realistically picked up features related to a single cyclone's evolution and structure. Individual storms can have two 24-hour periods of intensification that result in an NDR greater than 1, so any ECs that occurred in adjacent time steps that were no greater than 7.5° apart at T0 were considered as one event.

Other work evaluating cyclone detection and tracking methods has shown that differences in results do come from differences in methodology. The source of heterogeneity in the results of different tracking methods comes from data products and resolution differences (Hodges et al., 2003, 2011; Jung et al., 2006; X. L. Wang et al., 2016), differences in the criteria of extratropical cyclones (Allen et al., 2010b; Hoskins & Hodges, 2002b; E. Walker et al., 2020), and difference in analysis domains (i.e developing a tracking scheme for global versus regional domains) (Reale et al., 2019). While tracking using minima of mean sea level pressure or surface pressure has been successfully carried out in many studies (Benestad & Chen, 2006; Blender et al., 1997; Hanley & Caballero, 2012; Rudeva & Gulev, 2011; Trigo, 2006), there are documented

uncertainties in this approach. Many of these uncertainties are associated with weak low-pressure systems (Neu et al., 2012) or storms with a more complex structure (Hanley & Caballero, 2012). Due to these complicating factors in the development of a storm and to differences in data used for tracking, the exact frequency of cyclones per year remains one of the largest uncertainties (see Neu et al., 2012 for a review).

Despite these caveats, research has also shown that tracking is often most reliable for deep and extreme cyclones where low-pressure centers are prominent (Neu et al., 2012). This has been shown in mid-century reanalysis data and particularly for tracking methods in the northern hemisphere where observed data has had a longer, denser, and more reliable record than the southern hemisphere. While the exact frequency of extratropical cyclones is a source of disagreement between different datasets and methods, there is much stronger coherence in the interannual variability of cyclones detected by tracking methods (Neu et al., 2012). Additionally, the spatial distribution of cyclogenesis and cyclone tracks is well captured by several diverse methods and datasets (Allen et al., 2010b; Raible et al., 2008; E. Walker et al., 2020). These findings motivated the tracking methods used in this study, which are intentionally focused on the interannual variability of deep cyclones (ECs) with a clear definition and threshold criteria. We expect the greatest uncertainty in our methods to come from the data used in the study –motivating our use of four reanalysis datasets and their own records of ECs.

For a glimpse into the efficacy of our tracking methods, Figure 2.1 shows four consecutive time steps of MSLP for three randomly selected explosive cyclones. The black plus sign intersects the minimum MSLP value for that timestep. For each cyclone, our approach effectively follows the trajectory of the low-pressure center and does not

jump to other adjacent centers of MSLP. We have manually evaluated each storm tracked

by these methods by plotting the MSLP field along with our point detection scheme and

the algorithm performs very well at capturing the evolution of explosive cyclones.
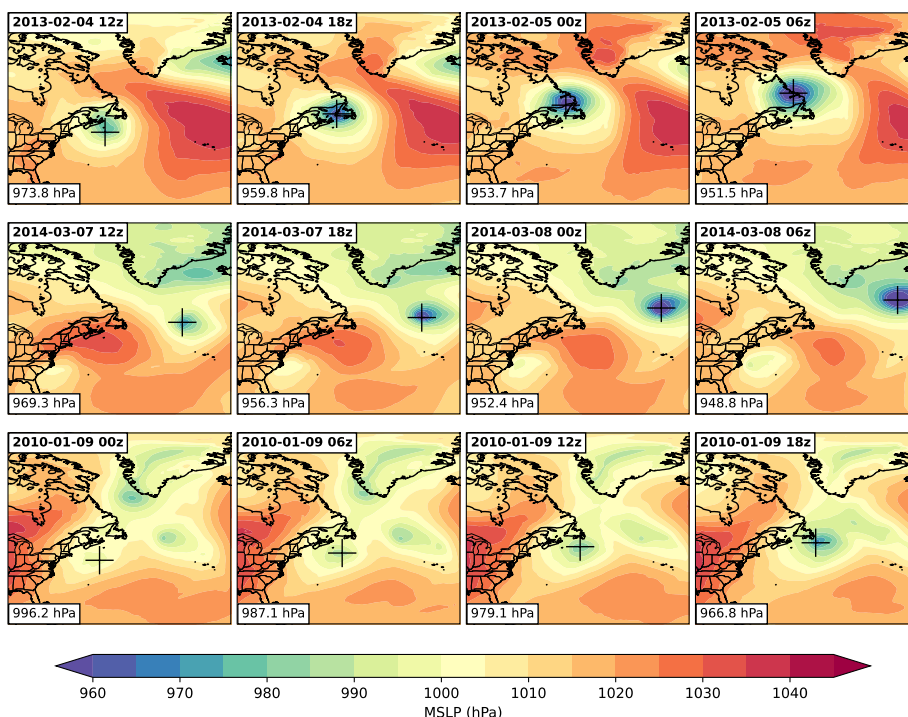
Figure 2.1. Three evolutions of explosive cyclones chosen at random. Each row represents four 6-hour time steps leading up to the explosive cyclogenesis threshold. The contour fill represents MSLP, and the black plus sign intersects the point of minimum MSLP detected by our tracking methods. The pressure at this grid point can be found in the bottom left corner each subplot while the date is in the top left corner.

We then determine the frequency of ECs for the cold season within two spatial

domains as defined by previous studies (Pinto et al., 2009; C.-C. Wang & Rogers, 2001).

ECs are grouped into coastal (90°W-60°W and 10°-45°N) and high-latitude domains

(60°W-0°W and 45°N-90°N), based on their latitude and longitudinal position 24 hours

before the criteria for explosive cyclogenesis was met (black dots in Fig 1b and 1c). Pinto

et al. (2009) showed that extreme cyclogenesis in the North Atlantic has two distinct

regions favorable for cyclogenesis near the low-latitude coast of North America and to the east of the southern tip of Greenland. While extratropical cyclones in the North Atlantic have long been classified into specific "types" based on their synoptic features, cyclogenesis mechanisms, and geographic location (Pinto et al., 2009; C.-C. Wang & Rogers, 2001), our focus is on the rapidly developing "bomb cyclones" and not further classification of these events. In addition to the two cyclogenesis regions highlighted by Pinto et al. (2009) and Wang et al. (C.-C. Wang & Rogers, 2001), these groupings are motivated largely by impacts – as cyclones forming near the east coast will have associated impacts on North America than high-latitude cyclones (where impacts can be heavily felt by Europe) (Gómara et al., 2014; LeComte, 2019).

2.3.2   Sources of Interannual Variability

To document the non-stationary relationship between teleconnection patterns and EC frequency, we use a 30-year rolling correlation between high-latitude/coastal EC frequency with teleconnection indices for the November-March average (e.g., EP-NP, PNA, AO, and NAO). These teleconnection indices are obtained from the National Oceanic and Atmospheric Administration's Physical Sciences Laboratory. We then use correlation and composite analysis of EC frequency for the cold season, averaged from November through March, with geopotential height (Z_{250}), wave activity flux (Takaya & Nakamura, 2001), stream function, velocity potential, wind divergence, and zonal wind at 250 hPa (U_{250}) as well as omega at 500 hPa. These data were all gathered from ERA5 monthly reanalysis data. For composite analysis, we selected years that surpassed a threshold of one-half standard deviation above the mean for both the frequency of ECs and for the EP-NP index. To compare how the relationship of ECs and North Atlantic

cyclogenesis mechanisms may have changed, we separately analyze the period from 1950

to 1984 (early period) compared to 1984 to 2019 (recent period). We chose 1984 as the

cutoff year to result in an equal sample size for comparison between the early and later

period. Changing the cutoff period to any time within the 1980s does not qualitatively

alter the results (not shown). The year in analysis corresponds to the year for the

November and December months of a November through March average. Finally, all

anomalies are defined as a deviation from climatology in each month from 1950 through

2020.

We also perform composite analysis of individual cyclone cases to examine the

cyclogenesis mechanisms. This analysis uses six-hourly ERA5 reanalysis data averaged

for the 12-hour period before the threshold of 1 Bergeron was met by an EC. In addition

to upper-level divergence, we compute the 850 hPa temperature advection and the

maximum Eady Growth Rate (EGR, Eady, 1949; Lindzen & Farrell, 1980) as a vertical

average from 300-500 hPa following Pinto et al. (2009) who showed that upper-level and

low-level EGR results were analogous for synoptic composites of extreme cyclones. The

EGR has been used extensively to approximate baroclinic instability in a storm:

$$\text{(2)} \qquad EGR = \frac{\left(0.3098 \times |f| \times \left|\frac{du}{dz}\right|\right)}{\left(\frac{g d\theta}{\theta dz}\right)^{\frac{1}{2}}}$$

where g represents the gravitational constant, f is the Coriolis parameter, and θ represents

potential temperature. The denominator represents the Brunt-Vaisala frequency which is

commonly denoted as N (Wallace & Hobbs, 2006)

2.3.3 Model Diagnostics in the CESM

To test the hypothesis that the recent amplification of the North Pacific wave-train and its association with EC frequency are forced by the ocean, we conducted modeling experiments using the National Center for Atmospheric Research (NCAR) fully coupled CESM version 1.0 (Shields et al. 2012) and an ocean data assimilation scheme (Chikamoto et al., 2019). CESM is comprised of ocean, sea ice, atmospheric, and land components. The resolution for ocean and sea-ice components is approximately 1° latitude by 3° longitude at the equator with a slight decrease in resolution at high latitudes and 60 vertical levels in the ocean. The atmospheric and land components are a T31 spectral grid with 26 atmospheric levels. Using this model configuration, we conducted two sets of partial ocean data assimilation runs as described below: the global (GLOB) and equatorial Pacific partial ocean assimilation (eqPAC) runs. Our approach is similar to the other model experiments, such as Atmospheric Model Intercomparison Projects (AMIP) (Alexander et al., 2002; D. L. Hartmann, 2015; Lau & Nath, 1996) and pacemaker experiments (Boer et al., 2016; Fosu, He, & Liguori, 2020; Kosaka & Xie, 2016), but can minimize the artificial model drift and initialization shocks by incorporating subsurface ocean information into the climate model as reported by previous studies (Chikamoto et al., 2015, 2016, 2019; Ham et al., 2017; Johnson et al., 2020; Purich et al., 2016; Stuivenvolt-Allen et al., 2021).

Configuring the GLOB and eqPAC runs consists of the following steps. We first conducted a historical simulation of the CESM with 10 ensemble members by prescribing natural and anthropogenic radiative forcing from 1850 to 1957. From this historical run, we selected initial conditions at January 1st, 1958 to conduct the ocean data assimilation run with 10-member ensemble. Next, we carried out ocean data assimilation runs by

incorporating three-dimensional ocean temperature and salinity anomalies taken from the

European Center for Medium-Range Weather Forecast's Ocean Reanalysis Product

(version 4) for the period 1958–2014 (Balmaseda et al., 2013a) along with prescribed

radiative forcing. The assimilation scheme used here is an incremental analysis update,

which is effective and computationally inexpensive compared to other methods (Bloom

et al., 1996; Huang et al., 2002). In the assimilation process, the ocean component of

CESM is updated by incorporating the ocean reanalysis over the global ocean (GLOB

run) or in the tropical Pacific only (10°S-10°N) across the Pacific Basin (eqPAC run).

Therefore, the model-simulated ocean variability in the assimilated region is consistent

with the ocean reanalysis while the rest of the climate system (including the extratropical

oceans) are free to evolve to the "observed" ocean forcing. The atmospheric variability

simulated by the GLOB and eqPAC runs indicate the contribution of ocean variability,

from the global ocean and tropical Pacific as well as the prescribed radiative forcing.

2.4   Interannual Variability of Coastal and High-Latitude Explosive Cyclones

The spatial distribution of our tracked ECs in the North Atlantic (Figure 2.2a)

show the greatest density of ECs occurring along the North Atlantic storm track, which is

consistent with other modern EC climatological studies (Allen et al., 2010a; Gómara et

al., 2016; Reale et al., 2019). Coastal cyclones have a meridionally tilted pattern in their

track (Figure 2.2b) while high-latitude cyclones exhibit a more zonal density pattern

(Figure 2.2c). These track patterns are consistent with the orientation of the gulf stream

current and the meridional tilt of the climatological jet stream in winter off the east coast

of North America. No noticeable trends are seen in the frequency (Figure 2.2d) or

minimum annual MSLP (not shown) of ECs within the last seventy years. However, we

find a significant increasing trend in the 30-year running variance of both coastal

(p=0.013) and high-latitude (p<0.01) EC frequency (Figure 2.2e). This suggests that

interannual variability in EC frequency has risen in the recent period that teleconnections

may have become more important for modulating EC frequency from November through

March. Finally, Coastal EC frequency is highly uncorrelated with high-latitude ECs

(r=0.07) supporting the need to separately analyze these groups.
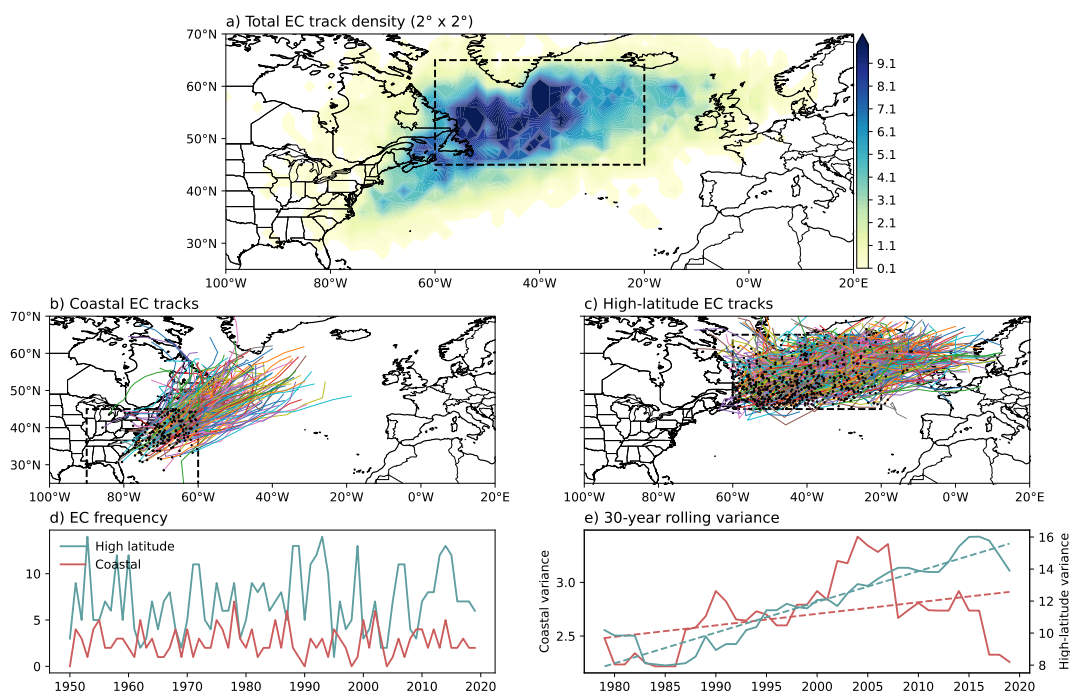
Figure 2.2. (a) Nov-Mar genesis density (Number of ECs per 2°x2° domain) of all ECs captured by our tracking methods from of 1950 through 2019 in ERA5. Tracks of (b) coastal and (c) high-latitude ECs along with the initial track point (a black marker). (d) Timeseries of EC frequency in the high-latitude (light blue) and coastal regions (red) during Nov-Mar from 1950 through 2019. (e) 30-year rolling variance of EC frequency (solid lines) along with the linear trend computed from least squares regression. Each trend is significantly different from a slope of 0 through use of the Wald Test with a t-distribution of the test statistic at the 95% confidence level. The dashed black line indicates the region in which coastal and high-latitude cyclones are grouped by.

The relationship between coastal ECs and upper-level geopotential height has

changed in the recent decades, shown by the correlation analysis in Figure 2.3a-c. The

correlation map of Z_{250} with coastal EC frequency during winter consists of positive

anomalies over Alaska/Western Canada and negative anomalies over the central North

Pacific and eastern North America (Fig 2a), resembling the EP-NP pattern. However,

their amplitudes are weak and insignificant, particularly for the 1950-1984 period (Fig

2b). In contrast, we find the clearer and significant Z_{250} anomaly pattern with a more

prominent wave-train translating across North America for the recent period of 1985-

2020 (Fig 2c), suggesting a strengthened relationship between coastal EC frequency and

the EP-NP pattern. Along with this wave-train, Figure 2.3c shows that coastal ECs have a

weak relationship with a negative NAO-like pattern, consistent with literature observing

the negative NAO results in a shift of the storm track to lower latitudes (Chartrand &

Pausata, 2020). This amplified relationship in the recent period is not seen for high-

latitude ECs (Fig 2d-f). Rather, a prominent positive NAO pattern is consistently

associated with enhanced EC frequency for the higher latitude storms.
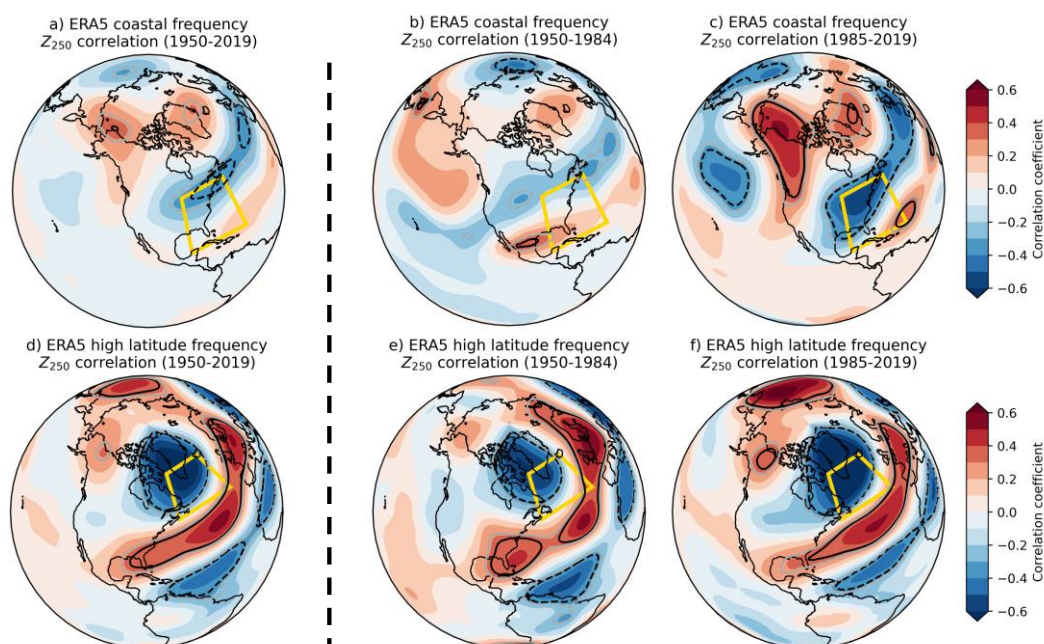
Figure 2.3. Correlation maps of Z_{250} with coastal EC frequency (top) and the high-latitude EC frequency (bottom) during November-March for (a,d) the entire analysis period, (b,e) 1950-1984, and (c,f) the recent period of 1985-2020. The black contour lines indicate the 95% confidence threshold for the correlation coefficient with the degrees of freedom equaling the number of the years in each correlation minus two using the Student's t-test. The yellow rectangle indicates the domain for coastal and high-latitude ECs.

2.5   Changes in Interannual Variability and Cyclogenesis Mechanisms

The wave-train pattern in Figure 2.3c suggests a Pacific climate influence on interannual variability of coastal EC frequency after 1985 through upper-level atmospheric dynamics. Through a 30-year rolling correlation with coastal EC frequency, Figure 2.4a shows that the EP-NP pattern has been highly correlated with coastal EC frequency in the recent decades. This growing relationship is present in the frequency of coastal ECs tracked from three different reanalysis datasets, ERA5, JRA55 and NCEP R1. The PNA pattern also depicts an increase in the correlation coefficient between coastal EC frequency and the cold-season teleconnection index except for the NCEP R1 record of coastal EC frequency (Figure 2.4b). We also note that the NAO and the Arctic Oscillation (AO) can have an impact on the high-latitude polar front jet (Hall et al., 2015) and their relationship with coastal EC frequency from ERA5 is increasing. However, the relationship between coastal EC frequency and the NAO and AO differs in each reanalysis dataset, introducing some uncertainty about the relationship of the arctic with coastal EC frequency. As the growing relationship of the EP-NP with coastal EC frequency is consistent in the three reanalysis datasets, it will be the focus of subsequent analysis.

The rolling correlations of the same teleconnection indices with the high-latitude EC frequency show a strong and persistent relationship between the NAO and high-

latitude EC frequency (not shown). The relationship between the NAO and high-latitude

EC frequency is consistent and significant for the entire period (1950-2020), which is

documented well by other studies (Gómara et al., 2016; Pinto et al., 2009).
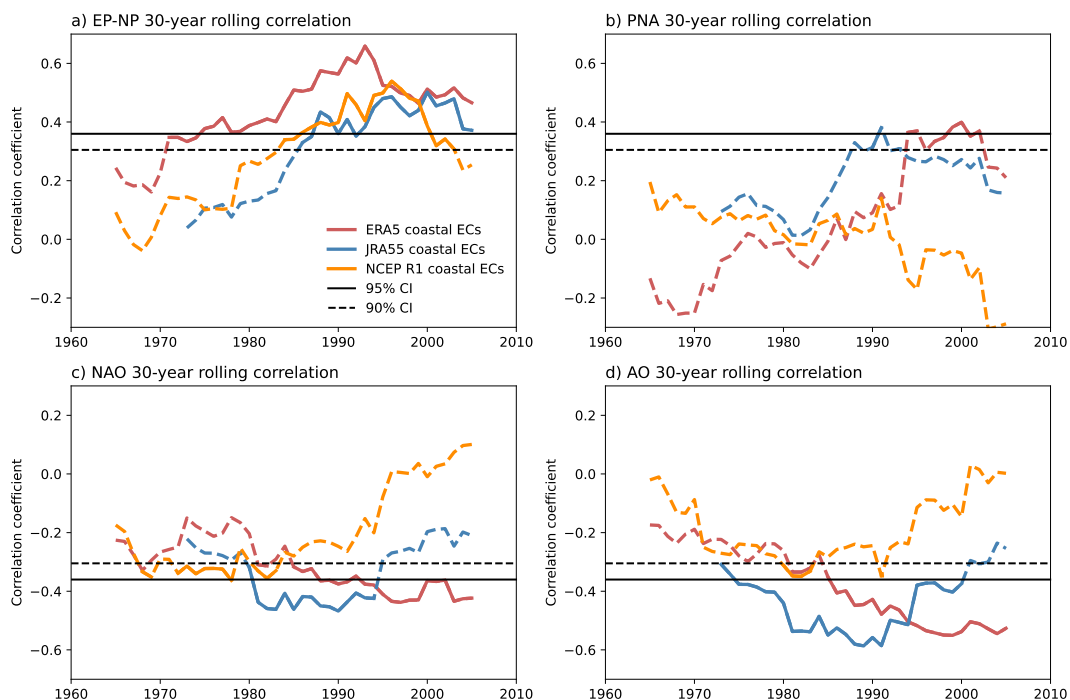
Figure 2.4. A 30-year rolling correlation between the November through March frequency of ECs tracked in ERA5 (red line), JRA55 (blue line) and NCEP R1 (orange line) with the (a) EP-NP, (b) PNA, (c) NAO, and (d) AO teleconnection indices. The time for each rolling correlation is calculated at the middle year for each 30-year period (i.e., the year 2000 corresponds to the correlation coefficient for 1985-2014). The horizontal dotted line and solid line indicate the significance thresholds for 28 degrees of freedom for the 90% and 95% confidence interval respectively. Solid lines indicate the periods with significant correlation surpassing the 90% confidence interval.

Figure 2.5a shows the correlation of the EP-NP index with Z_{250}, which

prominently features an arcing wave-train pattern that has a positive relationship with

Z_{250} over the central tropical Pacific. The early-period correlation shows that the upper-

level Z_{250} relationship with the EP-NP index was more localized to the Pacific and there

are less prominent relationships over North America (Figure 2.5b). For the recent period,

however, the relationship of Z_{250} with the EP-NP index has amplified over North

America (Figure 2.5c). This pattern is characteristic of a tropically induced

teleconnection which emanates from the central tropical Pacific. The associated wave-

train features a prominent positive relationship over the western coast of North America

and a deepened negative relationship over the east coast. The growing relationship

between the EP-NP index and EC frequency along with the changing upper-level

circulation features suggests that tropical Pacific variability could be an important driver

of EC frequency and cyclogenesis mechanisms along the east coast in the recent decades.
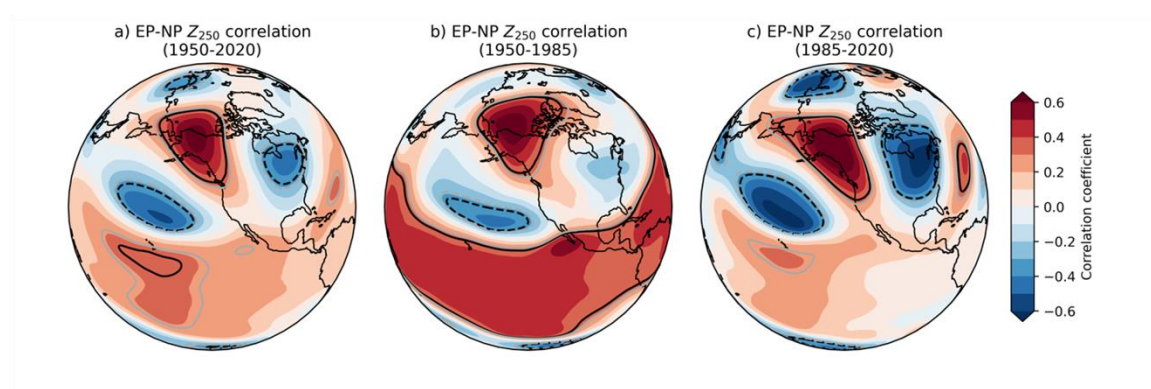
Figure 2.5. Correlation of the EP-NP index with Z_{250} from November through March for (a) the entire analysis period, (b) the early period 1950 through 1984 (c) and the recent period 1985 through 2020 (c). The black contour lines indicate the 95% confidence threshold for the correlation coefficient with the degrees of freedom equaling the number of the years in each correlation minus two.

The increasing relationship between the EP-NP and coastal EC frequency may be

partially explained by the strengthening of the negative relationship between the EP-NP

and upper-level Z_{250} over eastern North America. The amplified east-west dipole

structure in Z_{250} over North America would likely impact EC frequency through

enhanced jet stream activity and upper-level divergence associated with the amplified

pressure gradient. To examine the dynamic link between the EP-NP pattern and

cyclogenesis mechanisms, we made correlation maps of wind divergence at 250 hPa, zonal wind at 250 hPa (U_{250}), and latent heat flux at the ocean surface with the EP-NP index (Figure 2.6). Both 250 hPa divergence and zonal wind (U_{250}) as averages from November through March show an enhanced correlation with coastal EC frequency for the recent decades (Figure 2.6a-d). Upper-level divergence is an important factor to cyclogenesis in ECs and extreme extratropical cyclones because it facilitates baroclinicity that can result in rapid cyclogenesis (Baehr et al., 1999; Uccellini & Johnson, 1979; Ulbrich et al., 2009). The amplified gradient of Z_{250} anomalies associated with the EP-NP in the recent period (Figure 2.5c) results in a stronger upper-level jet stream over the east coast of North America (Figure 2.6d), another important ingredient for the genesis and steering of rapid cyclogenesis (Pinto et al., 2009). The relationship of the EP-NP with ocean surface latent heat flux (SLHF) results in shifted and a wide area of reduced SLHF in the recent era. Generally, it appears that the positive EP-NP is not associated with widespread increases in SLHF suggesting that the EP-NP impacts on cyclogenesis mechanisms are mostly associated with the upper-level (discussed more later).
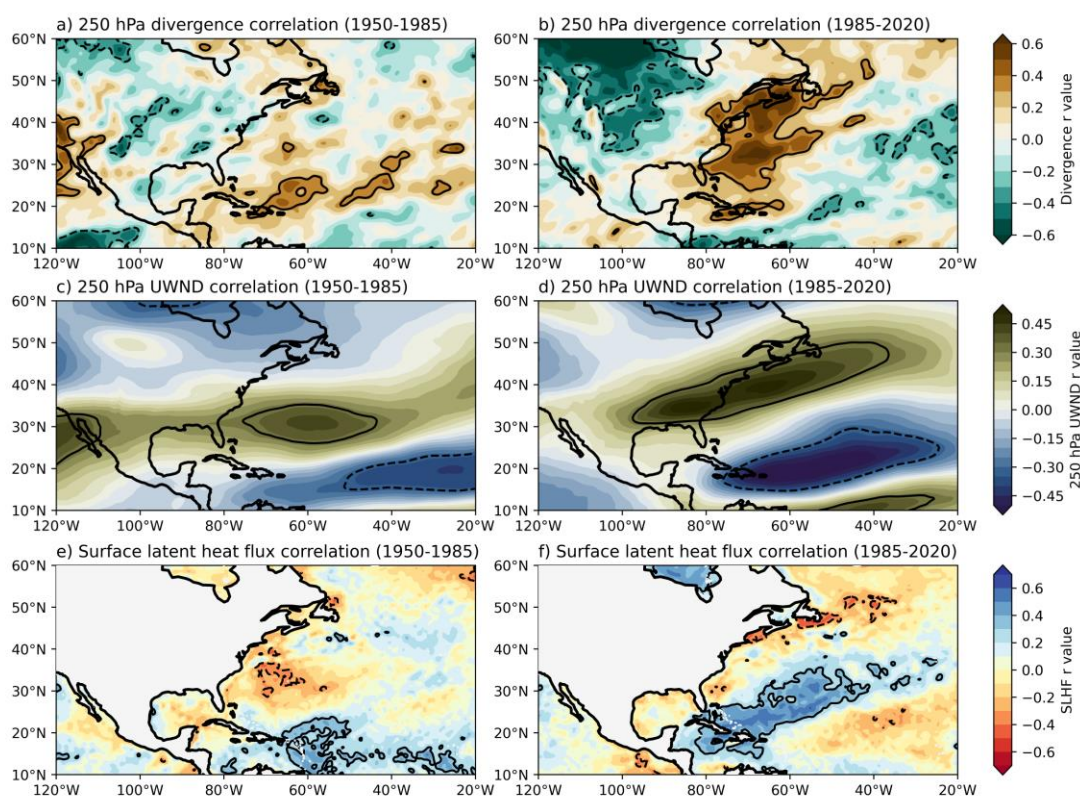
Figure 2.6. Correlation of the EP-NP index with (a,b) 250 hPa wind divergence, (c,d) 250 hPa zonal wind (U_{250}), and (e,f) SLHF for the early period (left) and the recent period (right). The black contour lines indicate the 95% confidence threshold for the correlation coefficient with the degrees of freedom equaling the number of the years in each correlation minus two.

All analysis to this point has been done with seasonal averages, but most of the processes that result in ECs occur on much shorter time scales. To determine if the synoptic scale cyclogenesis mechanisms associated with coastal ECs are impacted by the EP-NP pattern, we provide case composites which constitute 12-hour averages of divergence, U_{250}, EGR and latent heat flux for the 24-12 hours before the threshold of one Bergeron was met for each coastal EC. These composites are taken for ECs which occur during positive EP-NP events which are one standard deviation above the mean EP-NP index from 1950 through 2020, and then each group is split into the early (1950-

1984) and later periods (1985-2020). From the synoptic case composites in Figure 2.7, the recent period ECs which occurred during cold-seasons dominated by a positive EP-NP had more a stronger connection with upper-level dynamics along with the jet stream position. The orientation of the jet stream shows the zonally elongated pattern during ECs for the early period (Figure 2.7a), while the recent period features the meridionally tilted pattern associated with enhanced divergence anomalies near the east coast of North America (Figure 2.7b). The EGR composites largely mirror these same features: the zonal configuration in the early period (Figure 2.7c) and the amplified and meridionally tilted in the recent period (Figure 2.7d). The upper-level circulation features induced by the EP-NP are also associated with more distinct and organized temperature gradients that extend to lower layers which can be seen clearly at 850 hPa (Figure 2.7e,f). In the recent period, there is a more distinct gradient of cold-air advection and warm-air advection centered on the east coast of North America, a characteristic feature of baroclinic instability. Finally, the SLHF composites in Figure 2.7g and 2.7h show that this local ocean forcing associated with the positive EP-NP phase has decreased in the recent period. These results suggest that upper-level atmospheric dynamics associated with the EP-NP pattern, rather than near-surface thermodynamics, have become a more important cyclogenesis mechanism for coastal ECS.
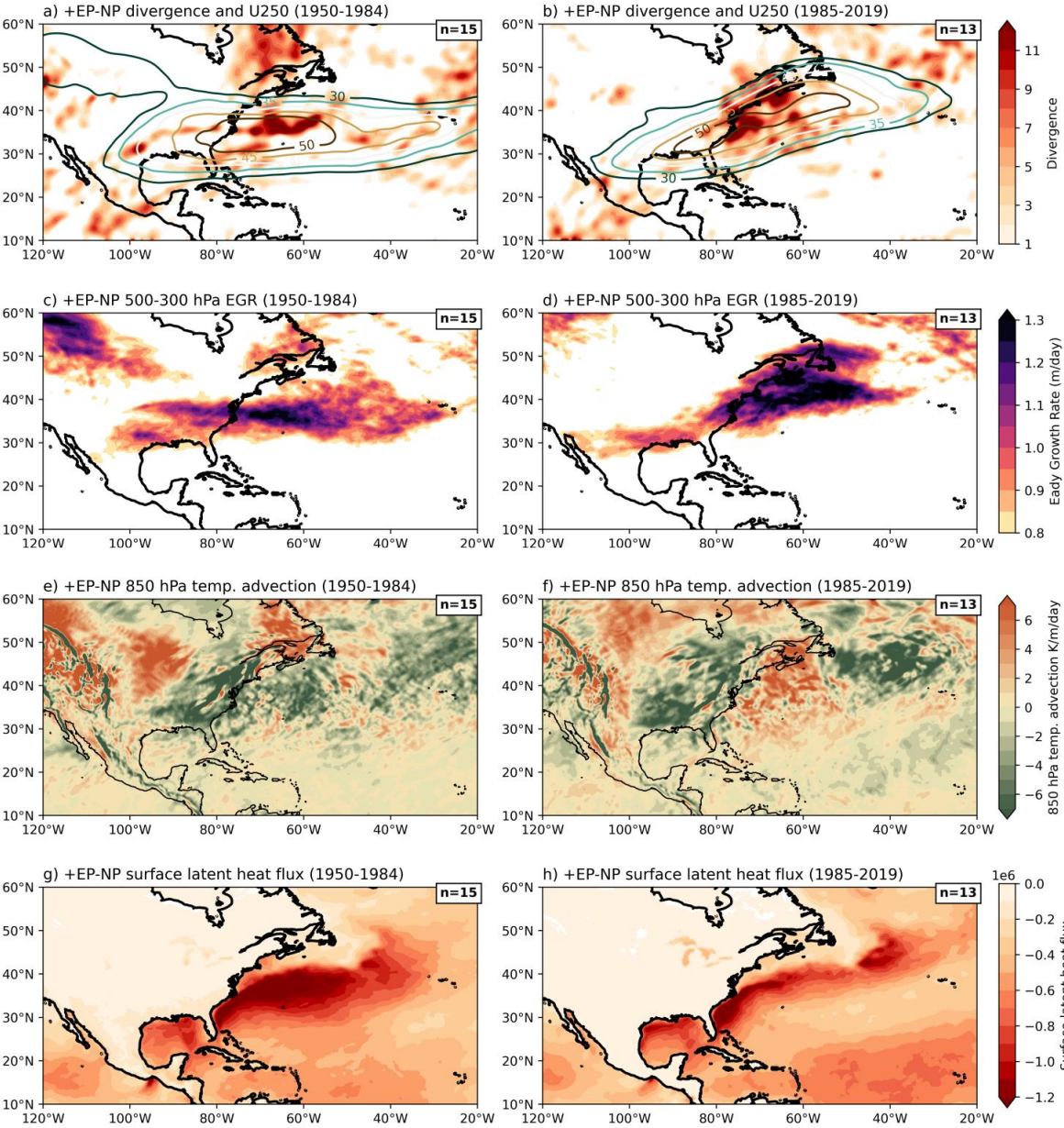
Figure 2.7. Positive EP-NP case composites of (a,b) wind divergence and zonal wind at 250 hPa, (c,d) 500-300 hPa EGR, (e,f) 850 hPa temperature advection, and (g,h) surface latent heat flux. The left column represents composites for the early period (1950–1984), while the right column are composites taken from the recent period (1985–2020). The sample size is included in the top right corner of each plot, indicating the number of ECs included in the analysis.

2.6 Growing Impact of the Tropical Pacific on Coastal ECs

The shift in the upper-level circulation features associated with coastal EC frequency and the EP-NP index can be seen in the stream function composites in Figure 2.8. This figure highlights that coastal EC frequency in the early period was more commonly associated with an anticyclonic circulation anomaly in the North Pacific. In the recent period, the stream function anomalies in the North Pacific have completely flipped compared to the early period (Fig. 2.8a and b) and are now more closely aligned with the EP-NP pattern (Fig. 2.8d). Additionally, the WAF (Takaya & Nakamura, 2001) shows wave energy propagation directed from the North Pacific towards the east coast of North America and the North Atlantic Ocean in the latter period.
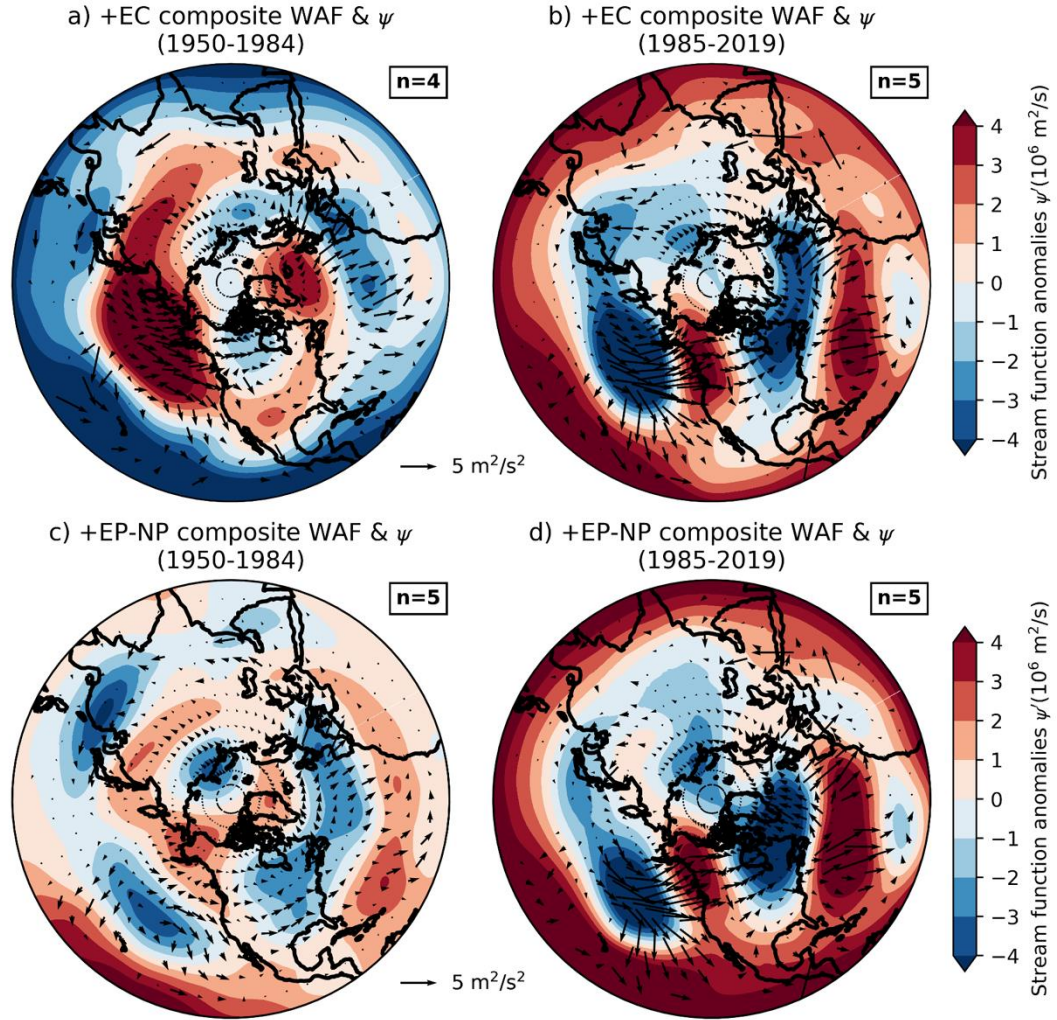
Figure 2.8. Composite maps of streamfunction anomalies at 250 hPa (contour fill) and WAF (vectors) for (a) large coastal EC frequency for 1950-1984, (b) large coastal EC frequency for 1985-2019, (c) positive phases of EP-NP index for 1950-1984, and (d) positive phases of EP-NP index for 1985-2019. The sample size is included in the top right corner of each plot, indicating the number of seasons included in the analysis.

To better depict the impact of the tropics on the emerging atmospheric wave train, Figure 2.9 presents composites of the positive phase of the EP-NP index with 500 hPa omega anomalies. In the last 35 years, upward motion associated with the EP-NP was enhanced in the central and western tropical Pacific (Figure 2.9a,b). Enhanced upward motion is also present in the northeast Pacific for the recent period, with an alternating

pattern of sinking and rising air that matches the observed changes in mid-latitude circulation associated with the EP-NP pattern. The linear trend in upward motion has some overlap with the composites of the positive EP-NP phase in the recent period, suggesting that climate change or low-frequency climate variability may contribute to strengthening the EP-NP pattern (Figure 2.9c).
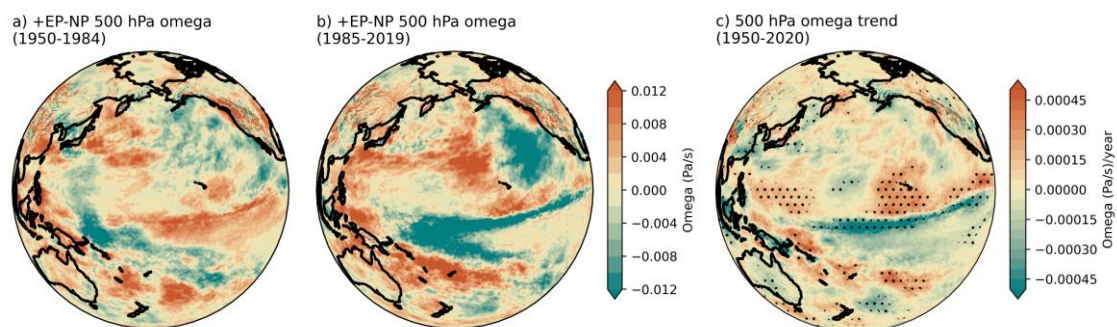
Figure 2.9. Composite maps of omega at 500hPa for the positive EP-NP phases in (a) the early period and (b) the recent period. (c) Linear trend in omega computed from least squares regression for the period of 1950-2020. Stippling marks areas significantly different from a slope of 0 through use of the Wald Test with a t-distribution of the test statistic at the 95% confidence interval.

These same features are supported by the 250 hPa velocity potential and divergent wind fields (Figure 2.10). There has been a large decrease in velocity potential in the western tropical Pacific and in the Northeastern Pacific, indicating an enhancement of upward motion within these regions, and increased potential for a source of Rossby wave activity that is known to induce atmospheric wave trains over North America (Held et al., 2002). Figure 2.10c shows the trend of velocity potential and divergent winds from 1950 through 2020, supporting that observed changes to the mean-state of the tropical Pacific are synchronous with the observed changes in variability.

a) +EP-NP velocity potential and divergent winds (1950-1984)
b) +EP-NP velocity potential and divergent winds (1985-2019)
c) Velocity and divergent wind trend (1950-2019)
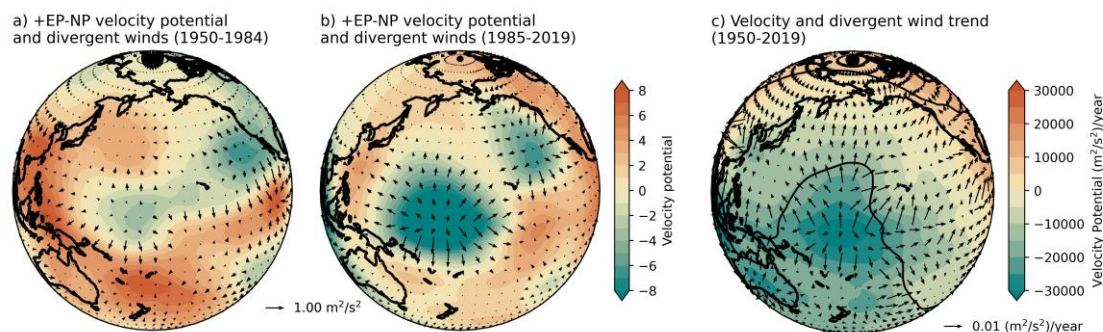
Figure 2.10. Same as Figure 2.9 but for velocity potential (shading) and divergent winds (vectors) at 250 hPa

Our analysis of reanalysis data suggests that changes in Pacific climate variability have resulted in impacts to the frequency of ECs in the North Atlantic. There remains a question of the exact forcing mechanisms for the emergence of the North Pacific wave-train, captured largely by the EP-NP pattern. Primary candidates include ocean forcing and atmospheric internal variability. Given the potential for a greater teleconnection associated with the EP-NP pattern sourced by the western tropical Pacific variability, the eqPAC and GLOB runs are useful tools for evaluating if ocean variability can account for the recent changes in atmospheric circulation. Figure 2.11 shows the composite of WAF and stream function at 250 hPa in the eqPAC and GLOB runs during positive EP-NP phases. The eqPAC simulates the recent enhancement of the wave-train over North America in association with the EP-NP, much like the pattern captured in reanalysis (Fig 9b, 7d). Since the eqPAC run includes the observed ocean temperature and salinity anomalies only in the tropical Pacific, this result highlights that the tropical Pacific forcing is a significant driver of the EP-NP pattern in the recent period. The magnitude of the EP-NP-like wave-train anomalies became much stronger in the GLOB run for the recent period (Fig 2.11d), indicating that the recent EP-NP pattern is also reinforced by

other ocean sources, such as the North Pacific (Newman et al., 2016) and the Atlantic (Cai et al., 2019; Johnson et al., 2020).

In the early period, however, the model simulated atmospheric teleconnections in the eqPAC and GLOB runs show a different pattern compared to the reanalysis results, particularly over North America (Fig 2.8c, 2.11a and 2.11c). Whereas the negative stream function anomalies emerge in the North Pacific in both the reanalysis product and the model simulations, their model simulated anomalies extend further eastward into the central US. Moreover, the eqPAC and GLOB runs simulate positive circulation anomalies stretching from Alaska to eastern Canada (Fig 2.11a and 2.11c), which contrasts with the positive anomalies limited over the Alaska/western Canada in ERA5 (Fig 2.8c). The discrepancies in the early period highlight that forcings other than ocean variability were previously more important for the EP-NP pattern. In the recent period however, the accurate simulation of the EP-NP by the GLOB and eqPAC runs show that the role of ocean variability has become more important.

a) +EP-NP composite WAF & ψ
eqPAC (1950-1984)

n=7

b) +EP-NP composite WAF & ψ
eqPAC (1985-2020)

n=8

$\longrightarrow$ 2 m²/s²

Stream function anomalies ψ'/(10⁶ m²/s)

c) +EP-NP composite WAF & ψ
GLOB (1950-1984)

n=7

d) +EP-NP composite WAF & ψ
GLOB (1985-2020)

n=8

$\longrightarrow$ 2 m²/s²

Stream function anomalies ψ'/(10⁶ m²/s)
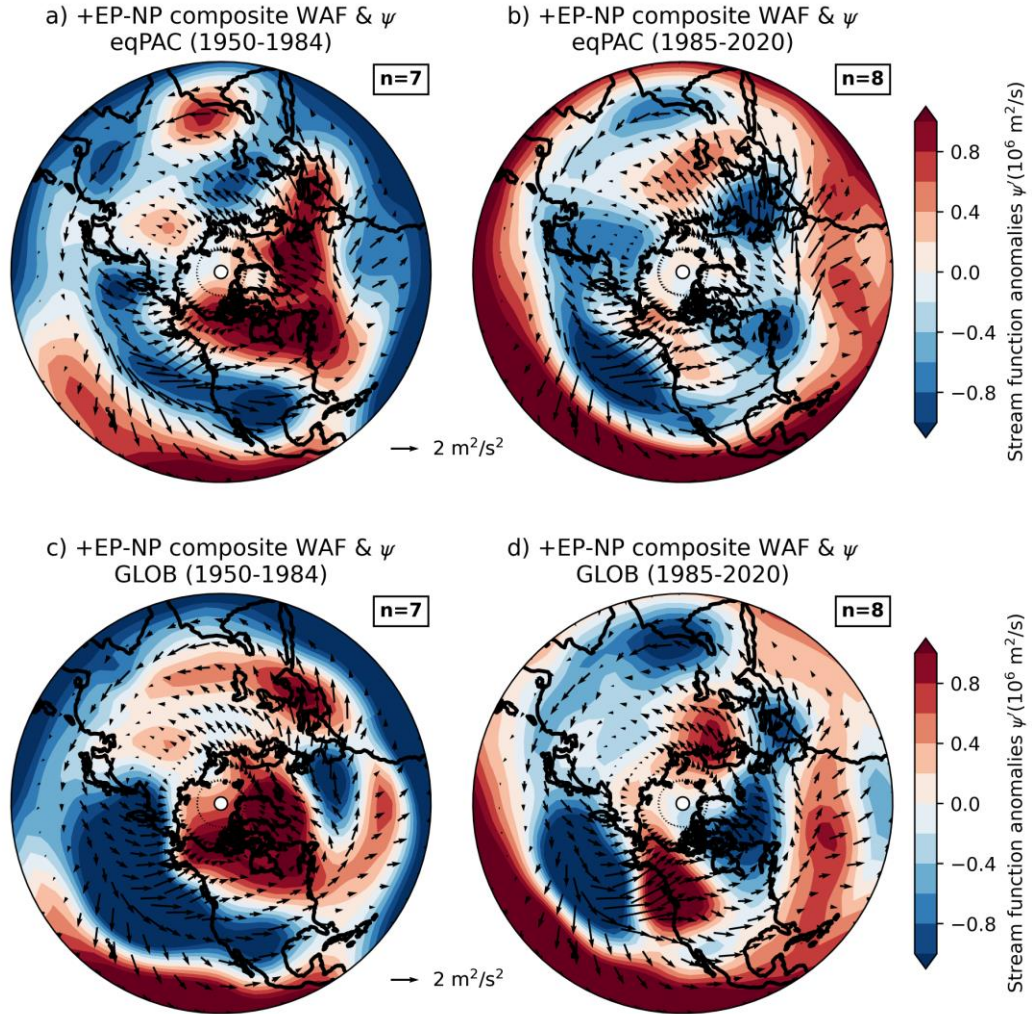
Figure 2.11. Composite maps of 250 hPa stream function (contour fill) and the WAF (vectors) for the positive EP-NP phase in (a,b) the eqPAC and the GLOB (c,d) runs for the early period (left) and the recent period (right panels).

We also provide composites of U_{250} and Z_{250} anomalies for the positive phase of the EP-NP index in the early and recent periods in the eqPAC and GLOB simulations (Figure 2.12). The eqPAC run depicts the EP-NP-like wave-train pattern of Z_{250} anomalies for the recent period (Figure 2.12a,b). We find the similar but more amplified wave train pattern of Z_{250} anomalies in the GLOB run compared to the eqPAC run (Figure 2.12c and d). As a result of wave propagation, the negative and positive Z_{250}

anomalies appear over the eastern North America and the North Atlantic for the recent period (Fig. 2.12b and d) although these features are unclear in the early period (Figure 2.12a,c). These pressure anomalies affect the jet stream position and contributes to coastal EC frequency through upper tropospheric dynamics (discussed more later). Our model experiments also support that recent variability in coastal EC frequency is modulated by the EP-NP pattern, which is captured by tropical Pacific Ocean forcing and well simulated by global ocean forcing.
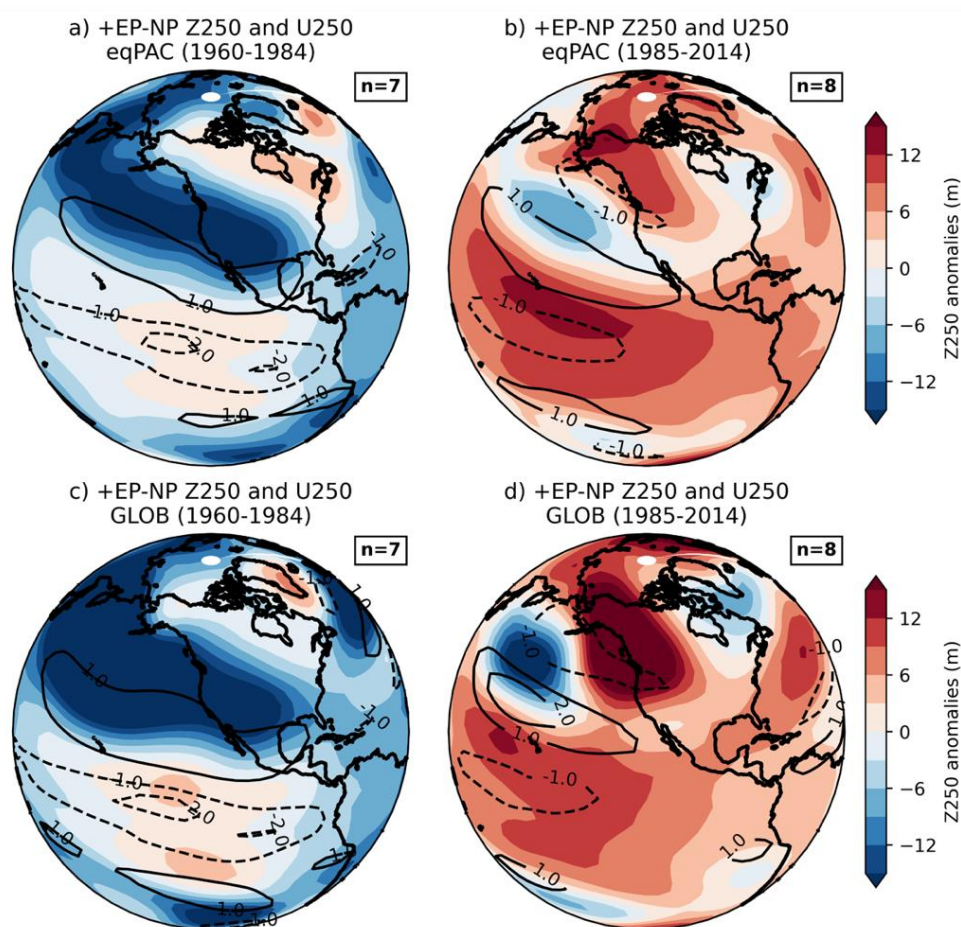
Figure 2.12. Composite maps of Z_{250} (contour fill) and U_{250} anomalies (contour line) for the positive EP-NP phases in (a,b) the eqPAC and (c,d) the GLOB runs for the early (left) and the recent periods (right panels).

2.7   Discussion

Our results show that the tropical Pacific can remotely affect coastal ECs through an atmospheric teleconnection over North America. Other case studies have described the processes involved in this cyclogenesis "teleconnection", generally showing that upstream perturbations result in adjacent eddy formation and eventually strong baroclinic energy conversion downstream which manifests in cyclogenesis (Chang, 1993; Orlanski & Sheldon, 1995). During this process, upper-level cyclogenesis mechanisms are the most important and the resulting storms generally fit into the category of Type-B cyclones described by Petterssen & Smebye (1971), and Deveson et al. (2002). These storms are classified as Type-B because they gain energy and instability mainly from the jet-stream region. In the early 2000s these type-B cyclones and upper-level cyclogenesis were found to be the dominant "flavor" of cyclones in the western North Atlantic (Gray & Dacre, 2006), generally supported by our work. However, an important caveat suggested by our work is that the dominant cyclone types and cyclogenesis mechanisms may change over longer analysis periods in conjunction with teleconnections.

Our study showed that coastal EC frequency relies on tropical Pacific and global ocean forcings for the recent decades, but the extent to which this relationship will continue to amplify, diminish or asymptote is currently unknown. The observed changes do not appear to be associated directly with ENSO, but rather with an enhanced teleconnection source in the western tropical Pacific (Fig 8). While other work has highlighted that similar ridge-trough patterns over North America can largely be explained by internal atmospheric variability, there is also evidence that ocean forcing in

the western tropical Pacific can increase the probability and amplitude of wave-train

patterns over North America (Deser et al., 2012; Teng & Branstator, 2017).

Accelerated warming in the arctic from anthropogenic climate change has also

been identified as a potential forcing for more amplified mid-latitude weather regimes (a

review on arctic mid-latitude linkages is provided by Cohen et al., 2020), but our results

highlight that the arctic forcing for coastal EC frequency may be secondary compared to

the tropics (D. L. Hartmann, 2015; McKinnon et al., 2016; Palmer, 2014). Notably, the

relationship between the AO index with coastal and high-latitude EC frequency is

increasing for ECs tracked in ERA5 (Fig. 3d and Fig. S1), but there is observational

uncertainty due to the spread between the three reanalysis datasets used in this study. In

contrast, NCEP R1, JRA and ERA5 coastal EC frequency agree upon the growing

relationship with the EP-NP index. Some observational uncertainty remains as objective

tracking has been shown to occasionally pick up "artificial" explosive systems (Allen et

al., 2010a), but the strong agreement between the three reanalysis datasets supports the

role of the EP-NP pattern.

The EP-NP spatial pattern in winter bears resemblance to the North American

Winter Dipole (Singh et al., 2016; Wang et al., 2015) and to the Pacific-North America

Pattern but correlations of these indices with the coastal ECs frequency are insignificant

(not shown). Because the EP-NP pattern has been characterized as a fall or spring pattern

rather than a winter pattern, the impact of EP-NP on North American extreme events may

have received less attention compared to those teleconnection patterns. Nevertheless,

notable changes have been reported in the leading empirical orthogonal function (EOF)

of wintertime geopotential height for November through January, which more closely

resembles the EP-NP and the North American Winter Dipole patterns (Chien et al.,

2019). Consistent with Chien et al., (2019), these two patterns have more become

strongly correlated for November through March (Figure 2.13).
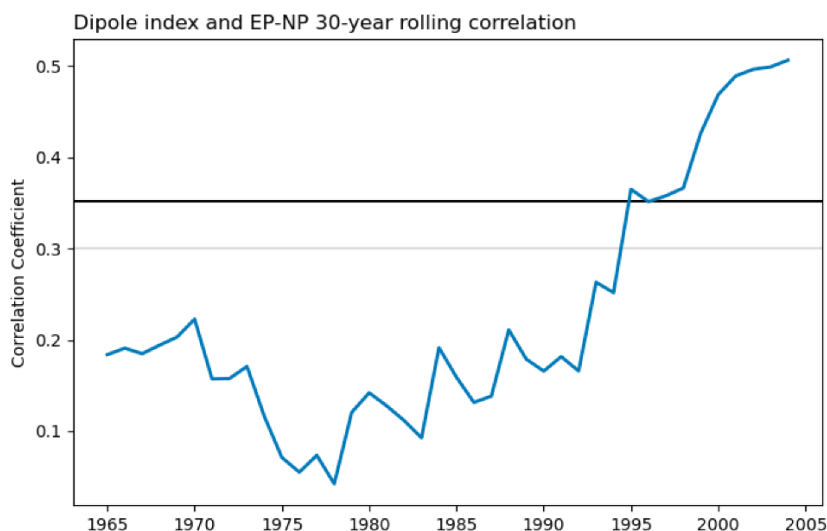
Figure 2.13. November through March "dipole-index" 30-year rolling correlation with the EP-NP index. The dipole index is calculated following Wang et al. (2015) by subtracting the monthly Z300 values between the ridge center (232.5-237.5°E & 47.5-52.5°N) from the trough center (282.5-287.5°E and 57.5-62.5°N) in NCEP R1. The horizontal black and gray lines indicate the 95% and 90% confidence intervals for 28 degrees of freedom.

Previous literature pointed out the increasing influence of the EP-NP on

temperature variability in the United States (Schulte & Lee, 2017) and the growing

impact of the zonal dipole of atmospheric pressure anomalies over North America (Singh

et al., 2016; Stuivenvolt-Allen & Wang, 2019; Wang et al., 2015, 2017). Our research

highlighted that the EP-NP pattern during the recent winter affects not only the large-

scale atmospheric circulations as described by the previous studies but also extreme

weather events, such as the coastal EC frequency. Therefore, our result suggests that

accurate seasonal forecast of EP-NP index would be crucial to mitigate damages from

severe winter storms in the east coast of North America.

2.8   Conclusions:

This study focuses on identifying the sources of interannual variability associated with EC frequency in the North Atlantic and determining the role of Pacific forcing in modulating EC frequency. Applying the EC tracking method to the reanalysis datasets, we found two independent modes of interannual variability for coastal and high-latitude EC frequency. The variances of EC frequency show noticeable increasing trends for the 1950-2020 period. Whereas the high-latitude EC frequency highly correlates with the NAO and the AO indices for the entire analysis period, the coastal EC frequency significantly correlates with the EP-NP index only for the recent decades. Coastal EC frequency during the last three decades exhibits a much stronger link to Pacific sourced climate variability – namely the atmospheric wave-train best characterized by the EP-NP teleconnection. Based on the observational data analysis, we found that the recent interannual variability of the EP-NP index is strongly linked to cyclogenesis mechanisms near the east coast of North America; Upper-level divergence, jet stream activity, and more organized regions of temperature advection, have all contributed to a greater association of the EP-NP pattern and coastal EC frequency. Our model experiments indicate that the equatorial Pacific Ocean and global ocean forcings are the main driver for the recent amplification regarding the EP-NP impacts on the coastal ECs frequency.

REFERENCES

Alexander, M. A., Bladé, I., Newman, M., Lanzante, J. R., Lau, N.-C., & Scott, J. D. (2002). The Atmospheric Bridge: The Influence of ENSO Teleconnections on Air–Sea Interaction over the Global Oceans. Journal of Climate, 15(16), 2205–2231. https://doi.org/10.1175/1520-0442(2002)015<2205:TABTIO>2.0.CO;2

Allen, J. T., Pezza, A. B., & Black, M. T. (2010a). Explosive Cyclogenesis: A Global Climatology Comparing Multiple Reanalyses. Journal of Climate, 23(24), 6468–6484. https://doi.org/10.1175/2010JCLI3437.1

Allen, J. T., Pezza, A. B., & Black, M. T. (2010b). Explosive Cyclogenesis: A Global Climatology Comparing Multiple Reanalyses. Journal of Climate, 23(24), 6468–6484. https://doi.org/10.1175/2010JCLI3437.1

Baehr, C., Pouponneau, B., Ayrault, F., & Joly, A. (1999). Dynamical Characterization of the FASTEX cyclogenesis cases. Quarterly Journal of the Royal Meteorological Society, 125(561), 3469–3494. https://doi.org/10.1002/qj.49712556117

Balmaseda, M. A., Mogensen, K., & Weaver, A. T. (2013). Evaluation of the ECMWF ocean reanalysis system ORAS4. Quarterly Journal of the Royal Meteorological Society, 139(674), 1132–1161. https://doi.org/10.1002/qj.2063

Benestad, R. E., & Chen, D. (2006). The use of a calculus-based cyclone identification method for generating storm statistics. Tellus A, 58(4), 473–486. https://doi.org/10.1111/j.1600-0870.2006.00191.x

Blender, R., Fraedrich, K., & Lunkeit, F. (1997). Identification of cyclone-track regimes in the North Atlantic. Quarterly Journal of the Royal Meteorological Society, 123(539), 727–741. https://doi.org/10.1002/qj.49712353910

Bloom, S. C., Takacs, L. L., Silva, A. M. da, & Ledvina, D. (1996). Data Assimilation Using Incremental Analysis Updates. Monthly Weather Review, 124(6), 1256–1271. https://doi.org/10.1175/1520-0493(1996)124<1256:DAUIAU>2.0.CO;2

Boer, G. J., Smith, D. M., Cassou, C., Doblas-Reyes, F., Danabasoglu, G., Kirtman, B., Kushnir, Y., Kimoto, M., Meehl, G. A., Msadek, R., Mueller, W. A., Taylor, K. E., Zwiers, F., Rixen, M., Ruprich-Robert, Y., & Eade, R. (2016). The Decadal Climate Prediction Project (DCPP) contribution to CMIP6. Geoscientific Model Development, 9(10), 3751–3777. https://doi.org/10.5194/gmd-9-3751-2016

Bosart, L. F. (1981). The Presidents' Day Snowstorm of 18–19 February 1979: A Subsynoptic-Scale Event. Monthly Weather Review, 109(7), 1542–1566. https://doi.org/10.1175/1520-0493(1981)109<1542:TPDSOF>2.0.CO;2

Bosart, L. F., & Lin, S. C. (1984). A Diagnostic Analysis of the Presidents' Day Storm Of February 1979. Monthly Weather Review, 112(11), 2148–2177. https://doi.org/10.1175/1520-0493(1984)112<2148:ADAOTP>2.0.CO;2

Branstator, G. (2014). Long-Lived Response of the Midlatitude Circulation and Storm Tracks to Pulses of Tropical Heating. Journal of Climate, 27(23), 8809–8826. https://doi.org/10.1175/JCLI-D-14-00312.1

Cai, W., Wu, L., Lengaigne, M., Li, T., McGregor, S., Kug, J.-S., Yu, J.-Y., Stuecker, M. F., Santoso, A., Li, X., Ham, Y.-G., Chikamoto, Y., Ng, B., McPhaden, M. J., Du, Y., Dommenget, D., Jia, F., Kajtar, J. B., Keenlyside, N., … Chang, P. (2019). Pantropical climate interactions. Science, 363(6430), eaav4236. https://doi.org/10.1126/science.aav4236

Chang, E. K. M. (1993). Downstream Development of Baroclinic Waves As Inferred from Regression Analysis. Journal of the Atmospheric Sciences, 50(13), 2038–2053. https://doi.org/10.1175/1520-0469(1993)050<2038:DDOBWA>2.0.CO;2

Chartrand, J., & Pausata, F. S. R. (2020). Impacts of the North Atlantic Oscillation on winter precipitations and storm track variability in southeast Canada and the northeast United States. Weather and Climate Dynamics, 1(2), 731–744. https://doi.org/10.5194/wcd-1-731-2020

Chikamoto, Y., Mochizuki, T., Timmermann, A., Kimoto, M., & Watanabe, M. (2016). Potential tropical Atlantic impacts on Pacific decadal climate trends. Geophysical Research Letters, 43(13), 7143–7151. https://doi.org/10.1002/2016GL069544

Chikamoto, Y., Timmermann, A., Luo, J.-J., Mochizuki, T., Kimoto, M., Watanabe, M., Ishii, M., Xie, S.-P., & Jin, F.-F. (2015). Skilful multi-year predictions of tropical trans-basin climate variability. Nature Communications, 6(1), 6869. https://doi.org/10.1038/ncomms7869

Chikamoto, Y., Timmermann, A., Widlansky, M. J., Zhang, S., & Balmaseda, M. A. (2019). A Drift-Free Decadal Climate Prediction System for the Community Earth System Model. Journal of Climate, 32(18), 5967–5995. https://doi.org/10.1175/JCLI-D-18-0788.1

Ciasto, L. M., Li, C., Wettstein, J. J., & Kvamstø, N. G. (2016). North Atlantic Storm-Track Sensitivity to Projected Sea Surface Temperature: Local versus Remote Influences. Journal of Climate, 29(19), 6973–6991. https://doi.org/10.1175/JCLI-D-15-0860.1

Cohen, J., Zhang, X., Francis, J., Jung, T., Kwok, R., Overland, J., Ballinger, T. J., Bhatt, U. S., Chen, H. W., Coumou, D., Feldstein, S., Gu, H., Handorf, D., Henderson, G., Ionita, M., Kretschmer, M., Laliberte, F., Lee, S., Linderholm, H. W., … Yoon, J. (2020). Divergent consensuses on Arctic amplification influence on midlatitude severe winter weather. Nature Climate Change, 10(1), 20–29. https://doi.org/10.1038/s41558-019-0662-y

Colucci, S. J. (1985). Explosive Cyclogenesis and Large-Scale Circulation Changes: Implications for Atmospheric Blocking. Journal of the Atmospheric Sciences, 42(24), 2701–2717. https://doi.org/10.1175/1520-0469(1985)042<2701:ECALSC>2.0.CO;2

Deser, C., Phillips, A., Bourdette, V., & Teng, H. (2012). Uncertainty in climate change projections: The role of internal variability. Climate Dynamics, 38(3), 527–546. https://doi.org/10.1007/s00382-010-0977-x

Deveson, A. C. L., Browning, K. A., & Hewson, T. D. (2002). A classification of FASTEX cyclones using a height-attributable quasi-geostrophic vertical-motion

diagnostic. Quarterly Journal of the Royal Meteorological Society, 128(579), 93–117. https://doi.org/10.1256/00359000260498806

Eady, E. T. (1949). Long Waves and Cyclone Waves. Tellus, 1(3), 33–52. https://doi.org/10.1111/j.2153-3490.1949.tb01265.x

Ebita, A., Kobayashi, S., Ota, Y., Moriya, M., Kumabe, R., Onogi, K., Harada, Y., Yasui, S., Miyaoka, K., Takahashi, K., Kamahori, H., Kobayashi, C., Endo, H., Soma, M., Oikawa, Y., & Ishimizu, T. (2011). The Japanese 55-year Reanalysis "JRA-55": An Interim Report. Sola, 7, 149–152. https://doi.org/10.2151/sola.2011-038

Fosu, B., He, J., & Liguori, G. (2020). Equatorial Pacific Warming Attenuated by SST Warming Patterns in the Tropical Atlantic and Indian Oceans. Geophysical Research Letters, 47(18), e2020GL088231. https://doi.org/10.1029/2020GL088231

Gall, R. (1976). The Effects of Released Latent Heat in Growing Baroclinic Waves. Journal of the Atmospheric Sciences, 33(9), 1686–1701. https://doi.org/10.1175/1520-0469(1976)033<1686:TEORLH>2.0.CO;2

Gómara, I., Pinto, J. G., Woollings, T., Masato, G., Zurita-Gotor, P., & Rodríguez-Fonseca, B. (2014). Rossby wave-breaking analysis of explosive cyclones in the Euro-Atlantic sector. Quarterly Journal of the Royal Meteorological Society, 140(680), 738–753. https://doi.org/10.1002/qj.2190

Gómara, I., Rodríguez-Fonseca, B., Zurita-Gotor, P., Ulbrich, S., & Pinto, J. G. (2016). Abrupt transitions in the NAO control of explosive North Atlantic cyclone development. Climate Dynamics, 47(9), 3091–3111. https://doi.org/10.1007/s00382-016-3015-9

Gray, S. L., & Dacre, H. F. (2006). Classifying dynamical forcing mechanisms using a climatology of extratropical cyclones. Quarterly Journal of the Royal Meteorological Society, 132(617), 1119–1137. https://doi.org/10.1256/qj.05.69

Gyakum, J. R. (1983). On the Evolution of the QE II Storm. II: Dynamic and Thermodynamic Structure. Monthly Weather Review, 111(6), 1156–1173. https://doi.org/10.1175/1520-0493(1983)111<1156:OTEOTI>2.0.CO;2

Hall, R., Erdélyi, R., Hanna, E., Jones, J. M., & Scaife, A. A. (2015). Drivers of North Atlantic Polar Front jet stream variability. International Journal of Climatology, 35(8), 1697–1720. https://doi.org/10.1002/joc.4121

Ham, Y.-G., Chikamoto, Y., Kug, J.-S., Kimoto, M., & Mochizuki, T. (2017). Tropical Atlantic-Korea teleconnection pattern during boreal summer season. Climate Dynamics, 49(7), 2649–2664. https://doi.org/10.1007/s00382-016-3474-z

Hanley, J., & Caballero, R. (2012). Objective identification and tracking of multicentre cyclones in the ERA-Interim reanalysis dataset. Quarterly Journal of the Royal Meteorological Society, 138(664), 612–625. https://doi.org/10.1002/qj.948

Hartmann, D. L. (2015). Pacific sea surface temperature and the winter of 2014. Geophysical Research Letters, 42(6), 1894–1902. https://doi.org/10.1002/2015GL063083

Held, I. M., Lyons, S. W., & Nigam, S. (1989). Transients and the Extratropical Response to El Niño. Journal of the Atmospheric Sciences, 46(1), 163–174. https://doi.org/10.1175/1520-0469(1989)046<0163:TATERT>2.0.CO;2

Held, I. M., Ting, M., & Wang, H. (2002). Northern Winter Stationary Waves: Theory and Modeling. Journal of Climate, 15(16), 2125–2144. https://doi.org/10.1175/1520-0442(2002)015<2125:NWSWTA>2.0.CO;2

Hersbach, H., Bell, B., Berrisford, P., Hirahara, S., Horányi, A., Muñoz-Sabater, J., Nicolas, J., Peubey, C., Radu, R., Schepers, D., Simmons, A., Soci, C., Abdalla, S., Abellan, X., Balsamo, G., Bechtold, P., Biavati, G., Bidlot, J., Bonavita, M., … Thépaut, J.-N. (2020). The ERA5 global reanalysis. Quarterly Journal of the Royal Meteorological Society, 146(730), 1999–2049. https://doi.org/10.1002/qj.3803

Hodges, K. I., Hoskins, B. J., Boyle, J., & Thorncroft, C. (2003). A Comparison of Recent Reanalysis Datasets Using Objective Feature Tracking: Storm Tracks and Tropical Easterly Waves. Monthly Weather Review, 131(9), 2012–2037. https://doi.org/10.1175/1520-0493(2003)131<2012:ACORRD>2.0.CO;2

Hodges, K. I., Lee, R. W., & Bengtsson, L. (2011). A Comparison of Extratropical Cyclones in Recent Reanalyses ERA-Interim, NASA MERRA, NCEP CFSR, and JRA-25. Journal of Climate, 24(18), 4888–4906. https://doi.org/10.1175/2011JCLI4097.1

Hoskins, B. J., & Ambrizzi, T. (1993). Rossby Wave Propagation on a Realistic Longitudinally Varying Flow. Journal of the Atmospheric Sciences, 50(12), 1661–1671. https://doi.org/10.1175/1520-0469(1993)050<1661:RWPOAR>2.0.CO;2

Hoskins, B. J., & Hodges, K. I. (2002a). New Perspectives on the Northern Hemisphere Winter Storm Tracks. Journal of the Atmospheric Sciences, 59(6), 1041–1061. https://doi.org/10.1175/1520-0469(2002)059<1041:NPOTNH>2.0.CO;2

Hoskins, B. J., & Hodges, K. I. (2002b). New Perspectives on the Northern Hemisphere Winter Storm Tracks. Journal of the Atmospheric Sciences, 59(6), 1041–1061. https://doi.org/10.1175/1520-0469(2002)059<1041:NPOTNH>2.0.CO;2

Hoskins, B. J., & Karoly, D. J. (1981). The Steady Linear Response of a Spherical Atmosphere to Thermal and Orographic Forcing. Journal of the Atmospheric Sciences, 38(6), 1179–1196. https://doi.org/10.1175/1520-0469(1981)038<1179:TSLROA>2.0.CO;2

Huang, B., Kinter, J. L., & Schopf, P. S. (2002). Ocean data assimilation using intermittent analyses and continuous model error correction. Advances in Atmospheric Sciences, 19(6), 965–992. https://doi.org/10.1007/s00376-002-0059-z

Johnson, Z. F., Chikamoto, Y., Wang, S.-Y. S., McPhaden, M. J., & Mochizuki, T. (2020). Pacific decadal oscillation remotely forced by the equatorial Pacific and the Atlantic Oceans. Climate Dynamics, 55(3), 789–811. https://doi.org/10.1007/s00382-020-05295-2

Jung, T., Gulev, S. K., Rudeva, I., & Soloviov, V. (2006). Sensitivity of extratropical cyclone characteristics to horizontal resolution in the ECMWF model. Quarterly Journal of the Royal Meteorological Society, 132(619), 1839–1857. https://doi.org/10.1256/qj.05.212

Kalnay, E., Kanamitsu, M., Kistler, R., Collins, W., Deaven, D., Gandin, L., Iredell, M., Saha, S., White, G., Woollen, J., Zhu, Y., Chelliah, M., Ebisuzaki, W., Higgins, W., Janowiak, J., Mo, K. C., Ropelewski, C., Wang, J., Leetmaa, A., … Joseph, D. (1996). The NCEP/NCAR 40-Year Reanalysis Project. Bulletin of the American Meteorological Society, 77(3), 437–472. https://doi.org/10.1175/1520-0477(1996)077<0437:TNYRP>2.0.CO;2

Konrad, C. E., & Colucci, S. J. (1988). Synoptic Climatology of 500 mb Circulation Changes during Explosive Cyclogenesis. Monthly Weather Review, 116(7), 1431–1443. https://doi.org/10.1175/1520-0493(1988)116<1431:SCOMCC>2.0.CO;2

Kosaka, Y., & Xie, S.-P. (2016). The tropical Pacific as a key pacemaker of the variable rates of global warming. Nature Geoscience, 9(9), 669–673. https://doi.org/10.1038/ngeo2770

Kuwano-Yoshida, A., & Asuma, Y. (2008). Numerical Study of Explosively Developing Extratropical Cyclones in the Northwestern Pacific Region. Monthly Weather Review, 136(2), 712–740. https://doi.org/10.1175/2007MWR2111.1

Lau, N.-C., & Nath, M. J. (1996). The Role of the "Atmospheric Bridge" in Linking Tropical Pacific ENSO Events to Extratropical SST Anomalies. Journal of Climate, 9(9), 2036–2057. https://doi.org/10.1175/1520-0442(1996)009<2036:TROTBI>2.0.CO;2

LeComte, D. (2019). U.S. Weather Highlights 2018: Another Historic Hurricane and Wildfire Season. Weatherwise, 72(3), 12–23. https://doi.org/10.1080/00431672.2019.1586492

Lindzen, R. S., & Farrell, B. (1980). A Simple Approximate Result for the Maximum Growth Rate of Baroclinic Instabilities. Journal of the Atmospheric Sciences, 37(7), 1648–1654. https://doi.org/10.1175/1520-0469(1980)037<1648:ASARFT>2.0.CO;2

Macdonald, B. C., & Reiter, E. R. (1988). Explosive Cyclogenesis over the Eastern United States. Monthly Weather Review, 116(8), 1568–1586. https://doi.org/10.1175/1520-0493(1988)116<1568:ECOTEU>2.0.CO;2

May, W., & Bengtsson, L. (1998). The signature of ENSO in the Northern Hemisphere midlatitude seasonal mean flow and high-frequency intraseasonal variability. Meteorology and Atmospheric Physics, 69(1), 81–100. https://doi.org/10.1007/BF01025185

McKinnon, K. A., Rhines, A., Tingley, M. P., & Huybers, P. (2016). Long-lead predictions of eastern United States hot days from Pacific sea surface temperatures. Nature Geoscience, 9(5), 389–394. https://doi.org/10.1038/ngeo2687

Miller, J. E. (1946). CYCLOGENESIS IN THE ATLANTIC COASTAL REGION OF THE UNITED STATES. Journal of the Atmospheric Sciences, 3(2), 31–44. https://doi.org/10.1175/1520-0469(1946)003<0031:CITACR>2.0.CO;2

Minobe, S., Kuwano-Yoshida, A., Komori, N., Xie, S.-P., & Small, R. J. (2008). Influence of the Gulf Stream on the troposphere. Nature, 452(7184), 206–209. https://doi.org/10.1038/nature06690

Neu, U., Akperov, M. G., Bellenbaum, N., Benestad, R., Blender, R., Caballero, R., Cocozza, A., Dacre, H. F., Feng, Y., Fraedrich, K., Grieger, J., Gulev, S., Hanley, J., Hewson, T., Inatsu, M., Keay, K., Kew, S. F., Kindem, I., Leckebusch, G. C., … Wernli, H. (2012). IMILAST: A Community Effort to Intercompare Extratropical Cyclone Detection and Tracking Algorithms. Bulletin of the American Meteorological Society, 94(4), 529–547. https://doi.org/10.1175/BAMS-D-11-00154.1

Newman, M., Alexander, M. A., Ault, T. R., Cobb, K. M., Deser, C., Di Lorenzo, E., Mantua, N. J., Miller, A. J., Minobe, S., Nakamura, H., Schneider, N., Vimont, D. J., Phillips, A. S., Scott, J. D., & Smith, C. A. (2016). The Pacific Decadal Oscillation, Revisited. Journal of Climate, 29(12), 4399–4427. https://doi.org/10.1175/JCLI-D-15-0508.1

Orlanski, I., & Sheldon, J. P. (1995). Stages in the energetics of baroclinic systems. Tellus A, 47(5), 605–628. https://doi.org/10.1034/j.1600-0870.1995.00108.x

Palmer, T. (2014). Record-breaking winters and global climate change. Science, 344(6186), 803–804. https://doi.org/10.1126/science.1255147

Petterssen, S., & Smebye, S. J. (1971). On the development of extratropical cyclones. Quarterly Journal of the Royal Meteorological Society, 97(414), 457–482. https://doi.org/10.1002/qj.49709741407

Pinto, J. G., Zacharias, S., Fink, A. H., Leckebusch, G. C., & Ulbrich, U. (2009). Factors contributing to the development of extreme North Atlantic cyclones and their relationship with the NAO. Climate Dynamics, 32(5), 711–737. https://doi.org/10.1007/s00382-008-0396-4

Purich, A., England, M. H., Cai, W., Chikamoto, Y., Timmermann, A., Fyfe, J. C., Frankcombe, L., Meehl, G. A., & Arblaster, J. M. (2016). Tropical Pacific SST Drivers of Recent Antarctic Sea Ice Trends. Journal of Climate, 29(24), 8931–8948. https://doi.org/10.1175/JCLI-D-16-0440.1

Raible, C. C., Della-Marta, P. M., Schwierz, C., Wernli, H., & Blender, R. (2008). Northern Hemisphere Extratropical Cyclones: A Comparison of Detection and Tracking Methods and Different Reanalyses. Monthly Weather Review, 136(3), 880–897. https://doi.org/10.1175/2007MWR2143.1

Reale, M., Liberato, M. L. R., Lionello, P., Pinto, J. G., Salon, S., & Ulbrich, S. (2019). A Global Climatology of Explosive Cyclones using a Multi-Tracking Approach. Tellus A: Dynamic Meteorology and Oceanography, 71(1), 1611340. https://doi.org/10.1080/16000870.2019.1611340

Rogers, E., & Bosart, L. F. (1986). An Investigation of Explosively Deepening Oceanic Cyclones. Monthly Weather Review, 114(4), 702–718. https://doi.org/10.1175/1520-0493(1986)114<0702:AIOEDO>2.0.CO;2

Rudeva, I., & Gulev, S. K. (2011). Composite Analysis of North Atlantic Extratropical Cyclones in NCEP–NCAR Reanalysis Data. Monthly Weather Review, 139(5), 1419–1446. https://doi.org/10.1175/2010MWR3294.1

Sanders, F. (1986). Explosive Cyclogenesis in the West-Central North Atlantic Ocean, 1981–84. Part I: Composite Structure and Mean Behavior. Monthly Weather Review, 114(10), 1781–1794. https://doi.org/10.1175/1520-0493(1986)114<1781:ECITWC>2.0.CO;2

Sanders, F., & Davis, C. A. (1988). Patterns of Thickness Anomaly for Explosive Cyclogenesis over the West-Central North Atlantic Ocean. Monthly Weather Review, 116(12), 2725–2730. https://doi.org/10.1175/1520-0493(1988)116<2725:POTAFE>2.0.CO;2

Sanders, F., & Gyakum, J. R. (1980). Synoptic-Dynamic Climatology of the "Bomb." Monthly Weather Review, 108(10), 1589–1606. https://doi.org/10.1175/1520-0493(1980)108<1589:SDCOT>2.0.CO;2

Schemm, S., Rivière, G., Ciasto, L. M., & Li, C. (2018). Extratropical Cyclogenesis Changes in Connection with Tropospheric ENSO Teleconnections to the North Atlantic: Role of Stationary and Transient Waves. Journal of the Atmospheric Sciences, 75(11), 3943–3964. https://doi.org/10.1175/JAS-D-17-0340.1

Schulte, J. A., & Lee, S. (2017). Strengthening North Pacific Influences on United States Temperature Variability. Scientific Reports, 7(1). https://doi.org/10.1038/s41598-017-00175-y

Silberberg, S. R., & Bosart, L. F. (1982). An Analysis of Systematic Cyclone Errors in the NMC LFM-II Model During the 1978–79 Cool Season. Monthly Weather Review, 110(4), 254–271. https://doi.org/10.1175/1520-0493(1982)110<0254:AAOSCE>2.0.CO;2

Singh, D., Swain, D. L., Mankin, J. S., Horton, D. E., Thomas, L. N., Rajaratnam, B., & Diffenbaugh, N. S. (2016). Recent amplification of the North American winter temperature dipole. Journal of Geophysical Research: Atmospheres, 121(17), 9911–9928. https://doi.org/10.1002/2016JD025116

Stuivenvolt-Allen, J., & Wang, S. S.-Y. (2019). Data Mining Climate Variability as an Indicator of U.S. Natural Gas. Frontiers in Big Data, 2. https://doi.org/10.3389/fdata.2019.00020

Stuivenvolt-Allen, J., Wang, S.-Y. S., Johnson, Z., & Chikamoto, Y. (2021). Atmospheric Rivers Impacting Northern California Exhibit a Quasi-Decadal Frequency. Journal of Geophysical Research: Atmospheres, 126(15), e2020JD034196. https://doi.org/10.1029/2020JD034196

Takaya, K., & Nakamura, H. (2001). A Formulation of a Phase-Independent Wave-Activity Flux for Stationary and Migratory Quasigeostrophic Eddies on a Zonally

Varying Basic Flow. Journal of the Atmospheric Sciences, 58(6), 608–627. https://doi.org/10.1175/1520-0469(2001)058<0608:AFOAPI>2.0.CO;2

Teng, H., & Branstator, G. (2017). Causes of Extreme Ridges That Induce California Droughts. Journal of Climate, 30(4), 1477–1492. https://doi.org/10.1175/JCLI-D-16-0524.1

Trigo, I. F. (2006). Climatology and interannual variability of storm-tracks in the Euro-Atlantic sector: A comparison between ERA-40 and NCEP/NCAR reanalyses. Climate Dynamics, 26(2), 127–143.

Uccellini, L. W. (1990). Processes Contributing to the Rapid Development of Extratropical Cyclones. In C. W. Newton & E. O. Holopainen (Eds.), Extratropical Cyclones: The Erik Palmén Memorial Volume (pp. 81–105). American Meteorological Society. https://doi.org/10.1007/978-1-944970-33-8_6

Uccellini, L. W., & Johnson, D. R. (1979). The Coupling of Upper and Lower Tropospheric Jet Streaks and Implications for the Development of Severe Convective Storms. Monthly Weather Review, 107(6), 682–703. https://doi.org/10.1175/1520-0493(1979)107<0682:TCOUAL>2.0.CO;2

Ulbrich, U., Fink, A. H., Klawa, M., & Pinto, J. G. (2001). Three extreme storms over Europe in December 1999. Weather, 56(3), 70–80. https://doi.org/10.1002/j.1477-8696.2001.tb06540.x

Ulbrich, U., Leckebusch, G. C., & Pinto, J. G. (2009). Extra-tropical cyclones in the present and future climate: A review. Theoretical and Applied Climatology, 96(1), 117–131. https://doi.org/10.1007/s00704-008-0083-8

Walker, E., Mitchell, D., & Seviour, W. (2020). The numerous approaches to tracking extratropical cyclones and the challenges they present. Weather, 75(11), 336–341. https://doi.org/10.1002/wea.3861

Wallace, J. M., & Hobbs, P. V. (2006). Atmospheric Science: An Introductory Survey. Elsevier.

Wang, C.-C., & Rogers, J. C. (2001). A Composite Study of Explosive Cyclogenesis in Different Sectors of the North Atlantic. Part I: Cyclone Structure and Evolution. Monthly Weather Review, 129(6), 1481–1499. https://doi.org/10.1175/1520-0493(2001)129<1481:ACSOEC>2.0.CO;2

Wang, S.-Y., Hipps, L., Gillies, R. R., & Yoon, J.-H. (2014). Probable causes of the abnormal ridge accompanying the 2013–2014 California drought: ENSO precursor and anthropogenic warming footprint. Geophysical Research Letters, 41(9), 3220–3226. https://doi.org/10.1002/2014GL059748

Wang, S.-Y. S., Huang, W.-R., & Yoon, J.-H. (2015). The North American winter 'dipole' and extremes activity: A CMIP5 assessment. Atmospheric Science Letters, 16(3), 338–345. https://doi.org/10.1002/asl2.565

Wang, S.-Y. S., Yoon, J.-H., Becker, E., & Gillies, R. (2017). California from drought to deluge. Nature Climate Change, 7, 465–468. https://doi.org/10.1038/nclimate3330

Wang, X. L., Feng, Y., Chan, R., & Isaac, V. (2016). Inter-comparison of extra-tropical cyclone activity in nine reanalysis datasets. Atmospheric Research, 181, 133–153. https://doi.org/10.1016/j.atmosres.2016.06.010

Wettstein, J. J., & Wallace, J. M. (2010). Observed Patterns of Month-to-Month Storm-Track Variability and Their Relationship to the Background Flow. Journal of the Atmospheric Sciences, 67(5), 1420–1437. https://doi.org/10.1175/2009JAS3194.1

Whitaker, J. S., & Davis, C. A. (1994). Cyclogenesis in a Saturated Environment. Journal of the Atmospheric Sciences, 51(6), 889–908. https://doi.org/10.1175/1520-0469(1994)051<0889:CIASE>2.0.CO;2

CHAPTER 3

ATMOSPHERIC RIVERS IMPACTING NORTHERN CALIFORNIA EXHIBIT A
QUASI-DECADAL FREQUENCY

3.1 Abstract

Periods of water surplus and deficit in Northern California follow a pronounced quasi-decadal cycle. This cycle is largely driven by the frequency of atmospheric rivers (AR), affecting the region's wet and dry periods. Our analyses demonstrate that the previously undocumented quasi-decadal cycle of AR frequency relies on moisture transport associated with the position and intensity of the Aleutian Low. In observations, the Aleutian Low is shown to covary with tropical Pacific sea surface temperature anomalies. A modeling experiment, which incorporates ocean observations from the equatorial Pacific into the fully coupled climate model, provides support that the quasi-decadal cycle of the Aleutian Low is forced by the tropical Pacific. Subsequently, the tropical Pacific modulates the wet season moisture transport towards California on decadal time scales. These results provide metrics for improving interannual-to-decadal prediction of AR activity, which drives hydrological cycles in Northern California.

3.2 Introduction

Water resources along the Pacific Coast of the United States are closely tied to the frequency and magnitude of cold-season precipitation associated with atmospheric rivers (ARs) (M. Dettinger, 2011). ARs transport large amounts of moisture from the tropics to the poles – and have been studied extensively on seasonal to annual timescales for their "drought busting" characteristics and potential flooding hazards (M. D. Dettinger, 2013; Gershunov et al., 2017; Guan et al., 2010). While the seasonal to annual variability is

important for surface hydrology a recent study in the Emerald Triangle region of

Northern California (Trinity, Mendocino and Humboldt counties, Figure 3.1a) showed

that longer scales, within a 10-to-17-year range, are the most prominent feature in the

region's surface and atmospheric moisture – stimulating interest in understanding the

source of this cycle (Morgan et al., 2021). These cycles are referred to as quasi-decadal

owing to their almost 10-year period. While the quasi-decadal cycle in atmospheric and

surface moisture was prominent in this sub-region of Northern California, one objective

of this research is to determine if the quasi-decadal cycle is a common feature for the rest

of Northern California (the area used for tracking the coastal entry of Northern California

ARs is shown in the black box on Figure 3.1b along with topography). Additionally,

because low-frequency atmospheric variability is largely affected by ocean variability,

our other objective is to evaluate the ocean's role in influencing this quasi-decadal cycle

and identify which component of the climate system maintains the quasi-decadal

variability in ARs.
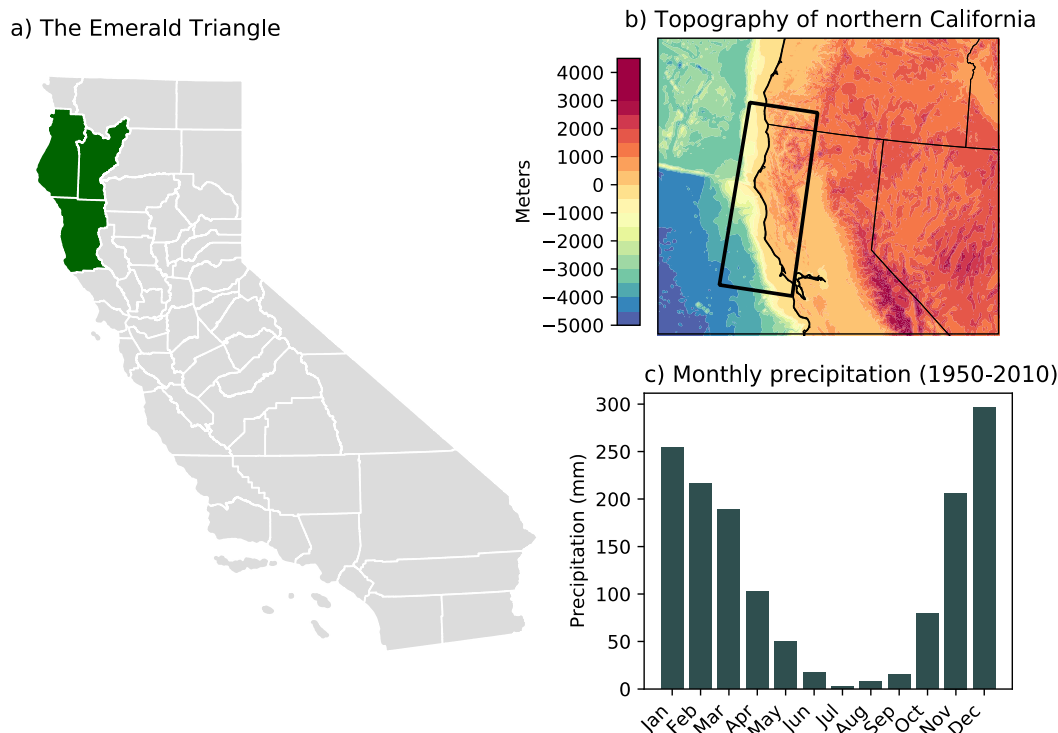
Figure 3.1. (a) County map of California with the Emerald Triangle (Humboldt, Mendocino and Trinity counties) shown in green. (b) Topographic map of Northern California with the black box indicating the area used for AR tracking. (c) Histogram of monthly precipitation from 1950 through 2020 in the boxed region from Figure 3.1b.

With a few exceptions (Gershunov et al., 2017; Guirguis et al., 2019), AR literature focuses on relatively short time scales. This can largely be explained by the short history of high-resolution climate data to analyze the frequency and characteristics of ARs and regional precipitation. These studies have highlighted three patterns of extra-tropical atmospheric circulation that affect interannual cycles of AR frequency during the wet season (November through March; Figure 3.1c): The Pacific North American (PNA) pattern, the North Pacific Oscillation (NPO), and the North American Winter Dipole (NAWD). These seasonal climate patterns can cycle between positive and negative phases, in which the location of the pressure anomalies is maintained, but the sign of the pressure anomaly is reversed. The negative phase of the PNA pattern has been associated

with enhanced AR activity in the Pacific Northwest, due to the negative pressure anomaly just offshore of the western U.S. (Guan et al., 2013; Guan & Waliser, 2015; Mundhenk et al., 2018). The NPO, characterized by a meridional pressure seesaw in the North Pacific, enhances moisture transport toward the central Pacific Coast (encompassing the Emerald Triangle region) during its negative phase (Tan et al., 2020). The last notable pattern is the NAWD, with a positive phase that is characterized by an amplified ridge over western North America and an amplified trough over the eastern part of the continent during the boreal winter (Wang et al., 2015). The NAWD strongly influences California's precipitation variability (O'Brien et al., 2019; Wang et al., 2017), but has not been studied directly with ARs and has not been studied for any cyclical behavior. Due to their known relationship with northern California precipitation and ARs, these extratropical patterns are analyzed as potential contributors to the quasi-decadal cycle.

Atmospheric cycles over long periods are heavily influenced by ocean variability (Patricola et al., 2020). Many previous studies point out that the El Niño Southern Oscillation (ENSO) impacts AR orientation, frequency, and intensity on interannual timescales (Bao et al., 2006; Guirguis et al., 2019; Higgins et al., 2000; Payne & Magnusdottir, 2014; Ryoo et al., 2013). On longer timescales, however, there is still uncertainty about the role of decadal ENSO or ENSO flavor (Timmermann et al., 2018) and how it affects AR activity (Guirguis et al., 2019; H.-M. Kim & Alexander, 2015). While the positive Pacific Decadal Oscillation (PDO) enhances AR activity for the Northeastern Pacific (Gershunov et al., 2017; X. Liu et al., 2016), its dominant cycle of 30-50 years (MacDonald & Case, 2005; Newman et al., 2016) does not compare with the quasi-decadal cycle in AR frequency over the Emerald Triangle. The last pattern of ocean

variability we analyze is the North Pacific Gyre Oscillation (NPGO) which modulates

water vapor transport to western North America and is characterized by strong decadal

variability (X. Liu et al., 2016; Lorenzo et al., 2008).

To evaluate the quasi-decadal cycle in ARs, it is important to have data with

sufficient length to account for the reduction in degrees of freedom when looking at

decadal variability. Additionally, tracking ARs requires data with a sufficient

representation of tropospheric moisture and winds to capture the features and frequency

of ARs. To satisfy these requirements, we adapted an AR tracking method from

Gershunov et al. (2017) and produced a frequency record of ARs reaching coastal

Northern California that spans more than seven decades. While a longer record of ARs is

desirable, the lack of observational data before the mid-20th century reduces the reliability

of atmospheric moisture and wind data in reanalysis (Hersbach et al., 2015; Slivinski et

al., 2019).

To identify the ocean and atmosphere's influence on the quasi-decadal cycle, we

evaluate the contributions of atmospheric teleconnection patterns and ocean variability in

the Pacific towards AR frequency during the wet season (November through the

following March). These months account for more than 80% of the region's annual

precipitation and are the most common months for landfalling ARs (Figure 3.1c)

(Guirguis et al., 2019). First, we show the relationship between ARs and the ocean in

observations. To validate the results of observations and provide potential primary

forcing mechanisms, we make use of a climate modelling experiment with the fully

coupled Community Earth System Model (CESM). Literature focused on decadal

variability and impacts to extra-tropical atmospheric circulation in the north Pacific has

often highlighted the tropical Pacific as a primary forcing (Di Lorenzo et al., 2010; Johnson et al., 2020; Rodgers et al., 2004; L. Wu et al., 2003). In particular, decadal components of ENSO variability have shown a strong relationship with precipitation and temperature variability in western North America (George & Ault, 2011). Through a three-dimensional assimilation of observed sea surface temperatures and salinity from the tropical Pacific alone, the CESM allows us to evaluate the role of the tropical Pacific in the quasi-decadal cycle and discuss the important climate features for modulating low-frequency variability in ARs for the entire Northern California region.

3.3 Data, Methods, and Modeling Experiment

3.3.1 Observational Data

Monthly precipitation (1890-2019) and soil moisture data (1948-2019) at 1° resolution were provided by the Global Precipitation Climatology Project Centre version 6.0 (Schneider et al., 2014) and the NOAA Climate Prediction Center (Fan & Dool, 2004), respectively. Streamflow data comprising the standardized average of 11 gauges within the Emerald Triangle with consistent records for at least 65 years in the United States Geological Survey (Morgan et al. 2020). Available climate indices (PNA, NPO, Niño 1+2, Niño 4, PDO, NPGO) were obtained from the NOAA Physical Science Laboratory (https://psl.noaa.gov/). The NAWD index was calculated following Wang et al. (2014a) by subtracting the area average of 300 hPa geopotential height anomalies at the center of the ridge location (132.5°-137.5°W and 47.5°N-52.5°N) from the 300 hPa geopotential height anomalies at the eastern trough center (77.5°-82.5°W and 57.5°-62.5°N). The monthly sea surface temperature (SST) data spanning 1948 to 2019 was provided by the Japanese Meteorological Agency's Centennial In-Situ Observation Based

Estimates (COBE) SST at 1° resolution (Ishii et al., 2005). Monthly and 6-hourly three-dimensional atmospheric variables, such as geopotential height (GPH), specific humidity, and horizontal winds come from the National Center for Environmental Prediction's Reanalysis (NCEP R1) from 1948 to 2019 (Kalnay et al., 1996). Results in NCEP R1 are compared with the Japanese Meteorological Agency's reanalysis (JRA-55) at 1.25°x 1.25° resolution (Ebita et al., 2011). The wet season is defined as the average from November through the following March with the year corresponding to the year during January. All observational data are processed as anomalies from the 1981-2010 climatology with the linear trend removed to minimize any climate change signal.

3.3.2 Atmospheric River Tracking

Slight changes in tracking methodology and the definitions of an AR can result in different frequencies and characteristics from automated AR detection (Rutz et al. 2019). To account for this, and produce a reliable and long-term index of ARs over northern California (125°-122.5°W and 37.5°-42.5°N), we adapted a tracking algorithm from Gershunov et al. (2017) with insight from Rutz et al. (2019) to be used in the NCEP R1 at 6-hour intervals. AR detection was based off of absolute thresholds, which is the recommended form of tracking for analyzing the relationship between ARs and large-scale atmospheric patterns (Rutz et al., 2019). These thresholds require minimum values of integrated vapor transport (IVT) at 250 $kg^1m^{-1}s^{-1}$ and total columnar integrated water vapor (IWV) at 15 mm. These thresholds filter out the background state and highlight anomalously high values of IVT and IWV that are uncommonly seen without AR conditions. IVT and IWV computations require the zonal and meridional components of wind at pressure levels from 1000 hPa to 300 hPa, specific humidity, and surface

pressure. To ensure that the threshold values over Northern California are part of a larger

corridor of enhanced vapor transport, counting an AR also requires a length requirement

in threshold values of IVT and IWV. Geometric requirements for AR detection were

limited to the length of the event, requiring at least 2500 km of continuous threshold

conditions of IVT and IWV. These threshold conditions were evaluated at the Northern

Californian coast as the entry point for landfalling ARs in the region and then their

characteristics were traced back, grid point by grid point until IVT and IWV conditions

were not met.

NCEP R1 has been shown to have biases in atmospheric vapor transport, but the

temporal variability of atmospheric vapor transport is accurate for well-observed regions

(Gutowski et al., 1997). To ensure AR tracking in NCEP R1 is accurate, we compared

results from our tracking with results from the Atmospheric River Intercomparison

Project's (ARTMIP) published Tier One Catalog for the same region and season (Shields

et al., 2018). These ARTMIP tracking routines were performed in the Modern-Era

Retrospective analysis for Research and Applications 2 (MERRA) reanalysis data at 0.5°

x 0.625° resolution, providing a test of how well the relatively coarse resolution of NCEP

R1 can replicate annual frequency characteristics of ARs. While the NCEP R1 tracking

was done over six-hour intervals, ARTMIP tracking was done over 3-hour intervals. To

account for this discrepancy, we used the ARTMIP algorithms which required a

minimum time (12–18 hours) for threshold values of IVT or IWV (or both) to classify an

AR. In Figure 3.2, highly coherent interannual variability is found between the developed

tracking algorithm and the results from ARTMIP's Tier One Catalog ($r = 0.80$ for the

overlap period from 1980–2017). The annual AR frequency magnitudes vary

significantly between NCEP R1 and the ARTMIP mean, which is unsurprising as there are similar differences in AR frequency magnitude between different algorithms within ARTMIP as well (Shields et al. 2018). To provide a second layer of verification that extends beyond the satellite era, the wet-season frequency of ARs was correlated with soil moisture, and precipitation for the tracking region (125°-122.5°W and 37.5°-42.5°N) and streamflow from the Emerald Triangle. A strong relationship between AR frequency, surface moisture, and precipitation shows that the AR frequency time series is physically meaningful for wet-season hydrology (Figure 3.3. Disparities in AR characteristics from tracking have been explored in other research (Shields et al., 2018) while this project is focused on interannual-to-decadal variability in frequency.
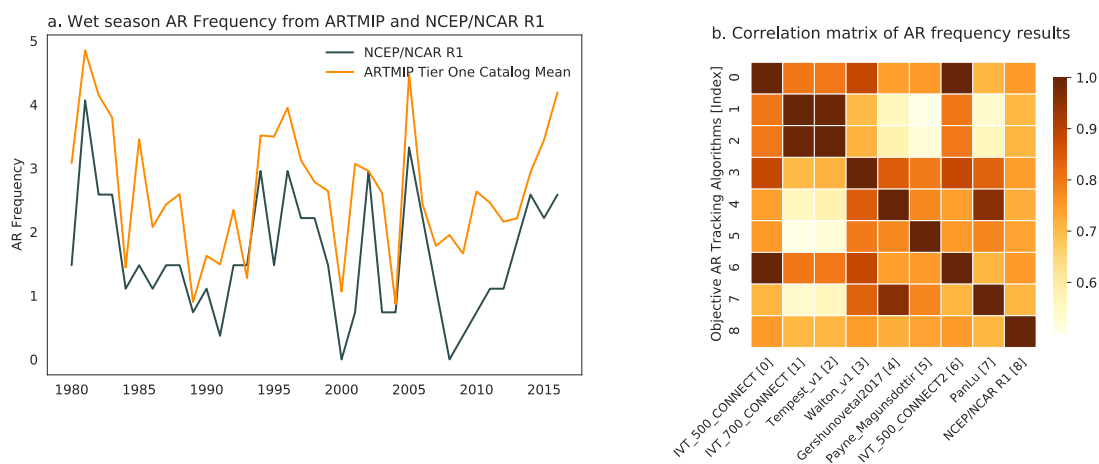
Figure 3.2 (a) AR frequency from objective tracking in NCEP R1 with AR frequency from the mean of 8 time-stitched algorithms from the ARTMIP Tier One Catalog (r=0.80). The wet-season frequency for NCEP R1 and the ARTMIP mean are standardized by diving the original time series by their standard deviation (b) Correlation matrix of the ARTMIP time-stitched algorithms and the results of the NCEP R1 tracking. All correlations surpass the 95% significance threshold for 38 degrees of freedom.
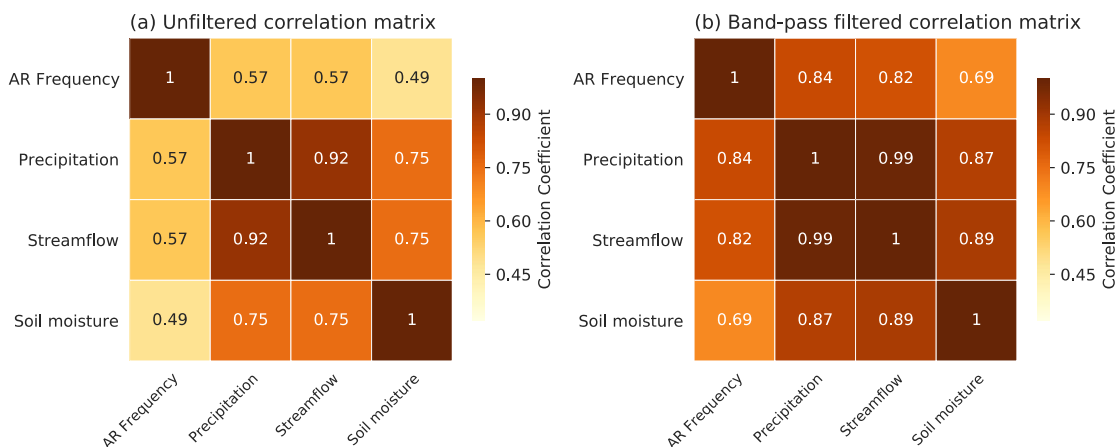
Figure 3.3 (a) AR frequency from objective tracking in NCEP R1 with AR frequency from the mean of 8 time-stitched algorithms from the ARTMIP Tier One Catalog. (b) Correlation matrix of the ARTMIP time-stitched algorithms and the results of the NCEP R1 tracking. All correlations in S2a surpass the 95% confidence interval for 60 degrees of freedom. All correlations in S2b also surpass the 95% confidence interval for 8 degrees of freedom.

3.3.3 A Climate Modeling Experiment

Observational data is a useful tool for evaluating the relationships between the ocean and atmosphere – but modeling experiments can be particularly helpful for identifying the primary forcing mechanisms. Numerous studies have found the tropical Pacific Ocean to be the source of decadal variability (Di Lorenzo et al., 2010; Rodgers et al., 2004; S. Wu et al., 2011) –stimulating interest in isolating the impacts of this region. To evaluate the ocean's response in modulating interannual to quasi-decadal variability in Northern Californian Ars, this study examines experiments conducted by NCAR's fully coupled Community Earth System Model (CESM) version 1.0. The CESM consists of ocean, atmospheric, land, and sea-ice components with 26 atmospheric levels and 60 vertical levels in the ocean. The ocean and sea-ice components comprise a curvature horizontal grid with approximately 1° latitude and 3° longitude resolution at the equator

but lower at higher latitudes. The atmosphere and land components have a T31 spectral grid (~3.75° resolution). Details of the model performance and settings can be found in Shields et al. (2012) and Chikamoto et al. (2015).

We ran a global ocean assimilation (GLOB run) and a historical assimilation comprising 10 ensemble members from initial conditions compiled from 10 random years in pre-industrial control simulations from 1958-2014. The historical simulation corresponds to the externally forced component from anthropogenic forcing. In the GLOB run, we prescribed the same radiative forcing as the historical run and assimilate 3-dimensional observed temperature and salinity anomalies into the ocean component of the model while the atmosphere is free to evolve from ocean forcing. The assimilated observed ocean data originates from the ECMWF ocean reanalysis product (version 4) from 1958-2014 (Balmaseda et al., 2013b), which is linearly interpolated from monthly to daily anomalies and added as forcing into the model's temperature and salinity tendency equations. To identify the equatorial Pacific's contribution to AR frequency, we further conduct a partial ocean assimilation using the same model configurations while assimilating the 3-dimensional observed salinity and temperature anomalies solely in the equatorial Pacific (10°S-10°N), with a buffering zone on the northern and southern boundaries of the assimilated domain. By only assimilating the equatorial Pacific Ocean information, namely the eqPAC run, the ocean and atmosphere components of CESM are free to evolve from equatorial Pacific forcing. Applications of the eqPAC method have

been documented in previous studies (Chikamoto et al., 2016; Chikamoto, Wang, et al., 2020; Johnson et al., 2018, 2020; Purich et al., 2016).

All model data presented in this study consists of the average from November through the following March. Anomalies in this study are defined as deviations from the climatological mean for 1981-2010, a range chosen because it was the most recent climate normal at the time of this writing, in observations and model run (World Meteorological Organization, 2017). To remove any climate change signal, linear trends are removed from all data.

3.3.4 Power Spectra and Bandpass Filtering

To isolate the temporal scales that are important for Northern California ARs, power spectra analysis is used to show which periods explain the most variance in relevant moisture variables. Each time series is linearly detrended and normalized before computing the power spectra, which uses Fourier analysis to determine which frequencies contribute the most variance to the time series. This analysis shows that the most prominent peak in the power spectra is 10 to 17 years for AR frequency, soil moisture, streamflow, and precipitation. Subsequently, we evaluate the relationship between unfiltered AR frequency and unfiltered climate variables (SST, 500 hPa GPH and IVT) which includes the total time-series variance and all scales of variability. To isolate the signal from the quasi-decadal cycle in ARs, we apply a bandpass filter which removes the variance not contributed by the 7-to-20-year oscillations. This window of time helps remove the influence of higher frequency ENSO variability (~4-6 years) along with lower frequency inter-decadal variability associated with the Interdecadal Pacific Oscillation (D'Arrigo et al., 2005; Mantua et al., 1997).

3.4 Observational Data Analysis

To help validate the tracking of ARs before the satellite era, correlations between AR frequency, and streamflow, precipitation and soil moisture for the Emerald Triangle are shown in Figure 3.4. Strong correlations between these variables and AR frequency indicate that the AR tracking before the satellite-era data provides physically meaningful AR metrics despite the stated shortcomings in NCEP R1. These results are consistent in both the unfiltered and the 7-to-20-year bandpass filtered data, supporting other studies highlighting pronounced decadal variability for Northern California (George & Ault, 2011; Wang et al., 2009). The power spectra analysis confirms these quasi-decadal cycles contribute significantly to the total variance of these hydrological variables, with spectral peaks at frequencies from about 10-17 years (Figure 3.4). Streamflow also exhibits a significant 4-year cycle although there are no such spectral peaks for the other hydrological variables (Figure 3.4). The 2-year spectral peak has been documented in western US hydrology and is likely related to the Biennial Annular Mode Oscillation (Johnstone, 2011). We focus on the quasi-decadal cycle because it is found in all moisture metrics for the region.
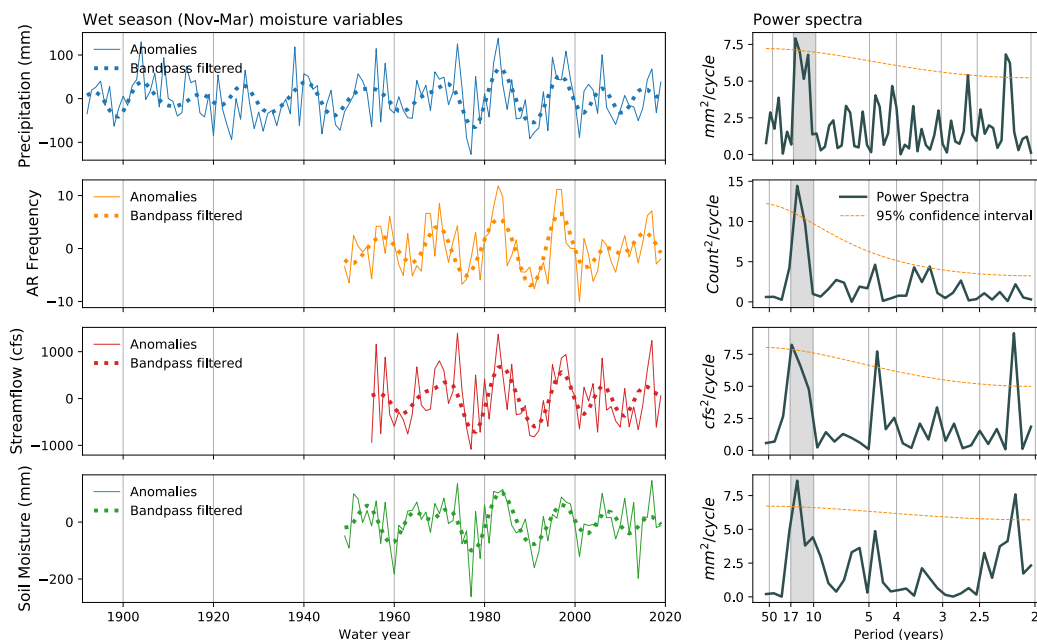
Figure 3.4. (Left column) Anomalies of precipitation, AR frequency, streamflow, and soil moisture along with the bandpass filtered time series. (Right column) Power spectra of the respective moisture variables with the 95% confidence interval represented by the power spectra of a first order Markov process. The gray shaded rectangle highlights the period of interest, the quasi-decadal frequency, from 10-17 years.

To examine the large-scale climate variability associated with the AR frequency, we made regression maps of 500 hPa geopotential height (Z500), IVT, and SST anomalies with AR frequency. Due to the stated deficiencies in NCEP R1, a comparison is also made with JRA-55 which yields analogous results when compared to Figure 3.5 (not shown). Two years before peaks of AR frequency, the regressions depict a north-south dipole of Z500 anomalies in the North Pacific, which resemble the NPO structure (Figure 3.5a). However, the moisture transport associated with NPO does not yet reach into Northern California (Figure 3.5b). At 1-year lead time, the negative Z500 anomaly is closer to the West Coast of North America (Figure 3.5d), enhancing the moisture transport toward Northern California (Figure 3.5e). The concurring regressions show the persistence of the negative Z500 anomaly in the northeast Pacific, with enhanced IVT

over Northern California (Figure 3.5g,h). Broad areas of tropical Pacific SST anomalies exhibit a significant relationship with AR frequency at a 1- to 0-year lead time (Figure 3.5f,i), but the main forcing for the quasi-decadal variability of ARs is still unclear. Regressions of observed and unfiltered Z500 and IVT with streamflow (not shown) depict features of the NAWD and the Pacific North American (PNA) pattern. The El Niño-like pattern in year-1 (Figure 35f) suggests that Northern California's hydroclimate variability is coupled with the ENSO transition phase rather than the peak ENSO phase (Wang et al., 2014a).
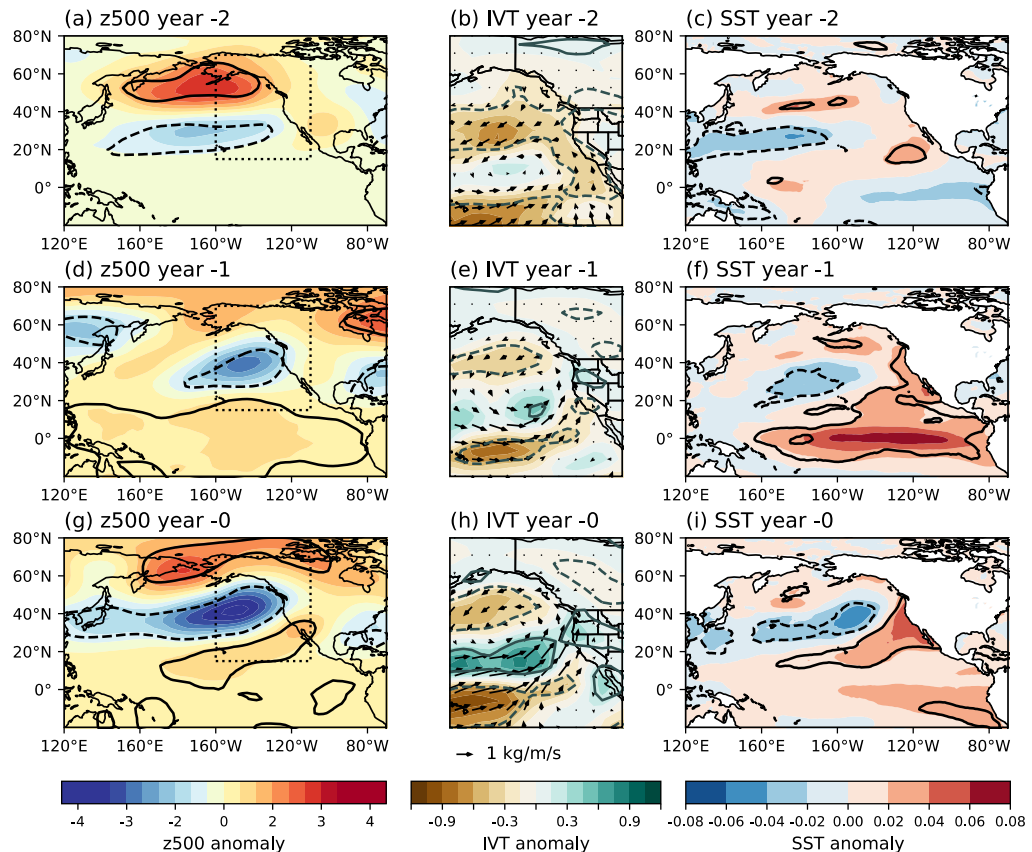
Figure 3.5. Regression maps of Z500, IVT and SST anomalies during the wet season at (a-c) -2, (d-f) -1, and (g-i) 0-year leads with the AR frequency for 1948–2020. Black contour lines indicate regions where the correlation between the climate variables and AR frequency surpass the 95% confidence interval. The dotted black box in a,d and g represents the spatial domain of the IVT in b, e and h.

When we apply a 7-to-20-year bandpass filter to all anomalies, a clear evolution can be found in Z500, IVT and SST. Tropical SST cooling at a 6-year lead results in an anti-cyclonic circulation anomaly over the northeast Pacific, inhibiting moisture transport into the region (Figure 3.6a-c). Positive SST anomalies in the west-tropical Pacific appear around the 3-year lead and the extra-tropical atmosphere facilitates more moisture transport to Southern California through the cyclonic circulation anomaly around the latitude band of 20-40N (Figure 3.6d-f). The concurrent regressions feature a deepened Aleutian Low (Figure 3.6g), enhanced tropical moisture transport (Figure 3.6h), and a broad area of tropical SST warming. The central Pacific is the main contributor to the maintenance of decadal variability for much of the Pacific basin (Deser et al., 2011; Knutson & Manabe, 1998; Yeh & Kirtman, 2005), but our results highlight that peak AR activity does not occur in tandem with central Pacific warming (Figure 3.6f). Instead, the ENSO impact on the hydroclimate of Northern California is delayed for about a year after the peak of the event. (Figure 3.6i).
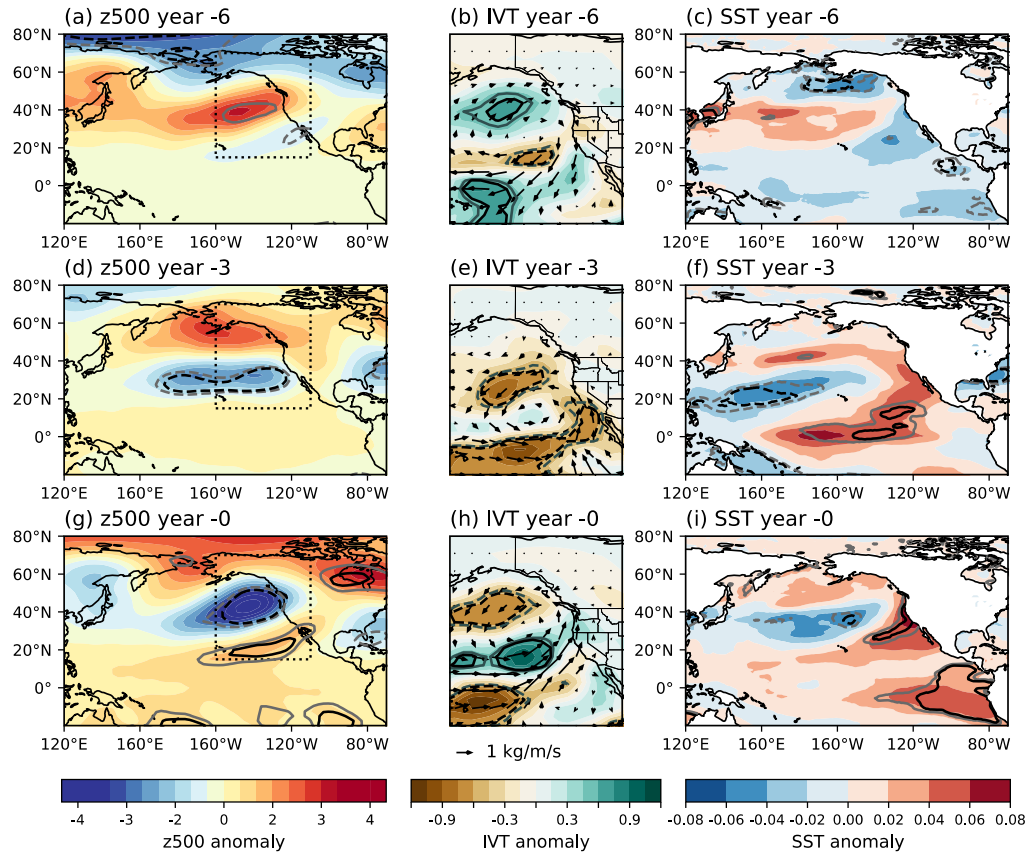
Figure 3.6. Regression maps of bandpass filtered Z500, IVT, and SST anomalies during the wet season at (a-c) -6, (d-f) -3, and (g-i) 0-year leads with bandpass filtered AR frequency for 1948–2020. The dotted rectangle in figures 3.6a, d, and g show the domain of figure 3.6b, e, and h. The significance testing has been adjusted to account for the reduction in degrees of freedom due to bandpass filtering (72 years of data with a 7-year frequency filter ~ 8 degrees of freedom). Black and gray contour lines indicate regions where the correlation between the climate variables and AR frequency surpass the 95% and 90% confidence interval respectively.

To further isolate climate variability with similar low-frequency oscillations to ARs, we applied power spectra to the teleconnection indices of interest. In the atmosphere, the NPO and the NAWD exhibit a pronounced 10-17-year periodicity. The PNA dominates on timescales around 3-4 years and 5-6 years, and thus is considered mostly irrelevant for the decadal variability of ARs (Figure 3.7a). We can also find the NAWD-like Z500 regression pattern with streamflow, but it is not clear in the regressions with AR

frequency (Figures 3.5,3.6). The common feature between each teleconnection and the

Z500 regression maps is the Aleutian Low that affects the moisture transport toward

Northern California. However, none of the patterns are accurately depicted in the

bandpass filtered data (Figure 3.6 a,d,g). By modulating the position and intensity of the

Aleutian low, it appears the NPO and NAWD are important for AR frequency but are not

a singular forcing for the quasi-decadal cycle in ARs. It is also possible that the

teleconnections could be simultaneously acting to diminish or enhance certain features.
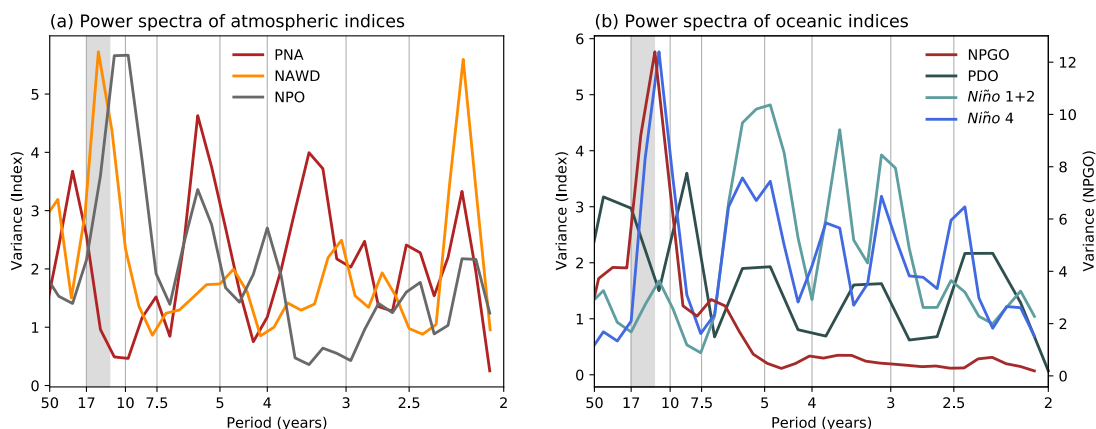
Figure 3.7. Power spectra of (a) atmospheric and (b) oceanic indices. Atmospheric indices include the PNA (red), the NAWD (orange), and the NPO (gray) whereas oceanic indices correspond to NPGO (red), PDO (dark blue), Niño 1+2 (light blue), and Niño 4 (blue) in the 5-month mean from November to the following March. The gray shaded rectangle highlights the period of interest, the quasi-decadal frequency, from 10-17 years.

For the oceanic indices, the NPGO and Niño-4 indices exhibit the most pronounced

decadal variability (Figure 3.7b) and the filtered regression maps indicate cyclical

behavior. We can find the same pattern with opposite signs of Pacific SST anomalies at

6- and 0-year lead times (Fig 3.6c and 3.6i). Consistent with this temporal evolution of

SST anomalies, Z500 anomalies also demonstrate the same pattern with opposite signs at

6- and 0-year lead times (Fig 3.6a and 3.6g). The SST regressions depict an NPGO-like

pattern 3 years before peak AR frequency with significant SST anomalies in the

equatorial Pacific through 6-, 3-, and 0-year leads. However, the decadal variability of the

NPGO (an extra-tropical mode) is tied to central Pacific warming and low-frequency

ENSO variability in the tropics (Di Lorenzo et al., 2010, 2015). This indicates the

relationship between ARs and the NPGO is largely stimulated by the tropical Pacific.

Observational analysis to this point has shown that the extratropical atmosphere

and tropical ocean exhibit an oscillatory behavior on a quasi-decadal scale that is

important for IVT transport and Z500 circulation anomalies for Northern California.

However, we have not yet isolated the main contributor of quasi-decadal variability. To

summarize the series of events linking the ocean to AR frequency, Figure 3.6 shows the

bandpass filtered teleconnection indices as well as their cross correlation with AR

frequency. The NAWD shows the strongest concurrent relationship with AR activity

between the atmospheric indices – with a negative relationship sensibly indicating that

more ARs occur in Northern California during wet seasons with anomalous low-pressure

over western North America. The decadal variability of the NPO is slightly out of phase

with AR frequency, with the autocorrelation showing the strongest positive relationship 2

years before peak AR activity. The stronger relationship between the NPO and AR

frequency in the unfiltered cross correlation shows that NPO variability is more important

for ARs on shorter time scales (also supported in the difference between Figure 3.5 and

Figure 3.6 regressions at half-phase lead). The PNA shows no leading relationship with

ARs and lacks a notable cycle in the autocorrelation, confirming it is not the major

forcing. The ocean indices show the same features present in the SST regression maps

(Figure 3.6) with onset central Pacific warming or a positive Niño 4 index leading peak

AR frequency by 2-3 years. In line with other literature, the peak NPGO follows central

Pacific warming and is a response to the NPO, but these coupled modes of atmospheric

and ocean variability exist 1-2 years before peak AR frequency (Di Lorenzo et al., 2010).

Additionally, the NAWD has been linked to central Pacific ENSO events at one year lead

through anomalous heating of the western north Pacific (Fosu et al., 2020; Wang et al.,

2014a). These features are detailed in Figure 3.5 and supported by the cross correlations

in Figure 3.8. Finally, the eastern Pacific warming shown by the Niño 1+2 index has a

strong and in-phase relationship with AR frequency.
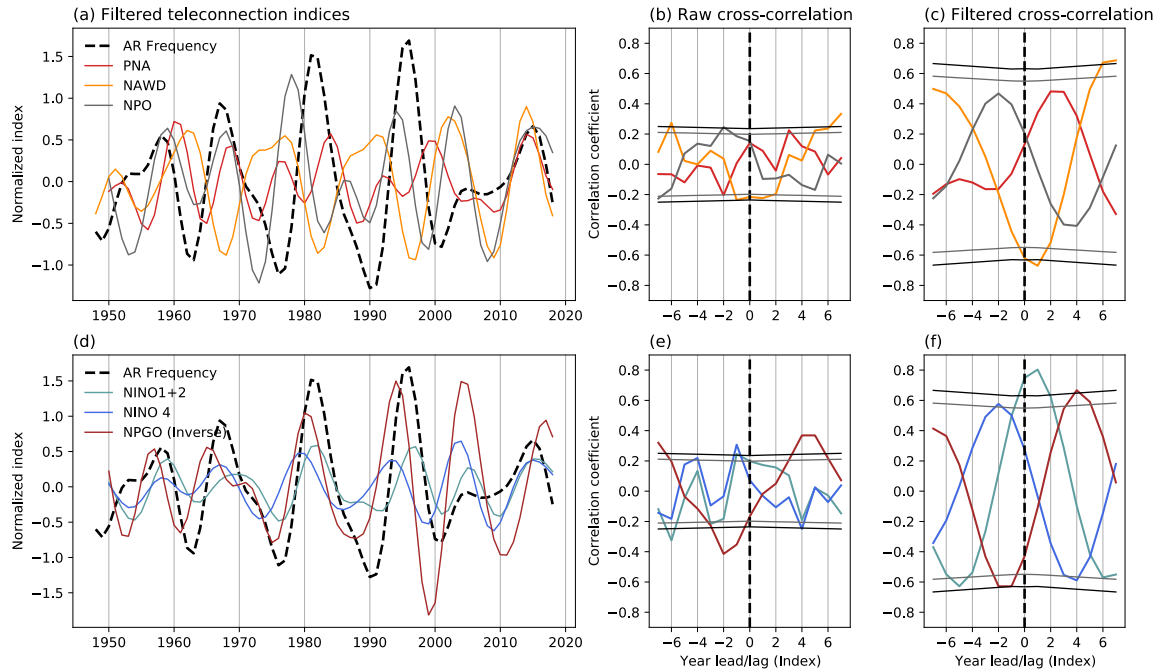
Figure 3.8. (a) Bandpass filtered atmospheric indices with the bandpass filtered AR frequency time series. (b) Cross-correlation between the unfiltered atmospheric indices and the AR frequency timeseries at lead and lag times. (c) Cross-correlation of the bandpass filtered atmospheric indices and AR frequency. The colors in 6b and 6c match the legend in 6a. (d) Bandpass filtered ocean indices with the bandpass filtered AR frequency time series. (e) Cross-correlation with unfiltered and (f) bandpass filtered ocean indices with AR frequency. The colors in 6e and 6f match the legend in 6d. The 90 and 95% significance thresholds are represented by the grey and black lines in 6b, c, e, and f – with the threshold changing to match the changing degrees of freedom in comparing the lead/lag relationships.

3.5 Tropical Pacific Modulation of ARs

Section 3 showed that both ocean (Niño 1+2 and 4, and the NPGO) and atmospheric variability (the NPO and the NAWD) are significantly related to the quasi-decadal cycle of AR frequency. However, the use of observations makes it difficult to isolate the atmospheric and oceanic forcings. Using the eqPAC of the CESM allows us to better evaluate the cause-and-effect response of AR frequency or extra-tropical atmospheric circulation to the tropical Pacific Ocean alone. To test the importance of the tropical Pacific for quasi-decadal variability in ARs, we created leading regressions of Z500 and SST in the model experiments (i.e., the eqPAC run) with AR frequency. In this model experiment, the simulated atmospheric pattern is the atmospheric response to the equatorial Pacific forcing alone.

To evaluate the model's ability to capture Z500 fields important for AR frequency and support the analysis in NCEP R1, Figure 3.9 shows a comparison of NCEP R1 Z500 with JRA-55 and the eqPAC Z500 when regressed with AR frequency. In the unfiltered data, the model does not capture the observed extratropical circulation at a 2-year lead. The observations show a clearly defined positive NPO-like pattern, with high-pressure in the central north Pacific around 60° N, and a low-pressure band around 30° N. Other research has shown that the stochastic NPO can force ENSO formation through the seasonal footprinting mechanism, driven by surface heat flux in the north Pacific (Alexander et al., 2010; B. T. Anderson, 2003; Vimont et al., 2001, 2003). As an SST assimilated model with the atmosphere free to evolve, stochastic extratropical circulation features like the NPO are not well captured by the model and not represented in the regression maps. This is one plausible explanation for why the 1-year leading regression

for the eqPAC run shows a less robust tropical response than the observed data, because the stated extratropical forcing for ENSO would be underrepresented.

Importantly, the 1-year lead and concurrent regressions show that the eqPAC and GLOB runs capture similar circulation features to observations. While the exact orientation and position of high- and low-pressure systems are shifted north by the model, the eqPAC run shows significant modulation of the Aleutian Low by the tropical Pacific (Figure 3.9). The noted differences between the model and reanalysis Z500 are either from model deficiencies in simulating the extratropical atmosphere or from the inability of the model to capture other forcings important for AR circulation features. The eqPAC also adequately captures the IVT features associated with the Niño 1+2 index, though the magnitude of IVT anomalies in the eqPAC is diminished compared to reanalysis (Figure 3.10). A higher resolution model would likely improve the fidelity of moisture transport and better resolve transient moisture transport (Zhao, 2020). The noted differences between the model and observations are either from model deficiencies in simulating the extratropical atmosphere or from the inability of the eqPAC to simulate other forcings important for extratropical circulation features.
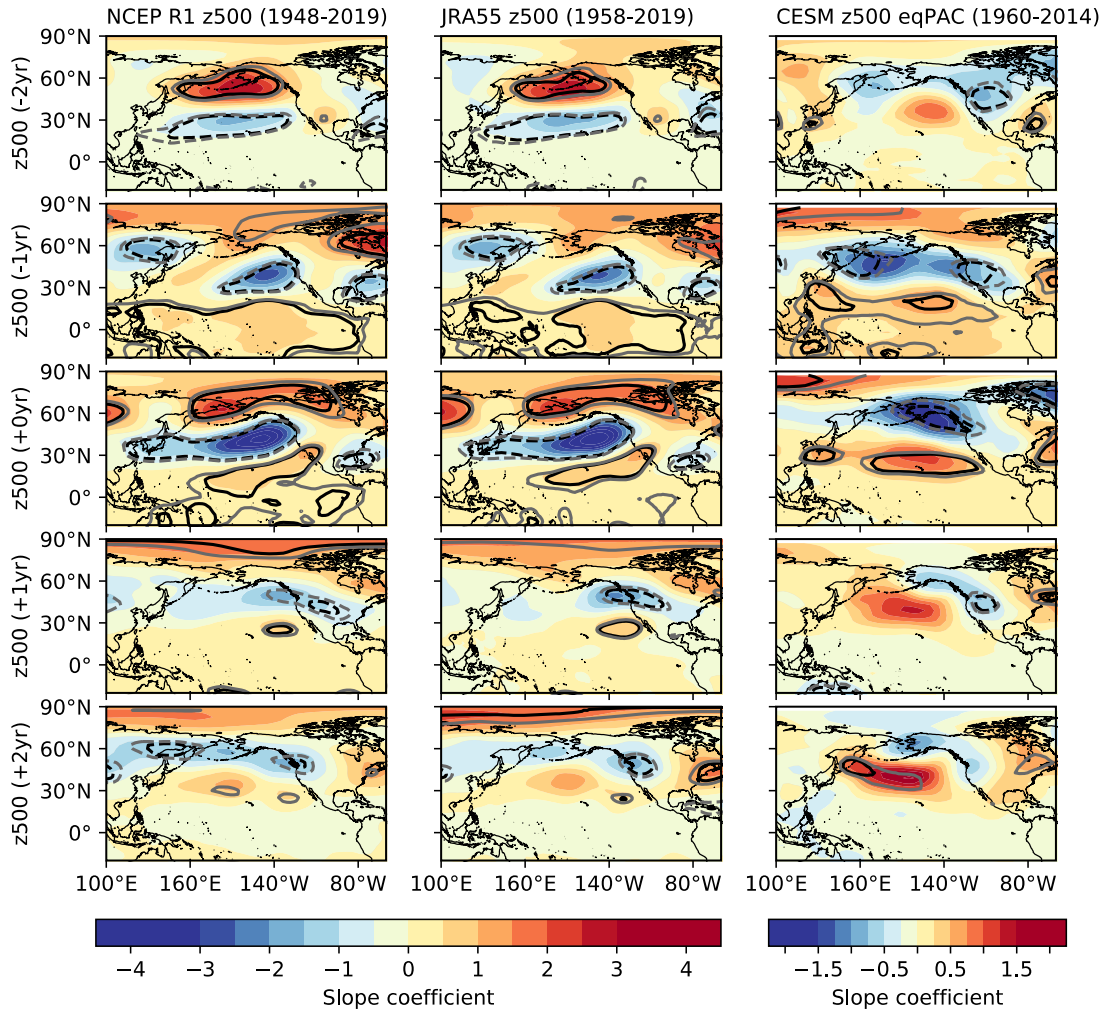
Figure 3.9. Lead/lag regressions of AR frequency with NCEP R1 Z500 (left column). JRA-55 (center column) and the eqPAC z500 (right column). Black and gray contour lines indicate regions where the correlation between Z500 and AR frequency surpass the 95% and 90% confidence interval respectively. The contour levels for the CESM are half the magnitude of the reanalysis data.
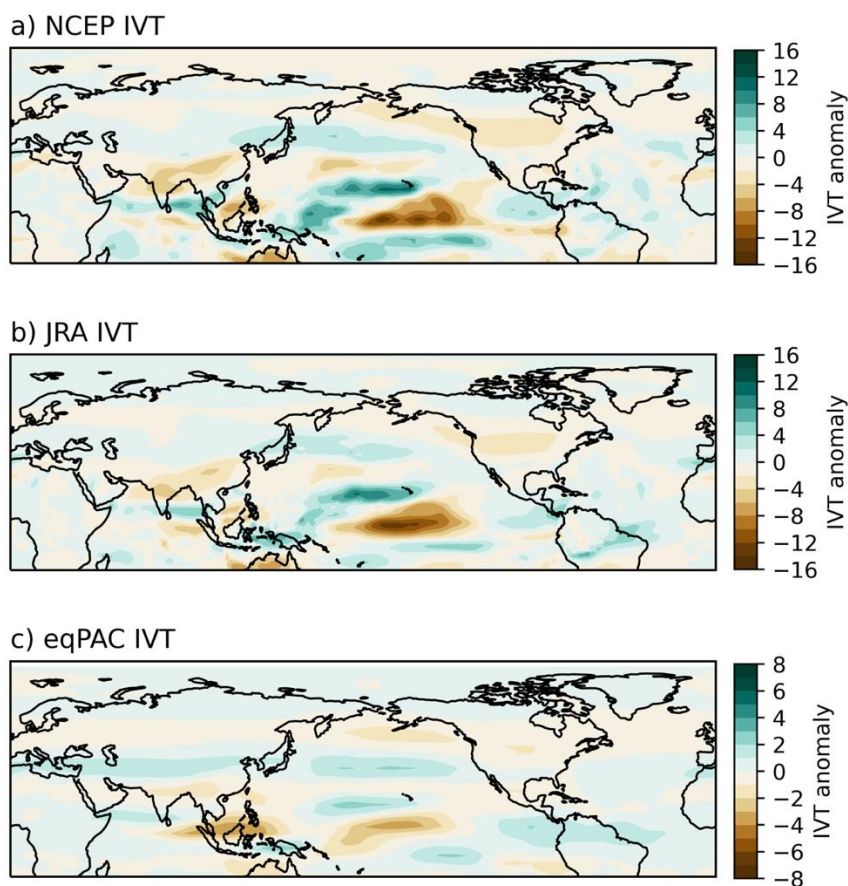
Figure 3.10. Regression maps of (a) NCEP, (b) JRA-55 and (c) eqPAC IVT anomalies during the wet season with Niño 1+2 anomalies. The contour level range for (c) is half that of the reanalysis data.

The SST and Z500 regressions from the eqPAC show similar cyclical features to observations, with the most prominent differences noted at the 6-year lead (Figure 3.11). Generally, the Z500 pattern is shifted to the north when compared to observational Z500. The deepened Aleutian Low with the adjacent subtropical high is still replicated in the regression patterns from the model—generally mirroring the observed relationship (Figure 3.6d,g). The Z500 patterns at the 3-year lead feature an elongated trough in the

north Pacific that stretches through north America. The IVT anomalies show that this period is accompanied with below average moisture transport from the tropics (Figure 3.11e). At 0-year lead, the low pressure in the north Pacific shifts east over the west coast of North America and is accompanied with enhanced IVT anomalies from the tropics (Figure 3.11g-h). The southwest-to-northeast orientation of the frontal zone in the Z500 field in observations at a 0-year lead (Figure 3.11) is not matched in the eqPAC. Additionally, the SST fields do not show the NPGO-like branch of positive SST anomalies spreading from the central Pacific to the North American coast for the concurrent regression. This suggests that these features are driven by factors other than the tropical Pacific or they might be a response to the meridional pressure dipole noted in the Z500 regressions with observations.

The eqPAC results show that tropical SST and salinity alone have substantial impacts on north Pacific extra-tropical circulation. Without the impact of the extra-tropical atmosphere, central Pacific warming one year prior to peak AR frequency and eastern Pacific ENSO result in a deepened Aleutian Low with a frontal boundary centered over Northern California (Figure 3.11). However, the IVT regressions result in features that match the observed circulation but lack the magnitude of the observed IVT and statistical significance. A more accurate simulation for extratropical moisture transport may be achieved with higher model resolution, the assimilation of extratropical SST and the inclusion of SST forcing from the North Pacific and the Atlantic (Chikamoto et al., 2020; Johnson et al., 2020; Zhao, 2020).
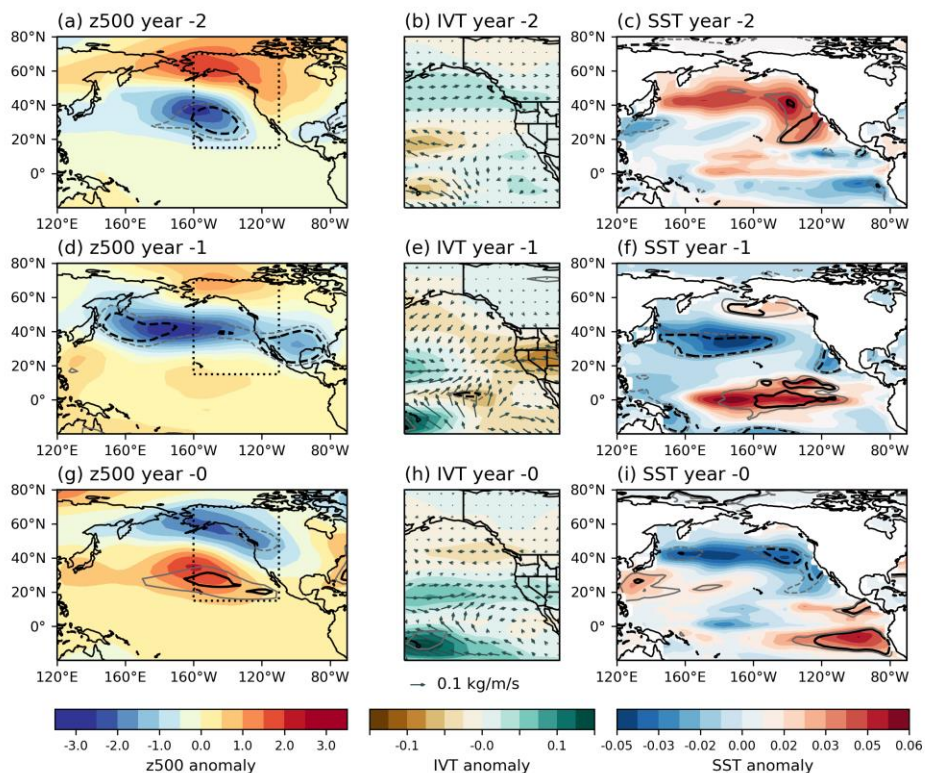
Figure 3.11. Regression maps of bandpass filtered Z500, IVT, and SST anomalies in the eqPAC during the wet season at (a-c) -6, (d-f) -3, and (g-i) 0-year leads with bandpass filtered AR frequency for 1960–2020. The dotted rectangle in figures 8a, d, and g show the domain of figure 4b, e, and h. Black and gray contour lines indicate regions where the correlation between Z500 and AR frequency surpass the 95% and 90% confidence interval respectively for 7 degrees of freedom.

3.6 Conclusions and Discussion

By analyzing 7 decades of wet-season AR frequency for Northern California, we show that AR frequency follows a pronounced quasi-decadal cycle with the region's surface and atmospheric moisture variables largely driven by tropical Pacific SST and salinity variability. Observational analysis highlights three important features for AR frequency on quasi-decadal scales:

1. A warming of the Central Pacific that accentuates the Aleutian Low 2-3 years before the peak of quasi-decadal AR frequency

2. A transition from central Pacific warming to eastern Pacific-type ENSO, and the associated eastward shift of the Aleutian Low to a position which facilitates positive IVT anomalies over Northern California

3. A consistent oscillation of the Aleutian Low over 10-to-17-year periods in tandem with the tropical Pacific warming/cooling, modulating AR frequency and wet-season moisture transport.

As the eqPAC run generally captures the extra-tropical response associated with enhanced ARs, we conclude that decadal variability in the tropical Pacific is essential for the frequency of Northern California ARs. However, the CESM-based eqPAC simulations at 3.75° resolution has differences in the Z500 field when compared with observations (Figure 3.8). The most notable differences are a northward shift in Z500 pressure anomalies and the mildly different orientation in the eqPAC (resulting in a more horizontally oriented frontal zone in the model). There are likely other extratropical factors not considered in this study that are important for the exact orientation and position of the Aleutian Low on the quasi-decadal timescale – potentially explained by internal variability or Arctic climate variability (Y. Chen & Zhai, 2011; Overland et al., 1999).

Interannual climate variability impacts AR characteristics (Guan et al., 2013; Patricola et al., 2020; Ralph et al., 2013) and surface water availability (Jones, 2000; Mo & Higgins, 1998), but the quasi-decadal cycle of ARs (Figure 1b,d) is also a fundamental hydrological component for Northern California that has been shown to limit reliable water access for some users (Morgan et al. 2020). While data limitations do exist and research should continue evaluating low-frequency variability as data records expand, our

study supports earlier findings that analysis of low-frequency AR variability is possible with mid-century reanalysis (Gershunov et al., 2017). In a region which has diverse temperature and precipitation responses to ENSO (O'Brien et al., 2019; Patricola et al., 2020), information facilitating climate prediction tools are lacking. Additionally, Northern California has an inherently difficult-to-predict AR-driven precipitation regime (Baggett et al., 2017), but tropical Pacific SST anomalies, specifically central Pacific warming, can serve as precursor patterns for improved decadal prediction of wet-season AR frequency and thus help inform water resource management decisions.

REFERENCES

Alexander, M. A., Vimont, D. J., Chang, P., & Scott, J. D. (2010). The Impact of Extratropical Atmospheric Variability on ENSO: Testing the Seasonal Footprinting Mechanism Using Coupled Model Experiments. Journal of Climate, 23(11), 2885–2901. https://doi.org/10.1175/2010JCLI3205.1

Anderson, B. T. (2003). Tropical Pacific sea-surface temperatures and preceding sea level pressure anomalies in the subtropical North Pacific. Journal of Geophysical Research: Atmospheres, 108(D23). https://doi.org/10.1029/2003JD003805

Baggett, C. F., Barnes, E. A., Maloney, E. D., & Mundhenk, B. D. (2017). Advancing atmospheric river forecasts into subseasonal-to-seasonal time scales. Geophysical Research Letters, 44(14), 7528–7536. https://doi.org/10.1002/2017GL074434

Balmaseda, M. A., Mogensen, K., & Weaver, A. T. (2013). Evaluation of the ECMWF ocean reanalysis system ORAS4. Quarterly Journal of the Royal Meteorological Society, 139(674), 1132–1161. https://doi.org/10.1002/qj.2063

Bao, J.-W., Michelson, S. A., Neiman, P. J., Ralph, F. M., & Wilczak, J. M. (2006). Interpretation of Enhanced Integrated Water Vapor Bands Associated with Extratropical Cyclones: Their Formation and Connection to Tropical Moisture. Monthly Weather Review, 134(4), 1063–1080. https://doi.org/10.1175/MWR3123.1

Chen, Y., & Zhai, P. (2011). Interannual to decadal variability of the winter Aleutian Low intensity during 1900–2004. Acta Meteorologica Sinica, 25(6), 710–724. https://doi.org/10.1007/s13351-011-0602-x

Chikamoto, Y., Johnson, Z. F., Wang, S.-Y. S., McPhaden, M. J., & Mochizuki, T. (2020). El Niño–Southern Oscillation Evolution Modulated by Atlantic Forcing. Journal of Geophysical Research: Oceans, 125(8), e2020JC016318. https://doi.org/10.1029/2020JC016318

Chikamoto, Y., Mochizuki, T., Timmermann, A., Kimoto, M., & Watanabe, M. (2016). Potential tropical Atlantic impacts on Pacific decadal climate trends. Geophysical Research Letters, 43(13), 7143–7151. https://doi.org/10.1002/2016GL069544

Chikamoto, Y., Timmermann, A., Luo, J.-J., Mochizuki, T., Kimoto, M., Watanabe, M., Ishii, M., Xie, S.-P., & Jin, F.-F. (2015). Skilful multi-year predictions of tropical trans-basin climate variability. Nature Communications, 6(1), 6869. https://doi.org/10.1038/ncomms7869

Chikamoto, Y., Wang, S.-Y. S., Yost, M., Yocom, L., & Gillies, R. R. (2020). Colorado River water supply is predictable on multi-year timescales owing to long-term ocean memory. Communications Earth & Environment, 1(1), 1–11. https://doi.org/10.1038/s43247-020-00027-0

D'Arrigo, R., Cook, E. R., Wilson, R. J., Allan, R., & Mann, M. E. (2005). On the variability of ENSO over the past six centuries. Geophysical Research Letters, 32(3). https://doi.org/10.1029/2004GL022055

Deser, C., Phillips, A. S., Tomas, R. A., Okumura, Y. M., Alexander, M. A., Capotondi, A., Scott, J. D., Kwon, Y.-O., & Ohba, M. (2011). ENSO and Pacific Decadal Variability in the Community Climate System Model Version 4. Journal of Climate, 25(8), 2622–2651. https://doi.org/10.1175/JCLI-D-11-00301.1

Dettinger, M. (2011). Climate Change, Atmospheric Rivers, and Floods in California – A Multimodel Analysis of Storm Frequency and Magnitude Changes1. JAWRA Journal of the American Water Resources Association, 47(3), 514–523. https://doi.org/10.1111/j.1752-1688.2011.00546.x

Dettinger, M. D. (2013). Atmospheric Rivers as Drought Busters on the U.S. West Coast. Journal of Hydrometeorology, 14(6), 1721–1732. https://doi.org/10.1175/JHM-D-13-02.1

Di Lorenzo, E., Cobb, K. M., Furtado, J. C., Schneider, N., Anderson, B. T., Bracco, A., Alexander, M. A., & Vimont, D. J. (2010). Central Pacific El Niño and decadal climate change in the North Pacific Ocean. Nature Geoscience, 3(11), 762–765. https://doi.org/10.1038/ngeo984

Di Lorenzo, E., Liguori, G., Schneider, N., Furtado, J. C., Anderson, B. T., & Alexander, M. A. (2015). ENSO and meridional modes: A null hypothesis for Pacific climate variability. Geophysical Research Letters, 42(21), 9440–9448. https://doi.org/10.1002/2015GL066281

Ebita, A., Kobayashi, S., Ota, Y., Moriya, M., Kumabe, R., Onogi, K., Harada, Y., Yasui, S., Miyaoka, K., Takahashi, K., Kamahori, H., Kobayashi, C., Endo, H., Soma, M., Oikawa, Y., & Ishimizu, T. (2011). The Japanese 55-year Reanalysis "JRA-55": An Interim Report. Sola, 7, 149–152. https://doi.org/10.2151/sola.2011-038

Fan, Y., & Dool, H. van den. (2004). Climate Prediction Center global monthly soil moisture data set at 0.5° resolution for 1948 to present. Journal of Geophysical Research: Atmospheres, 109(D10). https://doi.org/10.1029/2003JD004345

Fosu, B., He, J., & Wang, S.-Y. S. (2020). The influence of wintertime SST variability in the Western North Pacific on ENSO diversity. Climate Dynamics, 54(7), 3641–3654. https://doi.org/10.1007/s00382-020-05193-7

George, S. S., & Ault, T. R. (2011). Is energetic decadal variability a stable feature of the central Pacific Coast's winter climate? Journal of Geophysical Research: Atmospheres, 116(D12). https://doi.org/10.1029/2010JD015325

Gershunov, A., Shulgina, T., Ralph, F. M., Lavers, D. A., & Rutz, J. J. (2017). Assessing the climate-scale variability of atmospheric rivers affecting western North America. Geophysical Research Letters, 44(15), 7900–7908. https://doi.org/10.1002/2017GL074175

Guan, B., Molotch, N. P., Waliser, D. E., Fetzer, E. J., & Neiman, P. J. (2010). Extreme snowfall events linked to atmospheric rivers and surface air temperature via satellite measurements. Geophysical Research Letters, 37(20). https://doi.org/10.1029/2010GL044696

Guan, B., Molotch, N. P., Waliser, D. E., Fetzer, E. J., & Neiman, P. J. (2013). The 2010/2011 snow season in California's Sierra Nevada: Role of atmospheric rivers

and modes of large-scale variability. Water Resources Research, 49(10), 6731–6743. https://doi.org/10.1002/wrcr.20537

Guan, B., & Waliser, D. E. (2015). Detection of atmospheric rivers: Evaluation and application of an algorithm for global studies. Journal of Geophysical Research: Atmospheres, 120(24), 12514–12535. https://doi.org/10.1002/2015JD024257

Guirguis, K., Gershunov, A., Shulgina, T., Clemesha, R. E. S., & Ralph, F. M. (2019). Atmospheric rivers impacting Northern California and their modulation by a variable climate. Climate Dynamics, 52(11), 6569–6583. https://doi.org/10.1007/s00382-018-4532-5

Gutowski, W. J., Chen, Y., & Ötles, Z. (1997). Atmospheric Water Vapor Transport in NCEP–NCAR Reanalyses: Comparison with River Discharge in the Central United States. Bulletin of the American Meteorological Society, 78(9), 1957–1970. https://doi.org/10.1175/1520-0477(1997)078<1957:AWVTIN>2.0.CO;2

Hersbach, H., Peubey, C., Simmons, A., Berrisford, P., Poli, P., & Dee, D. (2015). ERA-20CM: A twentieth-century atmospheric model ensemble. Quarterly Journal of the Royal Meteorological Society, 141(691), 2350–2375. https://doi.org/10.1002/qj.2528

Higgins, R. W., Schemm, J.-K. E., Shi, W., & Leetmaa, A. (2000). Extreme Precipitation Events in the Western United States Related to Tropical Forcing. Journal of Climate, 13(4), 793–820. https://doi.org/10.1175/1520-0442(2000)013<0793:EPEITW>2.0.CO;2

Ishii, M., Shouji, A., Sugimoto, S., & Matsumoto, T. (2005). Objective analyses of sea-surface temperature and marine meteorological variables for the 20th century using ICOADS and the Kobe Collection. International Journal of Climatology, 25(7), 865–879. https://doi.org/10.1002/joc.1169

Johnson, Z. F., Chikamoto, Y., Luo, J.-J., & Mochizuki, T. (2018). Ocean Impacts on Australian Interannual to Decadal Precipitation Variability. Climate, 6(3), 61. https://doi.org/10.3390/cli6030061

Johnson, Z. F., Chikamoto, Y., Wang, S.-Y. S., McPhaden, M. J., & Mochizuki, T. (2020). Pacific decadal oscillation remotely forced by the equatorial Pacific and the Atlantic Oceans. Climate Dynamics, 55(3), 789–811. https://doi.org/10.1007/s00382-020-05295-2

Johnstone, J. A. (2011). A quasi-biennial signal in western US hydroclimate and its global teleconnections. Climate Dynamics, 36(3), 663–680. https://doi.org/10.1007/s00382-010-0755-9

Jones, C. (2000). Occurrence of Extreme Precipitation Events in California and Relationships with the Madden–Julian Oscillation. Journal of Climate, 13(20), 3576–3587. https://doi.org/10.1175/1520-0442(2000)013<3576:OOEPEI>2.0.CO;2

Kalnay, E., Kanamitsu, M., Kistler, R., Collins, W., Deaven, D., Gandin, L., Iredell, M., Saha, S., White, G., Woollen, J., Zhu, Y., Chelliah, M., Ebisuzaki, W., Higgins, W., Janowiak, J., Mo, K. C., Ropelewski, C., Wang, J., Leetmaa, A., … Joseph,

D. (1996). The NCEP/NCAR 40-Year Reanalysis Project. Bulletin of the American Meteorological Society, 77(3), 437–472. https://doi.org/10.1175/1520-0477(1996)077<0437:TNYRP>2.0.CO;2

Kim, H.-M., & Alexander, M. A. (2015). ENSO's Modulation of Water Vapor Transport over the Pacific–North American Region. Journal of Climate, 28(9), 3846–3856. https://doi.org/10.1175/JCLI-D-14-00725.1

Knutson, T. R., & Manabe, S. (1998). Model Assessment of Decadal Variability and Trends in the Tropical Pacific Ocean. Journal of Climate, 11(9), 2273–2296. https://doi.org/10.1175/1520-0442(1998)011<2273:MAODVA>2.0.CO;2

Liu, X., Ren, X., & Yang, X.-Q. (2016). Decadal Changes in Multiscale Water Vapor Transport and Atmospheric River Associated with the Pacific Decadal Oscillation and the North Pacific Gyre Oscillation. Journal of Hydrometeorology, 17(1), 273–285. https://doi.org/10.1175/JHM-D-14-0195.1

Lorenzo, E. D., Schneider, N., Cobb, K. M., Franks, P. J. S., Chhak, K., Miller, A. J., McWilliams, J. C., Bograd, S. J., Arango, H., Curchitser, E., Powell, T. M., & Rivière, P. (2008). North Pacific Gyre Oscillation links ocean climate and ecosystem change. Geophysical Research Letters, 35(8). https://doi.org/10.1029/2007GL032838

MacDonald, G. M., & Case, R. A. (2005). Variations in the Pacific Decadal Oscillation over the past millennium. Geophysical Research Letters, 32(8). https://doi.org/10.1029/2005GL022478

Mantua, N. J., Hare, S. R., Zhang, Y., Wallace, J. M., & Francis, R. C. (1997). A Pacific Interdecadal Climate Oscillation with Impacts on Salmon Production*. Bulletin of the American Meteorological Society, 78(6), 1069–1080. https://doi.org/10.1175/1520-0477(1997)078<1069:APICOW>2.0.CO;2

Mo, K. C., & Higgins, R. W. (1998). Tropical Influences on California Precipitation. Journal of Climate, 11(3), 412–430. https://doi.org/10.1175/1520-0442(1998)011<0412:TIOCP>2.0.CO;2

Morgan, B., Spangler, K., Stuivenvolt Allen, J., Morrisett, C. N., Brunson, M. W., Wang, S.-Y. S., & Huntly, N. (2021). Water Availability for Cannabis in Northern California: Intersections of Climate, Policy, and Public Discourse. Water, 13(1). https://doi.org/10.3390/w13010005

Mundhenk, B. D., Barnes, E. A., Maloney, E. D., & Baggett, C. F. (2018). Skillful empirical subseasonal prediction of landfalling atmospheric river activity using the Madden–Julian oscillation and quasi-biennial oscillation. Npj Climate and Atmospheric Science, 1(1), 1–7. https://doi.org/10.1038/s41612-017-0008-2

Newman, M., Alexander, M. A., Ault, T. R., Cobb, K. M., Deser, C., Di Lorenzo, E., Mantua, N. J., Miller, A. J., Minobe, S., Nakamura, H., Schneider, N., Vimont, D. J., Phillips, A. S., Scott, J. D., & Smith, C. A. (2016). The Pacific Decadal Oscillation, Revisited. Journal of Climate, 29(12), 4399–4427. https://doi.org/10.1175/JCLI-D-15-0508.1

O'Brien, J. P., O'Brien, T. A., Patricola, C. M., & Wang, S.-Y. S. (2019). Metrics for understanding large-scale controls of multivariate temperature and precipitation variability. Climate Dynamics, 53(7), 3805–3823. https://doi.org/10.1007/s00382-019-04749-6

Organization (WMO), W. M., & World Meteorological Organization (WMO). (2017). WMO Guidelines on the Calculation of Climate Normals (2017 edition). WMO.

Overland, J. E., Adams, J. M., & Bond, N. A. (1999). Decadal Variability of the Aleutian Low and Its Relation to High-Latitude Circulation. Journal of Climate, 12(5), 1542–1548. https://doi.org/10.1175/1520-0442(1999)012<1542:DVOTAL>2.0.CO;2

Patricola, C. M., O'Brien, J. P., Risser, M. D., Rhoades, A. M., O'Brien, T. A., Ullrich, P. A., Stone, D. A., & Collins, W. D. (2020). Maximizing ENSO as a source of western US hydroclimate predictability. Climate Dynamics, 54(1), 351–372. https://doi.org/10.1007/s00382-019-05004-8

Payne, A. E., & Magnusdottir, G. (2014). Dynamics of Landfalling Atmospheric Rivers over the North Pacific in 30 Years of MERRA Reanalysis. Journal of Climate, 27(18), 7133–7150. https://doi.org/10.1175/JCLI-D-14-00034.1

Purich, A., England, M. H., Cai, W., Chikamoto, Y., Timmermann, A., Fyfe, J. C., Frankcombe, L., Meehl, G. A., & Arblaster, J. M. (2016). Tropical Pacific SST Drivers of Recent Antarctic Sea Ice Trends. Journal of Climate, 29(24), 8931–8948. https://doi.org/10.1175/JCLI-D-16-0440.1

Ralph, F. M., Coleman, T., Neiman, P. J., Zamora, R. J., Dettinger, M. D., Ralph, F. M., Coleman, T., Neiman, P. J., Zamora, R. J., & Dettinger, M. D. (2013, April 12). Observed Impacts of Duration and Seasonality of Atmospheric-River Landfalls on Soil Moisture and Runoff in Coastal Northern California [Research-article]. Http://Dx.Doi.Org/10.1175/JHM-D-12-076.1. https://doi.org/10.1175/JHM-D-12-076.1

Rodgers, K. B., Friederichs, P., & Latif, M. (2004). Tropical Pacific Decadal Variability and Its Relation to Decadal Modulations of ENSO. Journal of Climate, 17(19), 3761–3774. https://doi.org/10.1175/1520-0442(2004)017<3761:TPDVAI>2.0.CO;2

Rutz, J. J., Shields, C. A., Lora, J. M., Payne, A. E., Guan, B., Ullrich, P., O'Brien, T., Leung, L. R., Ralph, F. M., Wehner, M., Brands, S., Collow, A., Goldenson, N., Gorodetskaya, I., Griffith, H., Kashinath, K., Kawzenuk, B., Krishnan, H., Kurlin, V., … Viale, M. (2019). The Atmospheric River Tracking Method Intercomparison Project (ARTMIP): Quantifying Uncertainties in Atmospheric River Climatology. Journal of Geophysical Research: Atmospheres, 124(24), 13777–13802. https://doi.org/10.1029/2019JD030936

Ryoo, J.-M., Kaspi, Y., Waugh, D. W., Kiladis, G. N., Waliser, D. E., Fetzer, E. J., & Kim, J. (2013). Impact of Rossby Wave Breaking on U.S. West Coast Winter Precipitation during ENSO Events. Journal of Climate, 26(17), 6360–6382. https://doi.org/10.1175/JCLI-D-12-00297.1

Schneider, U., Becker, A., Finger, P., Meyer-Christoffer, A., Ziese, M., & Rudolf, B. (2014). GPCC's new land surface precipitation climatology based on quality-controlled in situ data and its role in quantifying the global water cycle. Theoretical and Applied Climatology, 115(1), 15–40. https://doi.org/10.1007/s00704-013-0860-x

Shields, C. A., Bailey, D. A., Danabasoglu, G., Jochum, M., Kiehl, J. T., Levis, S., & Park, S. (2012). The Low-Resolution CCSM4. Journal of Climate, 25(12), 3993–4014. https://doi.org/10.1175/JCLI-D-11-00260.1

Shields, C. A., Rutz, J. J., Leung, L.-Y., Ralph, F. M., Wehner, M., Kawzenuk, B., Lora, J. M., McClenny, E., Osborne, T., Payne, A. E., Ullrich, P., Gershunov, A., Goldenson, N., Guan, B., Qian, Y., Ramos, A. M., Sarangi, C., Sellars, S., Gorodetskaya, I., … Nguyen, P. (2018). Atmospheric River Tracking Method Intercomparison Project (ARTMIP): Project goals and experimental design. Geoscientific Model Development, 11(6), 2455–2474. https://doi.org/10.5194/gmd-11-2455-2018

Slivinski, L. C., Compo, G. P., Whitaker, J. S., Sardeshmukh, P. D., Giese, B. S., McColl, C., Allan, R., Yin, X., Vose, R., Titchner, H., Kennedy, J., Spencer, L. J., Ashcroft, L., Brönnimann, S., Brunet, M., Camuffo, D., Cornes, R., Cram, T. A., Crouthamel, R., … Wyszyński, P. (2019). Towards a more reliable historical reanalysis: Improvements for version 3 of the Twentieth Century Reanalysis system. Quarterly Journal of the Royal Meteorological Society, 145(724), 2876–2908. https://doi.org/10.1002/qj.3598

Tan, Y., Zwiers, F., Yang, S., Li, C., & Deng, K. (2020). The Role of Circulation and Its Changes in Present and Future Atmospheric Rivers over Western North America. Journal of Climate, 33(4), 1261–1281. https://doi.org/10.1175/JCLI-D-19-0134.1

Timmermann, A., An, S.-I., Kug, J.-S., Jin, F.-F., Cai, W., Capotondi, A., Cobb, K. M., Lengaigne, M., McPhaden, M. J., Stuecker, M. F., Stein, K., Wittenberg, A. T., Yun, K.-S., Bayr, T., Chen, H.-C., Chikamoto, Y., Dewitte, B., Dommenget, D., Grothe, P., … Zhang, X. (2018). El Niño–Southern Oscillation complexity. Nature, 559(7715), 535–545. https://doi.org/10.1038/s41586-018-0252-6

Vimont, D. J., Battisti, D. S., & Hirst, A. C. (2001). Footprinting: A seasonal connection between the tropics and mid-latitudes. Geophysical Research Letters, 28(20), 3923–3926. https://doi.org/10.1029/2001GL013435

Vimont, D. J., Wallace, J. M., & Battisti, D. S. (2003). The Seasonal Footprinting Mechanism in the Pacific: Implications for ENSO. Journal of Climate, 16(16), 2668–2675. https://doi.org/10.1175/1520-0442(2003)016<2668:TSFMIT>2.0.CO;2

Wang, S.-Y., Gillies, R. R., Jin, J., & Hipps, L. E. (2009). Recent rainfall cycle in the Intermountain Region as a quadrature amplitude modulation from the Pacific decadal oscillation. Geophysical Research Letters, 36(2). https://doi.org/10.1029/2008GL036329

Wang, S.-Y., Hipps, L., Gillies, R. R., & Yoon, J.-H. (2014a). Probable causes of the abnormal ridge accompanying the 2013–2014 California drought: ENSO

precursor and anthropogenic warming footprint. Geophysical Research Letters, 41(9), 3220–3226. https://doi.org/10.1002/2014GL059748

Wang, S.-Y., Hipps, L., Gillies, R. R., & Yoon, J.-H. (2014b). Probable causes of the abnormal ridge accompanying the 2013–2014 California drought: ENSO precursor and anthropogenic warming footprint. Geophysical Research Letters, 41(9), 3220–3226. https://doi.org/10.1002/2014GL059748

Wang, S.-Y. S., Huang, W.-R., & Yoon, J.-H. (2015). The North American winter 'dipole' and extremes activity: A CMIP5 assessment. Atmospheric Science Letters, 16(3), 338–345. https://doi.org/10.1002/asl2.565

Wang, S.-Y. S., Yoon, J.-H., Becker, E., & Gillies, R. (2017). California from drought to deluge. Nature Climate Change, 7, 465–468. https://doi.org/10.1038/nclimate3330

Wu, L., Liu, Z., Gallimore, R., Jacob, R., Lee, D., & Zhong, Y. (2003). Pacific Decadal Variability: The Tropical Pacific Mode and the North Pacific Mode. Journal of Climate, 16(8), 1101–1120. https://doi.org/10.1175/1520-0442(2003)16<1101:PDVTTP>2.0.CO;2

Wu, S., Liu, Z., Zhang, R., & Delworth, T. L. (2011). On the observed relationship between the Pacific Decadal Oscillation and the Atlantic Multi-decadal Oscillation. Journal of Oceanography, 67(1), 27–35. https://doi.org/10.1007/s10872-011-0003-x

Yeh, S.-W., & Kirtman, B. P. (2005). Pacific decadal variability and decadal ENSO amplitude modulation. Geophysical Research Letters, 32(5). https://doi.org/10.1029/2004GL021731

Zhao, M. (2020). Simulations of Atmospheric Rivers, Their Variability, and Response to Global Warming Using GFDL's New High-Resolution General Circulation Model. Journal of Climate, 33(23), 10287–10303. https://doi.org/10.1175/JCLI-D-20-0241.1

CHAPTER 4
EMERGENCE OF A DECADAL HYDROCLIMATE REGIME IN THE WESTERN
UNITED STATES

4.1 Abstract

The diverse topography and climate of the western United States (US) has historically resulted in heterogeneous hydroclimate variability in space and time. However, as exemplified by recent drought events, hydroclimate variability can also affect the entire western US simultaneously with long-lasting impacts. Our findings show that the dominant mode of drought and precipitation variability has become more widespread and dominated by decadal variability. As a result, river discharge variability throughout the west has become more tightly coupled with precipitation and drought, and multi-year wet or dry periods have become more likely. This emergence of decadal hydroclimate variability is coupled with stronger decadal variability in North Pacific sea surface temperatures and upper-level atmospheric pressure along western North America. Evaluating the leading mode of precipitation variability in historical and future climate scenarios shows that climate change may end up decreasing low-frequency hydroclimate variability in the western US.

4.2 Introduction

Persistent droughts in the western United States (US) result in widespread impacts on water resources (Dettinger et al., 2015; Hidalgo et al., 2009; Martin et al., 2020; Zhou et al., 2018), agricultural production (Anderson et al., 2018; Chikamoto et al., 2020), and fire activity (Schoennagel et al., 2007; Seager et al., 2015; Westerling et al., 2003). In this region, drought variability contains a myriad of spatial and temporal scales, ranging from

local flash-drought (Chen et al., 2019) to interdecadal dry spells or pluvial periods (Ault et al., 2013; Cayan et al., 1998; Cook et al., 2011; Woodhouse et al., 2005). Additionally, the abnormal aridity of the early 21st century associated with anthropogenic climate change have resulted in more multi-year and widespread drought events (Gangopadhyay et al., 2019; Marshall et al., 2019; Stevenson et al., 2022; Williams et al., 2020, 2022). As most of the western states are currently facing continuous and severe drought conditions which have persisted since the start of the 2021 water year (or earlier), a better understanding of the dominant temporal and spatial variability of western US drought is needed to characterize our current situation.

Drought on interannual-to-decadal timescales is mainly attributed to two major sources of low-frequency ocean variability: El Niño Southern Oscillation (ENSO) and the Pacific Decadal Oscillation (PDO). ENSO most commonly affects seasonal-to-interannual hydrological variability with differing precipitation responses in the Northwest and Southwest (Cayan et al., 1998; Cole et al., 2002; McCabe & Dettinger, 1999; Ropelewski & Halpert, 1986), snow water equivalent (Cayan, 1996; Clark et al., 2001; Thakur et al., 2020), and streamflow (Tootle et al., 2005). On decadal timescales, the PDO can facilitate wet and dry cycles by altering the jet-stream location and strength in the North Pacific (Chikamoto et al., 2017, 2020; Cook et al., 2011; Goodrich, 2007; Hidalgo et al., 2009; McCabe et al., 2004; McCabe & Dettinger, 1999; S. Wang et al., 2014). Moreover, the geographical heterogeneity in the West results in unique local responses to these large-scale climate modes (Mock, 1996; Shinker, 2010) which have been documented in the frequency of atmospheric rivers in California (Cayan, 1996; Dettinger, 2016; Dettinger & Cayan, 2014; Morgan et al., 2021; Stuivenvolt-Allen et al.,

2021), the elevation of the Great Salt Lake (S.-Y. Wang et al., 2009, 2010), and
streamflow in the Colorado River Basin (Hidalgo & Dracup, 2003; Nowak et al., 2012).
Consequently, the dominant mode of drought variability is sensitive to geography,
drought metrics, and time periods of analysis.

In addition to these sensitivities, climate change and rapid climate shifts may alter the
dominant mode of drought variability in the western US through changes to large-scale
atmosphere-ocean dynamics. Chien et al (2019) pointed out that the leading mode of the
winter planetary waves has changed from the Pacific North America (PNA) pattern to the
North American Winter Dipole pattern around 1980s. Stuivenvolt-Allen et al., (2022) and
Schulte & Lee (2017) also demonstrated that a similar teleconnection which results in
alternating pressure anomalies over North America has become more important for North
American temperature and weather extremes proceeding 1980. These changes are
concurrent with the North Pacific climate shift in 1976, which resulted in rapid cooling in
the western North Pacific in conjunction with an emergence of warm sea surface
temperatures (SST) wrapping around the north, east (along the west coast of North
America), and south side of this cold SST anomaly (Latif & Barnett, 1996; Mantua et al.,
1997; Nitta & Yamada, 1989; Trenberth, 1990). There were documented shifts in
hydroclimate variability in the western US following 1976 (McCabe & Dettinger, 1999;
Nowak et al., 2012), however it is unknown if these changes were experienced by the
entire western region.

Our main objective is to revisit the dominant mode of drought variability for the
western US and analyze how this has changed in the last century in a changing Pacific
climate. To link drought in the western US to larger scale climate variability, we will

show the associated shifts in oceanic and atmospheric variability that accompany low-frequency drought in reanalysis data and in the Community Earth System Model Version 2 Large Ensemble (CESM2_LE). Finally, we will present future projections of the leading modes of precipitation variability to estimate the impact of climate change on decadal hydroclimate variability. This research builds off seminal findings and techniques used to analyze drought variability in the western US (Cayan et al., 1998; Cook et al., 2018; Hidalgo & Dracup, 2003) to demonstrate that decadal variability drought rapidly emerged and persisted as a dominant driver of pan-western US hydroclimate for the last four decades.

4.3 Data and methods

4.3.1 Drought, precipitation, and reanalysis data

For analyzing the spatial and temporal variability of drought in the western United States, we use the self-calibrated Palmer Drought Severity Index (PDSI) from the Parameter-elevation Regressions on Independent Slopes Model (PRISM) (Abatzoglou et al., 2017). The self-calibrated PDSI has proven more effective for comparing drought in different locations by adjusting the calculation of PDSI to the climate characteristics of a certain region (Wells et al., 2004). Monthly precipitation data (1930-2019) at 1° resolution were provided by the Global Precipitation Climatology Project Centre version 6.0 (Schneider et al., 2014) which is derived from quality controlled in situ observations.

SST and 250 hPa geopotential height data (z250) are gathered from the Japanese Meteorological Agency's Centennial In-Situ Observation Based Estimates (COBE) SST at 1° resolution and the National Center for Environmental Prediction's Reanalysis 1 dataset from 1948 to present (Ishii et al., 2005; Kalnay et al., 1996). As this study

concerns low-frequency drought variability, PDSI, precipitation, SST and z250 were

averaged by water-year: a mean of October of one year through September of the next.

4.3.2 Streamflow data

Monthly river discharge from the United States Geological Survey (USGS) was

acquired from 25 streamflow gauges for major rivers in the western United States. We

identified these 25 gauges because they have consistent (no periods of missing values)

records of river discharge from near 1930 until the present day for comparison with the

record of precipitation and PDSI data. Data for the Sacramento River starts in 1945, but

we included it to get a larger spatial sample that includes California. All river discharge

data is averaged into water-year means, linearly detrended, and then standardized by

dividing the data by its standard deviation As in Morgan et al. (2021), when multiple

gauges along the same river had a data record starting by 1935, the standardized from the

multiple gauges were averaged together. The USGS gauges used and the number of

gauges which represent each river can be found in Table 4.1.

Gauge Number	Site location	River group
USGS 09180500	Colorado River near Cisco, UT	Upper Colorado
USGS 09095500	Colorado River near Cameo, CO	Upper Colorado
USGS 09058000	Colorado River near Kremmling, CO	Upper Colorado
USGS 09380000	Colorado River at Lees Ferry, AZ	Lees Ferry
USGS 09382000	Paria River at Lees Ferry, AZ	Lower Colorado
USGS 09402500	Colorado River near Grand Canyon, AZ	Lower Colorado
USGS 09423000	Colorado River below Davis Dam, AZ-NV	Lower Colorado
USGS 09427520	Colorado River below Parker Dam, AZ-NV	Lower Colorado
USGS 09525500	Yuma Main Canal, AZ	Lower Colorado
USGS 09315000	Green River at Green River, UT	Green
USGS 09261000	Green River near Jensen, UT	Green
USGS 09211200	Green River below Fontenelle Reservoir, WY	Green
USGS 09365000	San Juan River at Farmington, NM	San Juan
USGS 09379500	San Juan River near Bluff, UT	San Juan
USGS 10322500	Humboldt River at Palisade, NV	Humboldt
USGS 10318500	Humboldt River near Elko, NV	Humboldt
USGS 10333000	Humbuldt River near Imlay, NV	Humboldt
USGS 11377100	Sacramento River at Bend Bridge, CA	Sacramento
USGS 11389500	Sacramento River at Colusa, CA	Sacramento
USGS 14038530	John Day River near John Day, OR	John Day
USGS 14046500	John Day River at Service Creek, OR	John Day
USGS 14048000	John Day River at McDonald Ferry, OR	John Day
USGS 13290450	Snake River at Hells Canyon Dam, ID-OR	Snake
USGS 13269000	Snake River at Weiser, ID	Snake
USGS 13334300	Snake River near Anatone, WA	Snake
USGS 13081500	Snake River at Howells Ferry,, ID	Snake

Table 4.1. USGS gauges

Table 4.1. A table of USGS gauges used to measure water-year hydroclimate variability. The "River Group" column refers to the names used in the manuscript and the respective gauges used for each respective river.

4.3.3 Variance decomposition and signal processing

To capture the spatial and temporal variability of drought and precipitation, we

use empirical orthogonal function (EOF) analysis of water-year anomalies. All climate

data in this study are analyzed as anomalies from the climatology (average of water-year

mean for the period of analysis). EOFs are computed from 1931 to 2019 for precipitation

as this is the available record of GPCC data and from 1931 to 2021 for PDSI. To

highlight a shift in the dominant mode of drought variability, EOFs are also computed for

the period from 1931 to 1975 (early period) and from 1976 to 2019 (recent period) over

the western United States (125°W-80°W and 30°N-52°N). We subsequently apply

Fourier and wavelet analysis to the leading principal component from EOF analysis to

isolate the dominant timescales of drought and precipitation variability (Grinsted et al.,

2004; Liu et al., 2007; Torrence & Compo, 1998; Torrence & Webster, 1999). These

same methods are applied to the historical and shared socioeconomic pathway 3-7.0

(SSP3-7) to understand the historical and potential future changes of the leading mode of

precipitation variability in the West.

One source of uncertainty in understanding low-frequency climate variability is

the relatively short record of in-situ climate data (Power et al., 2021). To combat this, we

use precipitation, SST and z250 from 50 ensemble members from the fully coupled

CESM2_LE historical run (Danabasoglu et al., 2020). The exact members used are listed

in Table 4.2. Each ensemble member is analyzed like the reanalysis data, as water-year

anomalies from the total period climatology (1901-2015), but we also remove the

ensemble mean (average of the 50 members varying in time) to focus on internal

variability. The time dimension of the 50 members is then stitched together, so that the

data is now shaped into 5700 years (50 members x 114 years), and EOF analysis is

applied to this time-stitched data to ensure that the same modes are being identified in

each member. The leading EOF of precipitation in the CESM2_LENS closely matches

the spatial pattern from the GPCC (Figure 4.1). Subsequently, the leading principal

component is then segmented into individual members, and we apply wavelet analysis to

find periods where decadal variability (8-16-years) is significant at the 95% confidence interval for at least 30 years. The same methods are used to obtain the leading EOFs of precipitation for the early period, the recent period and for near future (2020-2059) and end of century (2060-2099) climate projections.

Table 4.2. CESM2_LENS historical members included in Stuivenvolt-Allen et al. (2022)	
Macro perturbation (n=10)	Micro Perturbation (n=40)
1001	1231 (1-10)
1021	1251 (1-10)
1041	1281 (1-10)
1061	1301 (1-10
1081	
1101	
1121	
1141	
1161	
1181	

Table 4.2. Ensemble members used from the CESM2_LENS
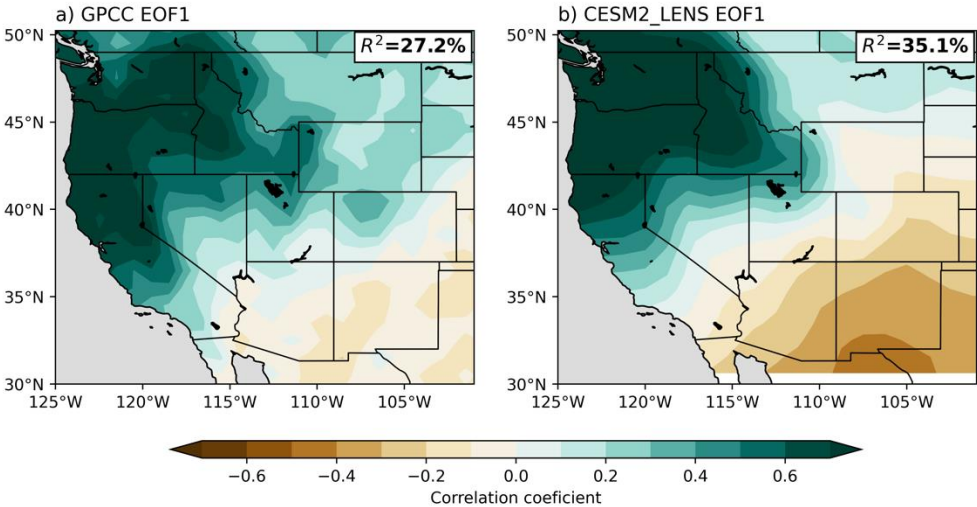
Figure 4.1. Leading EOF of precipitation for the western US expressed as correlation in the GPCC (a) and in the CESM2_LENS. Percent of variance explained by each EOF is embedded in the top right corner of the subplots.

4.4 Results and Discussion

4.4.1 Shift in the dominant frequency of pan-western drought

The temporal characteristics associated with the dominant mode of drought and precipitation variability have undergone a pronounced shift since the mid-1970s, motivating a separate treatment of the periods before and after 1975 (Figure 4.2). In analyzing precipitation, we can see the spatial pattern of the leading EOF pattern has drastically shifted as well. The early period was characterized by a northwest-southeast dipole pattern with anti-correlation between the Pacific Northwest and the rest of the focus area, to a pan-western pattern in the recent decades (Figure 4.3a,b). The dominant mode of precipitation variability is now associated with same sign impacts for almost all the western states. The changes to the leading EOF of PDSI largely mirrors precipitation (Figure 4.3d,e), showing a monopole-like pattern that is strongly correlated to drought in the entire western US. The importance of this shift is exemplified by the increased correlation between the leading modes of PDSI and precipitation with river discharge throughout the area (red dots). From the early period to the recent decades, drought has become more important and more tightly coupled with the discharge of major rivers throughout the west.
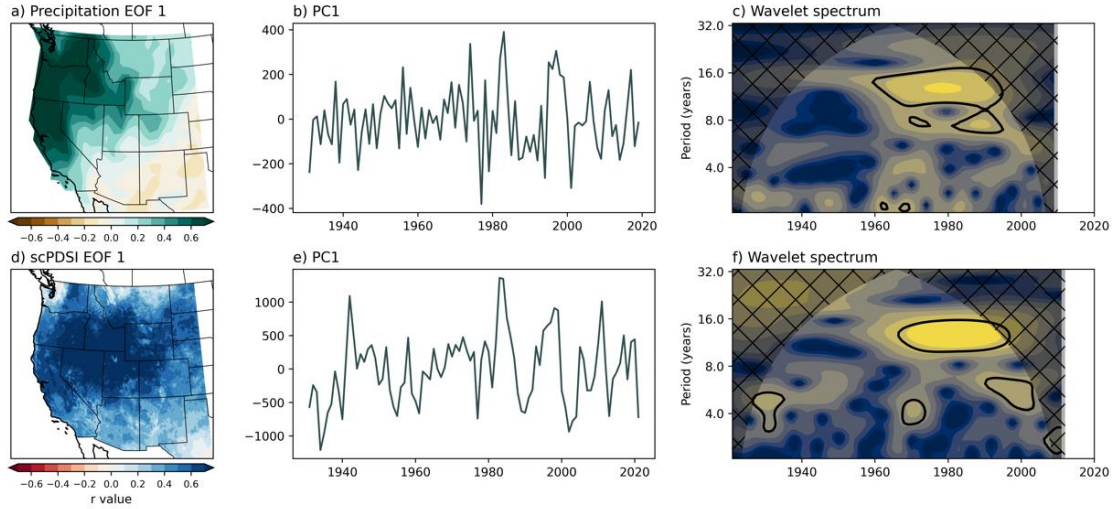
Figure 4.2. Leading EOF of precipitation from 1931-2019 (a), the associated principal component (b), and the wavelet spectrum of the principal component. Same as the top row, but for PDSI.
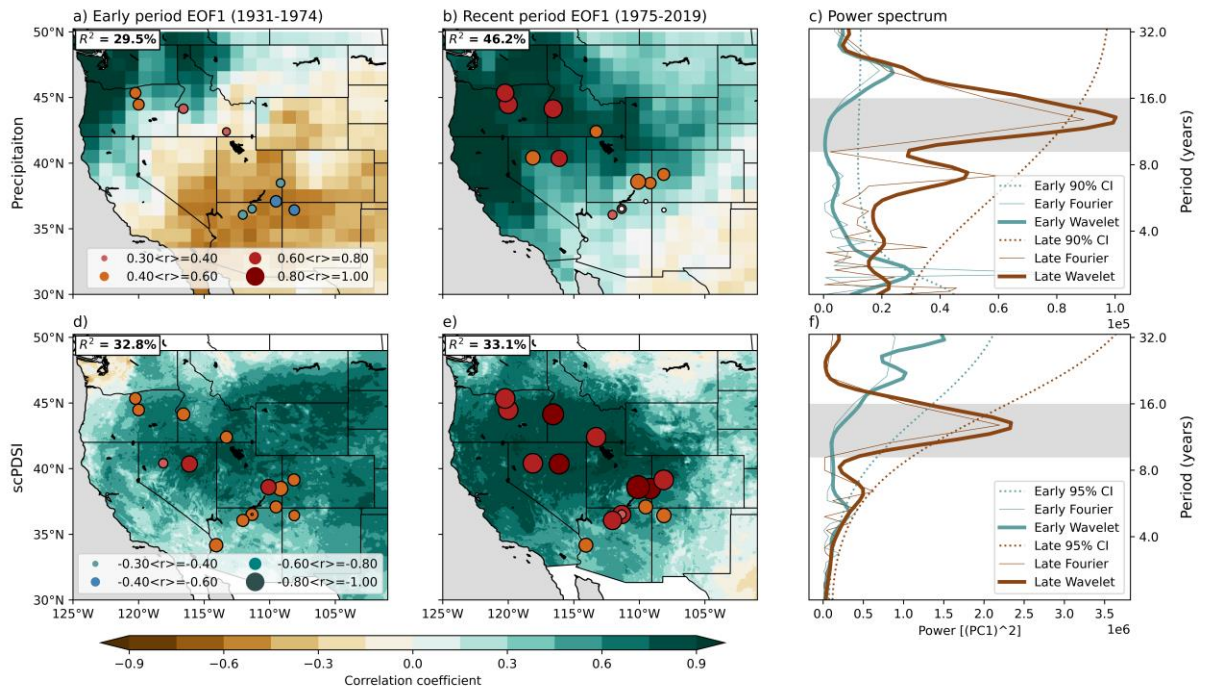
Figure 4.3. Dominant modes of variability in western US precipitation and drought along with their associated power spectra. EOF 1 of precipitation for the early period (a) and recent period (b). The red markers indicate the location and strength of the correlation coefficient between the leading principal component and river discharge for the USGS gauge in the respective location. Fourier and global wavelet power spectra of the early

and recent leading principal component from EOF analysis (c). Dotted lines indicate the 95% confidence threshold for statistical significance from a red-noise process. The bottom row shows the same analysis from (a-c) for PDSI (d-f).

More notable than the spatial shift in the leading modes is the shift in the dominant frequencies of temporal variability. Decadal variability (8-16 years) has become pronounced in both PDSI and precipitation's leading modes. This is shown through a comparison of the wavelet and Fourier spectrums, which highlight that decadal variability in the recent era explains a large fraction of the variance (power) of the total time series (Figure 4.2c,f, Figure 4.3c,d). Before 1975, it appears that western US hydroclimate fluctuated more chaotically, as the only significant peaks in explained variance can be seen at about two-year periods for precipitation and PDSI and four-six years for PDSI alone. Both cycles have been previously documented in western US hydroclimate, and they appear to be driven by ENSO (Cayan, 1996; Rajagopalan & Lall, 1998; Ropelewski & Halpert, 1986) or the biennial oscillation (Johnstone, 2011). Figure 4.4 depicts the second mode of PDSI and precipitation, which lacks widespread relationships with river discharge, underscoring the importance of the leading modes. Notably, decadal variability in precipitation was prominent in the second EOF during the early period. The spatial pattern also bears a resemblance to the leading EOF in the recent period, suggesting the dominant mode of precipitation has risen in rank since the early 20th century. However, this second mode still lacks the strong and widespread relationship with the Intermountain West shown in Figure 4.4.
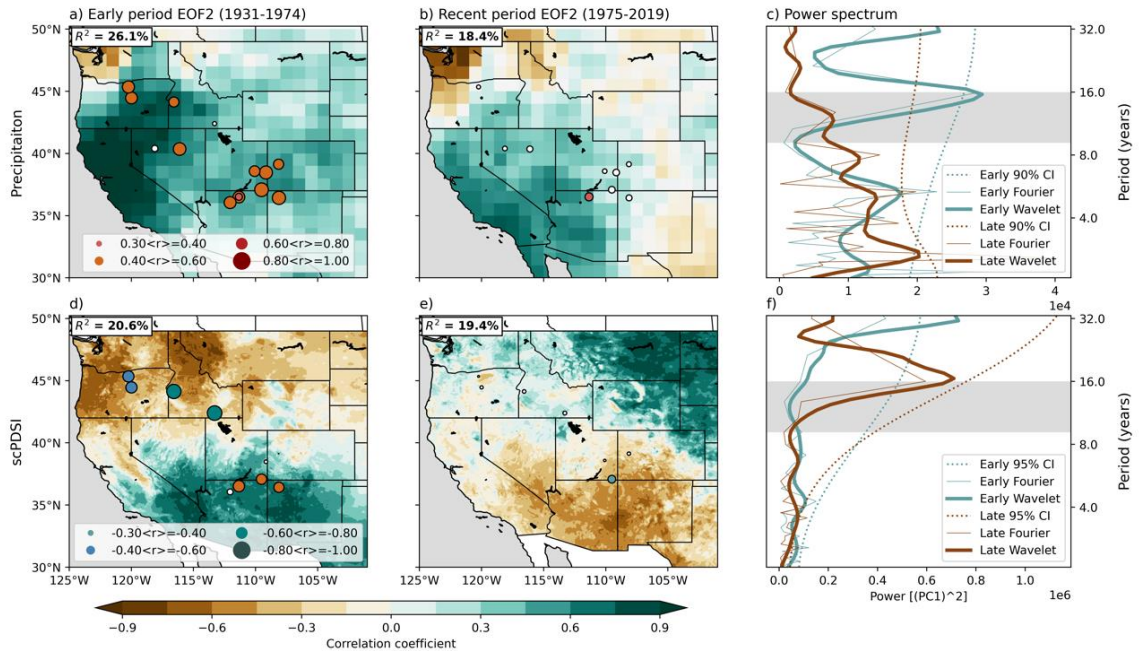
Figure 4.4. Second modes of variability in Western US precipitation and drought along with their associated power spectra. EOF 2 of standardized precipitation for the early period (a) and recent period (b). The red markers indicate the location and strength of the correlation coefficient between the leading principal component and river discharge for the USGS gauge in the respective location. Fourier and global wavelet power spectra of the early and recent leading principal component from EOF analysis (c). Dotted lines indicate the 95% confidence threshold for statistical significance from a red-noise process. The bottom row shows the same analysis from (a-c) for PDSI (d-f).

Decadal variability in precipitation and drought emerged in the leading mode of drought and precipitation around 1970 (Figure 4.2), as this is when the continuous wavelet transform began to pick up the significant low-frequency signal. Analogous results for the Upper Colorado River Basin were presented by Nowak et al. (2012) and Hidalgo & Dracup (2003). In addition to their results, we show that the emergence of the decadal signal is captured by almost all major rivers in the West. From the Snake in Oregon to the Colorado River at Lees Ferry, decadal variability became a significant factor in year-to-year fluctuations of river discharge in the 1970s (Figure 4.5b). Except for the San Juan River near the Four Corners, each river displays an emergence of

decadal variability (8-16-years) just after 1970 that persists through the 21st century (shown by the 95% confidence interval for each river's wavelet spectrum). There is no other period or cycle in river discharge that is shared by all these rivers, highlighting the large spatial extent of decadal hydroclimate variability from ~1970 to about 2010.
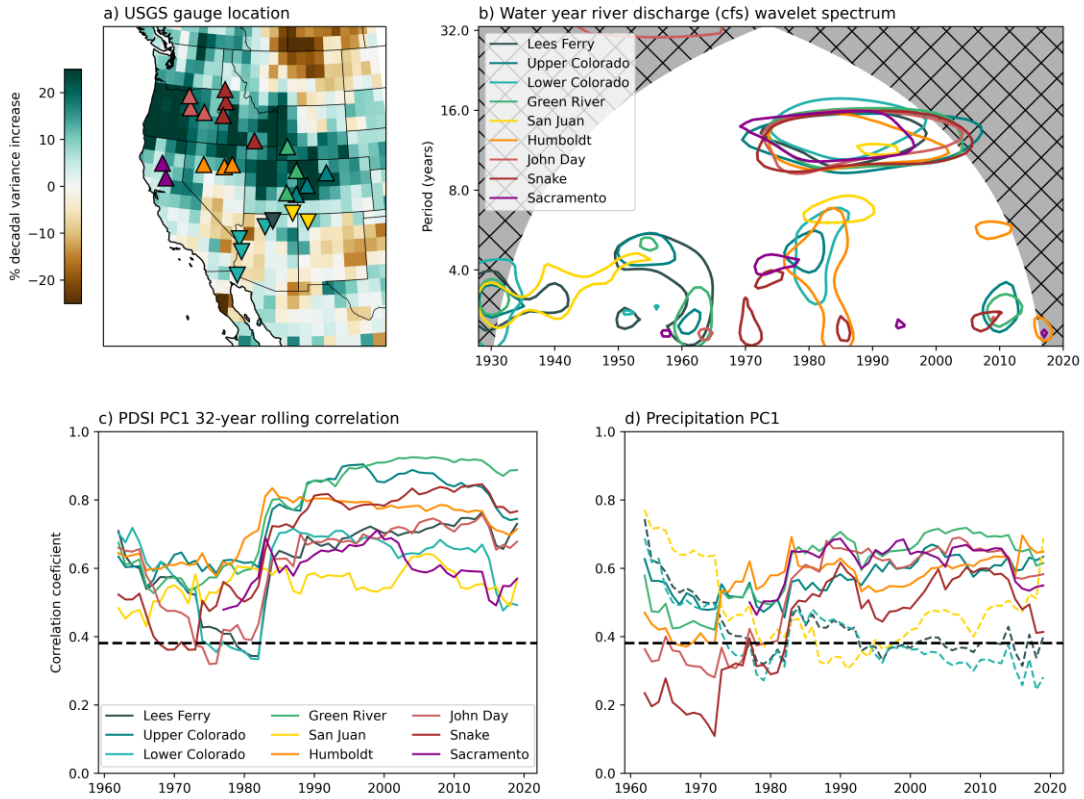
Figure 4.5. Difference in the percentage of variance explained by decadal cycles from the early period to the recent period (a, shading) along with the location of USGS gauges used in this study (markers). Triangles pointing up (down) indicate that the relationship between precipitation and river discharge is increasing (decreasing). The contour line of the 95% confidence threshold for the continuous wavelet power spectrum of river discharge averaged for each river (b). Included in (b) is the "cone of influence" which indicates regions of the wavelet spectrum where zero-padding in the Fourier transform introduces error into the data and hinders interpretation. The bottom row displays the 32-year rolling correlations for average river discharge with the leading principal components of PDSI and precipitation (c,d). The dashed black line indicates the 95% confidence threshold for the Pearson R correlation coefficient with 30 degrees of freedom.

From Figure 4.2 and Figure 4.5, it also appears that the decadal signal has waned in the last ten years. However, because the Fourier and wavelet transforms are applied to a finite-length time series, errors will occur at the ends of this data and may not accurately represent the decadal fluctuations in near-present data. It is unclear whether the decrease in significant decadal power is a true decrease or whether it is an artifact of the zero-padding involved in the Fourier transform (Torrence & Compo, 1998).

The growing relationship with drought and river discharge indicates a tighter coupling occurred between meteorological and hydrological drought during the period of pronounced decadal variability. Precipitation shows similar shifts in the northernmost rivers (Sacramento, Snake, John Day, Humboldt, Upper Colorado) but the relationship is decreasing for the gauges further to the south (Lower Colorado, Lees Ferry, San Juan). This is consistent given the northwest spatial shift of the leading mode of precipitation variability after 1970. As a result of rising decadal variability associated with precipitation and drought, multi-year persistence of river discharge has also increased, shown by the enhanced autocorrelation of river discharge in Figure 4.6. River discharge for the Colorado, the Green, the Humboldt, the San Juan and the Snake Rivers are now significantly autocorrelated at 1-year lead/lag and the autocorrelation remains significant for Lees Ferry at a 2-year lead/lag.
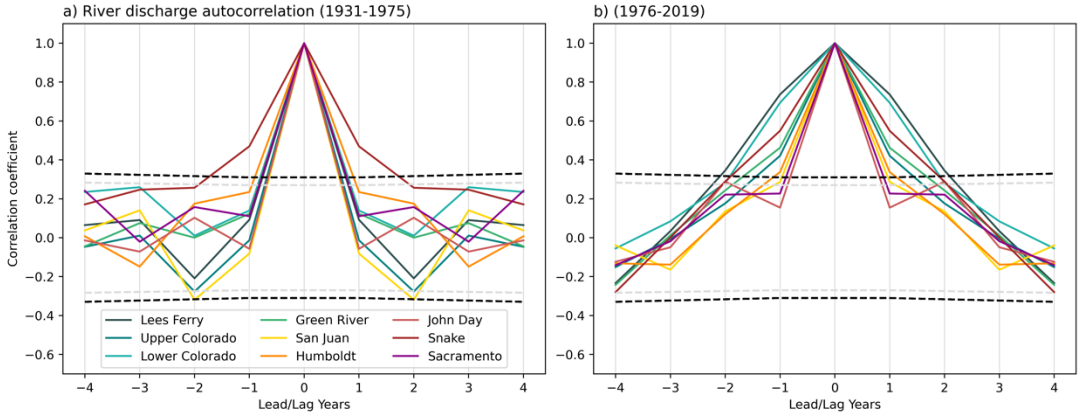
Figure 4.6. Autocorrelation between water-year averaged river-discharge for 9 major rivers in the western US in the early period (a) and recent period (b).

The emerging decadal signal is clearly captured by the leading mode of precipitation and PDSI, however, these EOFs explain less than 1/3rd of the total variance of precipitation and drought – stimulating interest in quantifying the importance of the emerging decadal variability on the total variance of precipitation and PDSI (Figure 4.7). This is accomplished by applying an 8-20-year bandpass filter to the anomalies of the gridded climate data and dividing the variance of the bandpass filtered data by the total variance of the unfiltered anomalies. In the recent period (1975-2019), the importance of decadal cycles has dramatically increased for large swaths of the focus area by greater than 25% for precipitation and upwards of 30% for PDSI (Figure 4.7a,b,c)
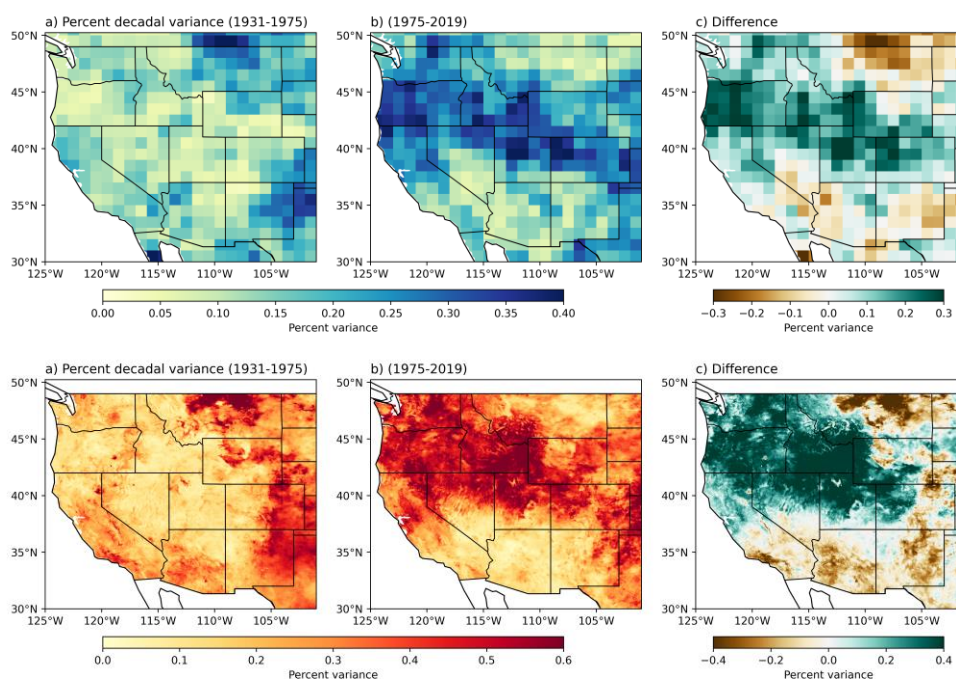
Figure 4.7. Ratio of decadal variance explained by 8-20-year variability in precipitation for the early period (a) and the recent period (b) along with the difference of the two periods (c). The bottom row shows the same analysis from (a-c) for PDSI (d-f).

4.4.2 Associated shifts in ocean and atmosphere variability

Figure 4.8 shows that large-scale circulation features in the North Pacific also experienced a rapid increase in the importance of decadal variability in the 1970s. From 1931 to 1975, decadal variability in SST was most dominant in the western and eastern tropical Pacific, and along the coast of western North America (Figure 4.8a). Much of the North Pacific in the recent era has greater than 40% of variance explained by decadal cycles with a spatial pattern that matches the observed shift in the North Pacific (Figure 4.7b) (Miller et al., 1994). The western tropical Pacific, the Kuroshio current region, and the SST adjacent to the west coast of North America experienced the largest increase in decadal variance (>30%). Similar findings are present in z250, as decadal variance

strongly emerged (~20% increase) in the east Asian sub-tropical jet stream and along the

coast of the western US (Figure 4.8d,e,f) – regions which heavily influence moisture

transport and drought variability for the western US (Teng & Branstator, 2017; S.-Y.

Wang et al., 2009; Zhang et al., 2022).
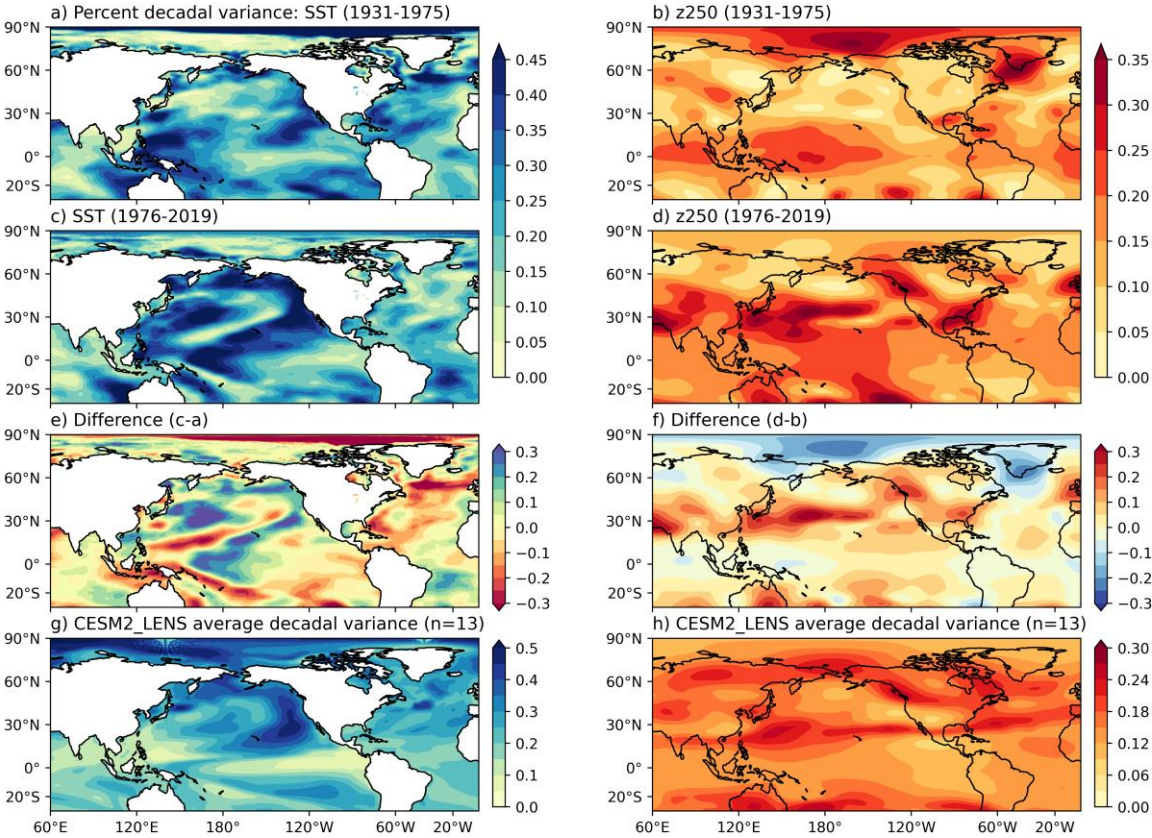
Figure 4.8. Percent of decadal variance explained by 8-20-year variability in SST and Z250 for the early period (a,b) and the recent period (c,d) along with the difference of the two periods (e,f). Average ratio of decadal variance explained by 8-20-year variability in SST (e) and z250 (f) for the 13 cases of amplified decadal variability in the leading principal component of western US precipitation in the CESM2_LENS.

To analyze the potential for the emergence of decadal hydroclimate variability to

be influenced by anthropogenic climate change, we first find similar periods of amplified

decadal variability in the CESM2_LENS historical run to ensure the models simulation of

decadal North Pacific climate variability is analogous to reanalysis. In total, 13 periods of

amplified decadal variability were found in 50 members from the CESM2_LENS. The average amount of variance explained by decadal cycles in SST shows a pattern that generally matches observations with the average power from the 13 cases concentrated along the West Coast of North America and spreading towards the western Tropical Pacific. Additionally, a center of action in the western North Pacific is captured by the average power from these cases. The decadal variance in z250 associated with these 13 cases also matches the observed period. Both reanalysis and CESM2_LENS show a band of amplified decadal variability around 30°N in the Pacific, likely from an expansion of the tropical Hadley cell. Additionally, the long-term cycles of precipitation are associated with prolonged atmospheric blocking or anomalously low-pressure as both the CESM2_LENS and reanalysis capture a pronounced decadal signal in upper-level pressure along the west coast of North America.

The ability of 12 members to capture periods where decadal variability explained a significant amount of variance in the leading EOF of western US precipitation suggests that these ensemble members have features that distinguish them from the other 38 members. As mean-state climate features can dictate and influence the expression of climate variability (Bayr et al., 2019; Di Carlo et al., 2022; Held & Ting, 1990; Li et al., 2020; Trenberth et al., 1998), we hypothesize that mean-state heating distributions or circulation features (i.e. jet-stream location and intensity) may shift and result in periods conducive for low-frequency variability in western US precipitation. First, using ERA20c Reanalysis we show the difference of the mean-state for SST, U250, and Z250 for the period with significant decadal variability (1974-2020) from the total period in this analysis (1930-2020) (Figure 4.9a-c). This analysis shows that the recent mean-state

climate has been characterized by a El Niño-like warming pattern when compared to the early period (1930-1974). The cooling of the central North Pacific along with the enhanced warming in the tropical Pacific is consistent with the Pacific climate shift of 1976 (Hartmann & Wendler, 2005; Meehl et al., 2009; Miller et al., 1994). There are notable changes in upper-level zonal wind as well, generally characterized by a strengthening, elongation, and slight southward shift of the North Pacific jet stream. Associated with these zonal wind changes and SST changes, the Z250 field shows a deepening of the Aleutian Low and an atmospheric wave-train over North America. Comparing these reanalysis features to the composite mean states from the CESM2_LENS shows generally similar differences from the ensemble mean. The most notable differences between the CESM2_LENS and reanalysis are difference in the strength of the Aleutian Low (Figure 4.9d-f) and the larger tropical signal present in the SST and Z250 fields in the CESM2_LENS (Figure 4.9d,f). While uncertainty remains in the efficacy of upper-level fields in 20th century reanalysis datasets (Laloyaux et al., 2018; Poli et al., 2016), the similarities between reanalysis and the CESM2_LENS results suggest that El Niño-like mean state patterns are conducive for decadal variability in western US precipitation. As global heating distributions, largely driven by heterogeneity in SSTs, are a fundamental factor in northern hemisphere circulation and stationary waves, (Chang, 2009; Held et al., 2002; Hoskins & Karoly, 1981) these low-frequency shifts in SST mean-states (Figure 4.9) may alter the dominant timescales of variability (Figure 4.8) in northern hemisphere circulation patterns and in-turn, precipitation.
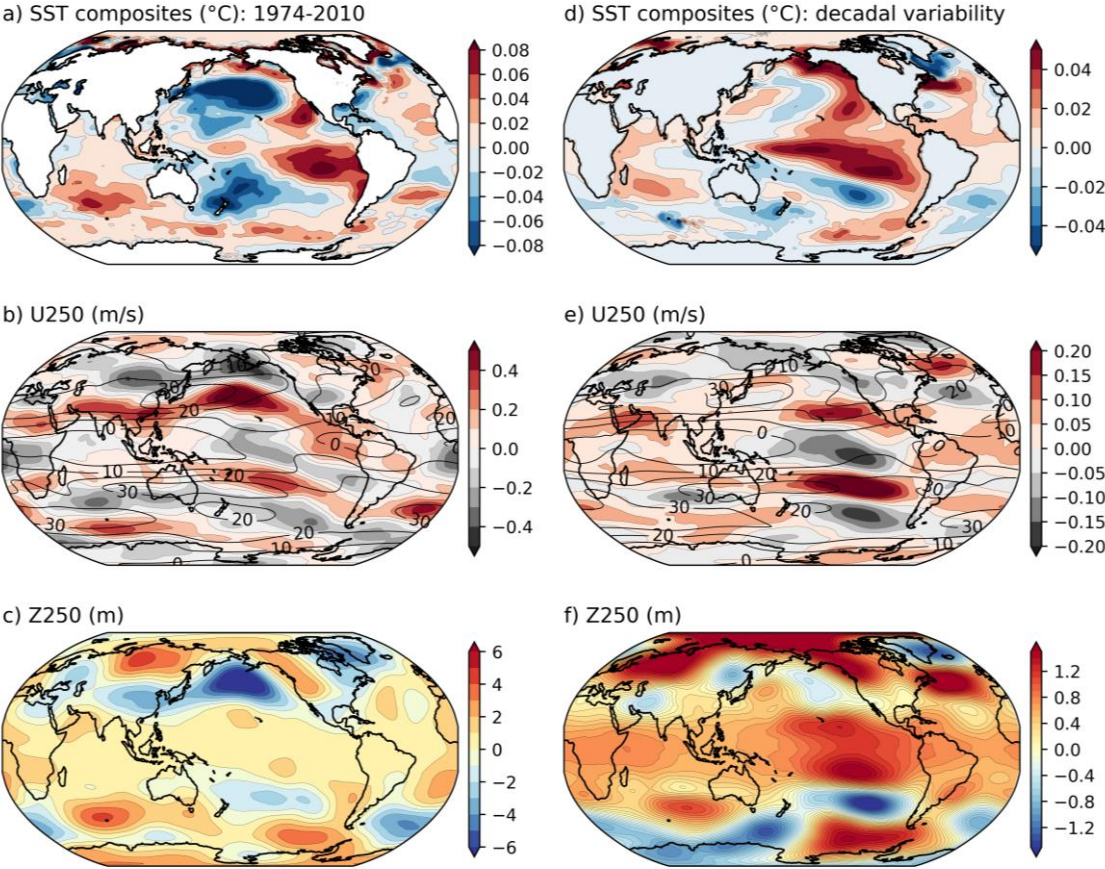
Figure 4.9. Difference of the 1974-2010 mean-state (a) SST, (b) U250 and (c) Z250 from the 1930-2010 mean-state in COBE SST data and ERA20c Reanalysis. Difference of the composite mean states of the 12 CESM2_LENS members (simulation years 1900-2014) with significant decadal variability in western US precipitation from the ensemble mean for (d) SST, (e) U250, and (f) Z250. Contours in (b) indicate the total period climatology of U250 while contours in (e) represent the CESM2_LENS ensemble mean for 1900-2014.

These interactions between climate mean-state conditions and variability are at the limit of current understanding and theory. This is partially due to the limitations of a relatively short observational record to study multi-decadal climate variability and change. Global climate models and idealized models have contributed greatly to our understanding about the interplay between low-frequency climate change/variability and higher-frequency phenomena (Cai et al., 2021; D'Arrigo et al., 2005; Enfield, 1989; Li et

al., 2020), but more mechanistic insight is needed to confidently link this El-Niño like warming pattern to North American decadal variability.

Decadal precipitation variability has been shown to be more predictable (McCabe & Dettinger, 1999), more widespread throughout the West (Figure 4.3), and more strongly associated with river discharge variability (Figure 4.3,4.5), but the extent to which this amplified decadal variability will continue is unknown. To estimate how important decadal hydroclimate variability will be in the warming future, we provide the leading EOF of precipitation for different time periods in the CESM2_LENS historical and SSP3-7 scenarios. The spatial pattern of EOF1 closely matches the leading EOF from the GPCC (Figure 4.1) and does not make any dramatic shifts from the historical into the SSP3-7 scenario (Figure 4.9a-d). The CESM2_LENS does capture an increase in decadal power from the early period to the recent period (Figure 4.10e,f), but low-frequency variability becomes less powerful into 21st century. The average Fourier and wavelet spectra for the 50 members show that high-frequency variability becomes more dominant under the enhanced warming scenario (Figure 4.10f). These results support recent findings that anthropogenic climate change will reduce the amplitude of Pacific decadal variability in the North Pacific (Sun et al., 2022). Associated with this preference for high-frequency variations, fluctuations in hydroclimate may become less predictable and more chaotic. Large uncertainties exist due to the importance of internal variability in Pacific decadal variability and model deficiencies in simulating hydroclimate variability (Capotondi et al., 2020; Deser et al., 2011, 2012; Lehner et al., 2019; Power et al., 2021; Sun et al., 2022). Further assessment will be needed to elucidate the relationship between anthropogenic climate change and amplified states of Pacific decadal variability.
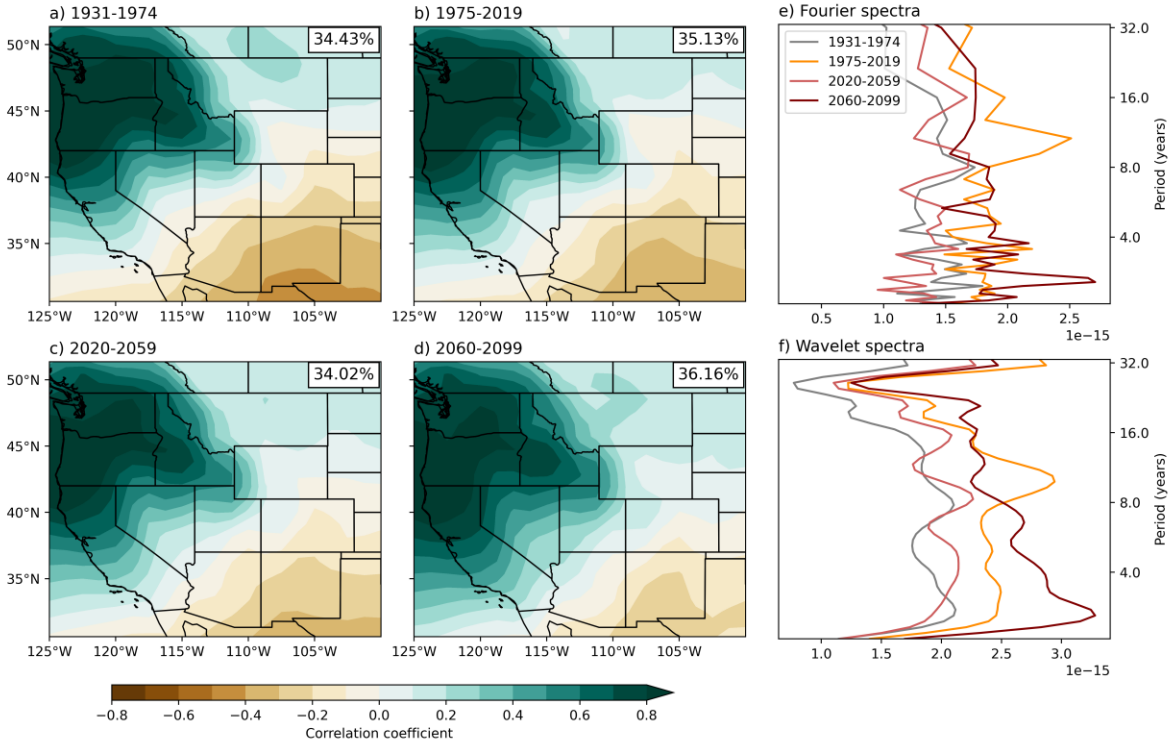
Figure 4.10. Leading EOF of precipitation in the CESM2_LENS historical (1931-2014) and SSP3-7 (2015-2099) scenario for (a) the early period, (b) the recent period, (c) the recent future (c, 2020-2059) and (d) the end of century (2060-2099). The power spectra of the leading principal component from the 50 ensemble members using Fourier methods (a) and the wavelet spectral methods (f) for each period.

4.5 Conclusions

After the mid-1970s, decadal variability became the dominant timescale of variability in precipitation, PDSI, and streamflow for the western US. From the Pacific Northwest into the Colorado Rockies, the variance explained by decadal cycles increased of precipitation and drought increased by 20-40%. During this period, interannual hydrological and meteorological drought (as captured by streamflow and precipitation/PDSI) became more tightly coupled and multi-year droughts or wet periods were increasingly common, suggesting that empirical prediction tools may have become more useful in the last 40 years (McCabe & Dettinger, 1999).

These large changes in western US hydroclimate are associated with prominent increases of decadal variance in SST and z250 in the North Pacific (Miller et al., 1994; Yeh et al., 2011). In finding similar periods of amplified decadal variability in western US precipitation within the CESM2_LENS, the observed SST and z250 features closely match the cases from the model suggesting that decadal variability is commonly augmented through mechanisms analogous to what the Pacific has experienced in recent decades. Future projections of the leading mode of precipitation show that climate change may preferentially result in higher frequency variability of precipitation (Sun et al., 2022) which has historically been less predictable and less tightly coupled to hydrologic drought (McCabe & Dettinger, 1999). However, more work is needed to further understand the role of anthropogenic forcing and the possibility that climate change may alter the likelihood or magnitude of similar periods of decadal hydroclimate variability.

REFERENCES

Abatzoglou, J. T., McEvoy, D. J., & Redmond, K. T. (2017). The West Wide Drought Tracker: Drought Monitoring at Fine Spatial Scales. *Bulletin of the American Meteorological Society*, *98*(9), 1815–1820. https://doi.org/10.1175/BAMS-D-16-0193.1

Anderson, W., Seager, R., Baethgen, W., & Cane, M. (2018). Trans-Pacific ENSO teleconnections pose a correlated risk to agriculture. *Agricultural and Forest Meteorology*, *262*, 298–309. https://doi.org/10.1016/j.agrformet.2018.07.023

Ault, T. R., Cole, J. E., Overpeck, J. T., Pederson, G. T., George, S. S., Otto-Bliesner, B., Woodhouse, C. A., & Deser, C. (2013). The Continuum of Hydroclimate Variability in Western North America during the Last Millennium. *Journal of Climate*, *26*(16), 5863–5878. https://doi.org/10.1175/JCLI-D-11-00732.1

Bayr, T., Domeisen, D. I. V., & Wengel, C. (2019). The effect of the equatorial Pacific cold SST bias on simulated ENSO teleconnections to the North Pacific and California. *Climate Dynamics*, *53*(7), 3771–3789. https://doi.org/10.1007/s00382-019-04746-9

Cai, W., Santoso, A., Collins, M., Dewitte, B., Karamperidou, C., Kug, J.-S., Lengaigne, M., McPhaden, M. J., Stuecker, M. F., Taschetto, A. S., Timmermann, A., Wu, L., Yeh, S.-W., Wang, G., Ng, B., Jia, F., Yang, Y., Ying, J., Zheng, X.-T., … Zhong, W. (2021). Changing El Niño–Southern Oscillation in a warming climate. *Nature Reviews Earth & Environment*, *2*(9), 628–644. https://doi.org/10.1038/s43017-021-00199-z

Capotondi, A., Deser, C., Phillips, A. S., Okumura, Y., & Larson, S. M. (2020). ENSO and Pacific Decadal Variability in the Community Earth System Model Version 2. *Journal of Advances in Modeling Earth Systems*, *12*(12), e2019MS002022. https://doi.org/10.1029/2019MS002022

Cayan, D. R. (1996). Interannual Climate Variability and Snowpack in the Western United States. *Journal of Climate*, *9*(5), 928–948. https://doi.org/10.1175/1520-0442(1996)009<0928:ICVASI>2.0.CO;2

Cayan, D. R., Dettinger, M. D., Diaz, H. F., & Graham, N. E. (1998). Decadal Variability of Precipitation over Western North America. *Journal of Climate*, *11*(12), 3148–3166. https://doi.org/10.1175/1520-0442(1998)011<3148:DVOPOW>2.0.CO;2

Chang, E. K. M. (2009). Diabatic and Orographic Forcing of Northern Winter Stationary Waves and Storm Tracks. *Journal of Climate*, *22*(3), 670–688. https://doi.org/10.1175/2008JCLI2403.1

Chen, L. G., Gottschalck, J., Hartman, A., Miskus, D., Tinker, R., & Artusa, A. (2019). Flash Drought Characteristics Based on U.S. Drought Monitor. *Atmosphere*, *10*(9), 498. https://doi.org/10.3390/atmos10090498

Chikamoto, Y., Timmermann, A., Widlansky, M. J., Balmaseda, M. A., & Stott, L. (2017). Multi-year predictability of climate, drought, and wildfire in southwestern

North America. *Scientific Reports*, *7*(1), 6568. https://doi.org/10.1038/s41598-017-06869-7

Chikamoto, Y., Wang, S.-Y. S., Yost, M., Yocom, L., & Gillies, R. R. (2020). Colorado River water supply is predictable on multi-year timescales owing to long-term ocean memory. *Communications Earth & Environment*, *1*(1), 1–11. https://doi.org/10.1038/s43247-020-00027-0

Clark, M. P., Serreze, M. C., & McCabe, G. J. (2001). Historical effects of El Nino and La Nina events on the seasonal evolution of the montane snowpack in the Columbia and Colorado River Basins. *Water Resources Research*, *37*(3), 741–757. https://doi.org/10.1029/2000WR900305

Cole, J. E., Overpeck, J. T., & Cook, E. R. (2002). Multiyear La Niña events and persistent drought in the contiguous United States. *Geophysical Research Letters*, *29*(13), 25-1-25–4. https://doi.org/10.1029/2001GL013561

Cook, B. I., Seager, R., & Miller, R. L. (2011). On the Causes and Dynamics of the Early Twentieth-Century North American Pluvial. *Journal of Climate*, *24*(19), 5043–5060. https://doi.org/10.1175/2011JCLI4201.1

Cook, B. I., Williams, A. P., Mankin, J. S., Seager, R., Smerdon, J. E., & Singh, D. (2018). Revisiting the Leading Drivers of Pacific Coastal Drought Variability in the Contiguous United States. *Journal of Climate*, *31*(1), 25–43. https://doi.org/10.1175/JCLI-D-17-0172.1

Danabasoglu, G., Lamarque, J.-F., Bacmeister, J., Bailey, D. A., DuVivier, A. K., Edwards, J., Emmons, L. K., Fasullo, J., Garcia, R., Gettelman, A., Hannay, C., Holland, M. M., Large, W. G., Lauritzen, P. H., Lawrence, D. M., Lenaerts, J. T. M., Lindsay, K., Lipscomb, W. H., Mills, M. J., … Strand, W. G. (2020). The Community Earth System Model Version 2 (CESM2). *Journal of Advances in Modeling Earth Systems*, *12*(2), e2019MS001916. https://doi.org/10.1029/2019MS001916

D'Arrigo, R., Cook, E. R., Wilson, R. J., Allan, R., & Mann, M. E. (2005). On the variability of ENSO over the past six centuries. *Geophysical Research Letters*, *32*(3). https://doi.org/10.1029/2004GL022055

Deser, C., Phillips, A., Bourdette, V., & Teng, H. (2012). Uncertainty in climate change projections: The role of internal variability. *Climate Dynamics*, *38*(3), 527–546. https://doi.org/10.1007/s00382-010-0977-x

Deser, C., Phillips, A. S., Tomas, R. A., Okumura, Y. M., Alexander, M. A., Capotondi, A., Scott, J. D., Kwon, Y.-O., & Ohba, M. (2011). ENSO and Pacific Decadal Variability in the Community Climate System Model Version 4. *Journal of Climate*, *25*(8), 2622–2651. https://doi.org/10.1175/JCLI-D-11-00301.1

Dettinger, M. (2016). Historical and Future Relations Between Large Storms and Droughts in California. *San Francisco Estuary and Watershed Science*, *14*(2). https://doi.org/10.15447/sfews.2016v14iss2art1

Dettinger, M., & Cayan, D. R. (2014). Drought and the California Delta—A Matter of Extremes. *San Francisco Estuary and Watershed Science*, *12*(2). https://doi.org/10.15447/sfews.2014v12iss2art4

Dettinger, M., Udall, B., & Georgakakos, A. (2015). Western water and climate change. *Ecological Applications*, *25*(8), 2069–2093. https://doi.org/10.1890/15-0938.1

Di Carlo, E., Ruggieri, P., Davini, P., Tibaldi, S., & Corti, S. (2022). ENSO teleconnections and atmospheric mean state in idealised simulations. *Climate Dynamics*. https://doi.org/10.1007/s00382-022-06261-w

Enfield, D. B. (1989). El Niño, past and present. *Reviews of Geophysics*, *27*(1), 159–187. https://doi.org/10.1029/RG027i001p00159

Gangopadhyay, S., McCabe, G., Pederson, G., Martin, J., & Littell, J. S. (2019). Risks of hydroclimatic regime shifts across the western United States. *Scientific Reports*, *9*(1), 6303. https://doi.org/10.1038/s41598-019-42692-y

Goodrich, G. B. (2007). Influence of the Pacific Decadal Oscillation on Winter Precipitation and Drought during Years of Neutral ENSO in the Western United States. *Weather and Forecasting*, *22*(1), 116–124. https://doi.org/10.1175/WAF983.1

Grinsted, A., Moore, J. C., & Jevrejeva, S. (2004). Application of the cross wavelet transform and wavelet coherence to geophysical time series. *Nonlinear Processes in Geophysics*, *11*(5/6), 561–566. https://doi.org/10.5194/npg-11-561-2004

Hartmann, B., & Wendler, G. (2005). The Significance of the 1976 Pacific Climate Shift in the Climatology of Alaska. *Journal of Climate*, *18*(22), 4824–4839. https://doi.org/10.1175/JCLI3532.1

Held, I. M., & Ting, M. (1990). Orographic versus Thermal Forcing of Stationary Waves: The Importance of the Mean Low-Level Wind. *Journal of the Atmospheric Sciences*, *47*(4), 495–500. https://doi.org/10.1175/1520-0469(1990)047<0495:OVTFOS>2.0.CO;2

Held, I. M., Ting, M., & Wang, H. (2002). Northern Winter Stationary Waves: Theory and Modeling. *Journal of Climate*, *15*(16), 2125–2144. https://doi.org/10.1175/1520-0442(2002)015<2125:NWSWTA>2.0.CO;2

Hidalgo, H. G., Das, T., Dettinger, M. D., Cayan, D. R., Pierce, D. W., Barnett, T. P., Bala, G., Mirin, A., Wood, A. W., Bonfils, C., Santer, B. D., & Nozawa, T. (2009). Detection and Attribution of Streamflow Timing Changes to Climate Change in the Western United States. *Journal of Climate*, *22*(13), 3838–3855. https://doi.org/10.1175/2009JCLI2470.1

Hidalgo, H. G., & Dracup, J. A. (2003). ENSO and PDO Effects on Hydroclimatic Variations of the Upper Colorado River Basin. *Journal of Hydrometeorology*, *4*(1), 5–23. https://doi.org/10.1175/1525-7541(2003)004<0005:EAPEOH>2.0.CO;2

Hoskins, B. J., & Karoly, D. J. (1981). The Steady Linear Response of a Spherical Atmosphere to Thermal and Orographic Forcing. *Journal of the Atmospheric*

Sciences, *38*(6), 1179–1196. https://doi.org/10.1175/1520-0469(1981)038<1179:TSLROA>2.0.CO;2

Ishii, M., Shouji, A., Sugimoto, S., & Matsumoto, T. (2005). Objective analyses of sea-surface temperature and marine meteorological variables for the 20th century using ICOADS and the Kobe Collection. *International Journal of Climatology*, *25*(7), 865–879. https://doi.org/10.1002/joc.1169

Johnstone, J. A. (2011). A quasi-biennial signal in western US hydroclimate and its global teleconnections. *Climate Dynamics*, *36*(3), 663–680. https://doi.org/10.1007/s00382-010-0755-9

Kalnay, E., Kanamitsu, M., Kistler, R., Collins, W., Deaven, D., Gandin, L., Iredell, M., Saha, S., White, G., Woollen, J., Zhu, Y., Chelliah, M., Ebisuzaki, W., Higgins, W., Janowiak, J., Mo, K. C., Ropelewski, C., Wang, J., Leetmaa, A., … Joseph, D. (1996). The NCEP/NCAR 40-Year Reanalysis Project. *Bulletin of the American Meteorological Society*, *77*(3), 437–472. https://doi.org/10.1175/1520-0477(1996)077<0437:TNYRP>2.0.CO;2

Laloyaux, P., de Boisseson, E., Balmaseda, M., Bidlot, J.-R., Broennimann, S., Buizza, R., Dalhgren, P., Dee, D., Haimberger, L., Hersbach, H., Kosaka, Y., Martin, M., Poli, P., Rayner, N., Rustemeier, E., & Schepers, D. (2018). CERA-20C: A Coupled Reanalysis of the Twentieth Century. *Journal of Advances in Modeling Earth Systems*, *10*(5), 1172–1195. https://doi.org/10.1029/2018MS001273

Latif, M., & Barnett, T. P. (1996). Decadal Climate Variability over the North Pacific and North America: Dynamics and Predictability. *Journal of Climate*, *9*(10), 2407–2423. https://doi.org/10.1175/1520-0442(1996)009<2407:DCVOTN>2.0.CO;2

Lehner, F., Wood, A. W., Vano, J. A., Lawrence, D. M., Clark, M. P., & Mankin, J. S. (2019). The potential to reduce uncertainty in regional runoff projections from climate models. *Nature Climate Change*, *9*(12), 926–933. https://doi.org/10.1038/s41558-019-0639-x

Li, R. K. K., Woollings, T., O'Reilly, C., & Scaife, A. A. (2020). Effect of the North Pacific Tropospheric Waveguide on the Fidelity of Model El Niño Teleconnections. *Journal of Climate*, *33*(12), 5223–5237. https://doi.org/10.1175/JCLI-D-19-0156.1

Liu, Y., Liang, X. S., & Weisberg, R. H. (2007). Rectification of the Bias in the Wavelet Power Spectrum. *Journal of Atmospheric and Oceanic Technology*, *24*(12), 2093–2102. https://doi.org/10.1175/2007JTECHO511.1

Mantua, N. J., Hare, S. R., Zhang, Y., Wallace, J. M., & Francis, R. C. (1997). A Pacific Interdecadal Climate Oscillation with Impacts on Salmon Production*. *Bulletin of the American Meteorological Society*, *78*(6), 1069–1080. https://doi.org/10.1175/1520-0477(1997)078<1069:APICOW>2.0.CO;2

Marshall, A. M., Abatzoglou, J. T., Link, T. E., & Tennant, C. J. (2019). Projected Changes in Interannual Variability of Peak Snowpack Amount and Timing in the Western United States. *Geophysical Research Letters*, *46*(15), 8882–8892. https://doi.org/10.1029/2019GL083770

Martin, J. T., Pederson, G. T., Woodhouse, C. A., Cook, E. R., McCabe, G. J., Anchukaitis, K. J., Wise, E. K., Erger, P. J., Dolan, L., McGuire, M., Gangopadhyay, S., Chase, K. J., Littell, J. S., Gray, S. T., St. George, S., Friedman, J. M., Sauchyn, D. J., St-Jacques, J.-M., & King, J. (2020). Increased drought severity tracks warming in the United States' largest river basin. *Proceedings of the National Academy of Sciences*, *117*(21), 11328–11336. https://doi.org/10.1073/pnas.1916208117

McCabe, G. J., & Dettinger, M. D. (1999). Decadal variations in the strength of ENSO teleconnections with precipitation in the western United States. *International Journal of Climatology*, *19*(13), 1399–1410. https://doi.org/10.1002/(SICI)1097-0088(19991115)19:13<1399::AID-JOC457>3.0.CO;2-A

McCabe, G. J., Palecki, M. A., & Betancourt, J. L. (2004). Pacific and Atlantic Ocean influences on multidecadal drought frequency in the United States. *Proceedings of the National Academy of Sciences*, *101*(12), 4136–4141. https://doi.org/10.1073/pnas.0306738101

Meehl, G. A., Hu, A., & Santer, B. D. (2009). The Mid-1970s Climate Shift in the Pacific and the Relative Roles of Forced versus Inherent Decadal Variability. *Journal of Climate*, *22*(3), 780–792. https://doi.org/10.1175/2008JCLI2552.1

Miller, A. J., Cayan, D. R., Barnett, T. P., Graham, N. E., & Oberhuber, J. M. (1994). The 1976-77 Climate Shift of the Pacific Ocean. *Oceanography*, *7*(1), 21–26.

Mock, C. J. (1996). Climatic Controls and Spatial Variations of Precipitation in the Western United States. *Journal of Climate*, *9*(5), 1111–1125. https://doi.org/10.1175/1520-0442(1996)009<1111:CCASVO>2.0.CO;2

Morgan, B., Spangler, K., Stuivenvolt Allen, J., Morrisett, C. N., Brunson, M. W., Wang, S.-Y. S., & Huntly, N. (2021). Water Availability for Cannabis in Northern California: Intersections of Climate, Policy, and Public Discourse. *Water*, *13*(1). https://doi.org/10.3390/w13010005

Nitta, T., & Yamada, S. (1989). Recent Warming of Tropical Sea Surface Temperature and Its Relationship to the Northern Hemisphere Circulation. *Journal of the Meteorological Society of Japan. Ser. II*, *67*(3), 375–383. https://doi.org/10.2151/jmsj1965.67.3_375

Nowak, K., Hoerling, M., Rajagopalan, B., & Zagona, E. (2012). Colorado River Basin Hydroclimatic Variability. *Journal of Climate*, *25*(12), 4389–4403. https://doi.org/10.1175/JCLI-D-11-00406.1

Poli, P., Hersbach, H., Dee, D. P., Berrisford, P., Simmons, A. J., Vitart, F., Laloyaux, P., Tan, D. G. H., Peubey, C., Thépaut, J.-N., Trémolet, Y., Hólm, E. V., Bonavita, M., Isaksen, L., & Fisher, M. (2016). ERA-20C: An Atmospheric Reanalysis of the Twentieth Century. *Journal of Climate*, *29*(11), 4083–4097. https://doi.org/10.1175/JCLI-D-15-0556.1

Power, S., Lengaigne, M., Capotondi, A., Khodri, M., Vialard, J., Jebri, B., Guilyardi, E., McGregor, S., Kug, J. S., Newman, M., McPhaden, M. J., Meehl, G., Smith, D., Cole, J., Emile-Geay, J., Vimont, D., Wittenberg, A. T., Collins, M., Kim, G. I.,

… Henley, B. J. (2021). Decadal climate variability in the tropical Pacific: Characteristics, causes, predictability, and prospects. *Science*, *374*(6563), eaay9165. https://doi.org/10.1126/science.aay9165

Rajagopalan, B., & Lall, U. (1998). Interannual variability in western US precipitation. *Journal of Hydrology*, *210*(1), 51–67. https://doi.org/10.1016/S0022-1694(98)00184-X

Ropelewski, C. F., & Halpert, M. S. (1986). North American Precipitation and Temperature Patterns Associated with the El Niño/Southern Oscillation (ENSO). *Monthly Weather Review*, *114*(12), 2352–2362. https://doi.org/10.1175/1520-0493(1986)114<2352:NAPATP>2.0.CO;2

Schneider, U., Becker, A., Finger, P., Meyer-Christoffer, A., Ziese, M., & Rudolf, B. (2014). GPCC's new land surface precipitation climatology based on quality-controlled in situ data and its role in quantifying the global water cycle. *Theoretical and Applied Climatology*, *115*(1), 15–40. https://doi.org/10.1007/s00704-013-0860-x

Schoennagel, T., Veblen, T. T., Kulakowski, D., & Holz, A. (2007). Multidecadal Climate Variability and Climate Interactions Affect Subalpine Fire Occurrence, Western Colorado (usa). *Ecology*, *88*(11), 2891–2902. https://doi.org/10.1890/06-1860.1

Schulte, J. A., & Lee, S. (2017). Strengthening North Pacific Influences on United States Temperature Variability. *Scientific Reports*, *7*(1). https://doi.org/10.1038/s41598-017-00175-y

Seager, R., Hooks, A., Williams, A. P., Cook, B., Nakamura, J., & Henderson, N. (2015). Climatology, Variability, and Trends in the U.S. Vapor Pressure Deficit, an Important Fire-Related Meteorological Quantity. *Journal of Applied Meteorology and Climatology*, *54*(6), 1121–1141. https://doi.org/10.1175/JAMC-D-14-0321.1

Shinker, J. J. (2010). Visualizing Spatial Heterogeneity of Western U.S. Climate Variability. *Earth Interactions*, *14*(10), 1–15. https://doi.org/10.1175/2010EI323.1

Stevenson, S., Coats, S., Touma, D., Cole, J., Lehner, F., Fasullo, J., & Otto-Bliesner, B. (2022). Twenty-first century hydroclimate: A continually changing baseline, with more frequent extremes. *Proceedings of the National Academy of Sciences*, *119*(12), e2108124119. https://doi.org/10.1073/pnas.2108124119

Stuivenvolt-Allen, J., Wang, S.-Y. S., Johnson, Z., & Chikamoto, Y. (2021). Atmospheric Rivers Impacting Northern California Exhibit a Quasi-Decadal Frequency. *Journal of Geophysical Research: Atmospheres*, *126*(15), e2020JD034196. https://doi.org/10.1029/2020JD034196

Sun, W., Wang, B., Liu, J., & Dai, Y. (n.d.). Recent changes of Pacific decadal variability shaped by greenhouse forcing and internal variability. *Journal of Geophysical Research: Atmospheres*, *n/a*(n/a), e2021JD035812. https://doi.org/10.1029/2021JD035812

Teng, H., & Branstator, G. (2017). Causes of Extreme Ridges That Induce California Droughts. *Journal of Climate*, *30*(4), 1477–1492. https://doi.org/10.1175/JCLI-D-16-0524.1

Thakur, B., Kalra, A., Lakshmi, V., Lamb, K. W., Miller, W. P., & Tootle, G. (2020). Linkage between ENSO phases and western US snow water equivalent. *Atmospheric Research*, *236*, 104827. https://doi.org/10.1016/j.atmosres.2019.104827

Tootle, G. A., Piechota, T. C., & Singh, A. (2005). Coupled oceanic-atmospheric variability and U.S. streamflow. *Water Resources Research*, *41*(12). https://doi.org/10.1029/2005WR004381

Torrence, C., & Compo, G. P. (1998). A Practical Guide to Wavelet Analysis. *Bulletin of the American Meteorological Society*, *79*(1), 61–78. https://doi.org/10.1175/1520-0477(1998)079<0061:APGTWA>2.0.CO;2

Torrence, C., & Webster, P. J. (1999). Interdecadal Changes in the ENSO–Monsoon System. *Journal of Climate*, *12*(8), 2679–2690. https://doi.org/10.1175/1520-0442(1999)012<2679:ICITEM>2.0.CO;2

Trenberth, K. E. (1990). Recent Observed Interdecadal Climate Changes in the Northern Hemisphere. *Bulletin of the American Meteorological Society*, *71*(7), 988–993. https://doi.org/10.1175/1520-0477(1990)071<0988:ROICCI>2.0.CO;2

Trenberth, K. E., Branstator, G. W., Karoly, D., Kumar, A., Lau, N.-C., & Ropelewski, C. (1998). Progress during TOGA in understanding and modeling global teleconnections associated with tropical sea surface temperatures. *Journal of Geophysical Research: Oceans*, *103*(C7), 14291–14324. https://doi.org/10.1029/97JC01444

Wang, S., Huang, J., He, Y., & Guan, Y. (2014). Combined effects of the Pacific Decadal Oscillation and El Niño-Southern Oscillation on Global Land Dry–Wet Changes. *Scientific Reports*, *4*(1), 6651. https://doi.org/10.1038/srep06651

Wang, S.-Y., Gillies, R. R., Jin, J., & Hipps, L. E. (2009). Recent rainfall cycle in the Intermountain Region as a quadrature amplitude modulation from the Pacific decadal oscillation. *Geophysical Research Letters*, *36*(2). https://doi.org/10.1029/2008GL036329

Wang, S.-Y., Gillies, R. R., Jin, J., & Hipps, L. E. (2010). Coherence between the Great Salt Lake Level and the Pacific Quasi-Decadal Oscillation. *Journal of Climate*, *23*(8), 2161–2177. https://doi.org/10.1175/2009JCLI2979.1

Wells, N., Goddard, S., & Hayes, M. J. (2004). A Self-Calibrating Palmer Drought Severity Index. *Journal of Climate*, *17*(12), 2335–2351. https://doi.org/10.1175/1520-0442(2004)017<2335:ASPDSI>2.0.CO;2

Westerling, A. L., Gershunov, A., Brown, T. J., Cayan, D. R., & Dettinger, M. D. (2003). Climate and Wildfire in the Western United States. *Bulletin of the American Meteorological Society*, *84*(5), 595–604. https://doi.org/10.1175/BAMS-84-5-595

Williams, A. P., Cook, B. I., & Smerdon, J. E. (2022). Rapid intensification of the emerging southwestern North American megadrought in 2020–2021. *Nature Climate Change*, *12*(3), 232–234. https://doi.org/10.1038/s41558-022-01290-z

Williams, A. P., Cook, E. R., Smerdon, J. E., Cook, B. I., Abatzoglou, J. T., Bolles, K., Baek, S. H., Badger, A. M., & Livneh, B. (2020). Large contribution from anthropogenic warming to an emerging North American megadrought. *Science*, *368*(6488), 314–318. https://doi.org/10.1126/science.aaz9600

Woodhouse, C. A., Kunkel, K. E., Easterling, D. R., & Cook, E. R. (2005). The twentieth-century pluvial in the western United States. *Geophysical Research Letters*, *32*(7). https://doi.org/10.1029/2005GL022413

Yeh, S.-W., Kang, Y.-J., Noh, Y., & Miller, A. J. (2011). The North Pacific Climate Transitions of the Winters of 1976/77 and 1988/89. *Journal of Climate*, *24*(4), 1170–1183. https://doi.org/10.1175/2010JCLI3325.1

Zhang, W., Hari, V., S-Y Wang, S., LaPlante, M. D., Garfin, G., Affram, G., & Kumar, R. (2022). Fewer Troughs, Not More Ridges, Have Led to a Drying Trend in the Western United States. *Geophysical Research Letters*, *49*(1), e2021GL097089. https://doi.org/10.1029/2021GL097089

Zhou, T., Voisin, N., Leng, G., Huang, M., & Kraucunas, I. (2018). Sensitivity of Regulated Flow Regimes to Climate Change in the Western United States. *Journal of Hydrometeorology*, *19*(3), 499–515. https://doi.org/10.1175/JHM-D-17-0095.1

CHAPTER 5
GENERAL CONCLUSIONS

5.1 Impacts of the Changing Pacific

This dissertation has stepped through many climate processes in the Pacific Basin to show how they influence the occurrence of drought, ARs, and ECs. Taking a step back from the nuanced findings, I can highlight two general conclusions:

1. The year-to-year frequency of impactful weather events in North America is strongly tied to the background climate conditions and the impacts of Pacific climate variability,

2. The drifts or changes in Pacific climate variability and mean-state conditions can result in changing relationships between impactful weather and the background state.

In Chapter 1, a stated motivation for carrying out this work was that an improved understanding of the mechanisms by which climate can result in more impactful weather over the course of a season may result in improved metrics for outlooks or predictions of these events. The findings from Chapter 1 and 2 highlight that the tropical Pacific induces northern hemispheric circulation patterns associated with the frequency of ARs and ECs; the relationship of ARs and ECs with the tropical Pacific may provide metrics to improve statistical outlooks of AR and EC activity on seasonal to interannual timescales. However, the second general conclusion suggests that the predictability associated with tropical Pacific forcing is non-stationary (Coopersmith et al., 2014; McCabe & Dettinger, 1999; Miller et al., 1994). Further, moving from empirical research to operational

prediction is a large-step and many unknowns exist regarding the potential skill, error, and utility of seasonal AR or EC outlooks. Some examples which use prediction schemes involving ENSO or tropical Pacific variability as a metric for the prediction of severe weather probabilities have been proposed by DeFlorio et al. (2018, 2019), Lee et al. (2016), and DeGaetano et al. (2002) and provide paths for future work. Generally, these works find useable skill on subseasonal-to-seasonal timescales using tropical Pacific SSTs and the Madden Julian Oscillation (W. Zhang et al., 2022).

The second stated motivation of this work was to describe the recent drifts of the climate system as the relationships between impactful weather and climate are likely changing in this non-stationary system. Chapter 1 showed that Pacific climate variability, namely the EP-NP pattern, was previously unimportant for the year-to-year fluctuations in ECs. However, the trends and shifting pattern of teleconnections from the tropical pacific have been associated with an amplified wave-train over North America with opposite impacts on the western and eastern half of the continent (Schulte & Lee, 2017). Finally, one of the most interesting conclusions regarding non-stationarity comes from Chapter 4, in which the changing Pacific is not just linked to mean-state changes (Miller et al., 1994; Yeh et al., 2011), but also to changes in the variance and year-to-year persistence of pan-western drought and precipitation.

5.2 Future Directions

The conclusions in each chapter are mostly related to climate variability, but future work should continue to explore the role of anthropogenic climate change in driving the observed shifts in Pacific climate and the associated changes to drought and ECs. Over the last 40 years, decadal variability has remained powerful largely in

association with a lack of a warming trend in the central tropical Pacific that has resulted in a strengthening of the climatological east-west SST gradient (DiNezio et al., 2009; Fosu, He, & Liguori, 2020; Seager et al., 2022). While most studies conclude this trend to be a product of internal variability (Kestin et al., 1998; Timmermann et al., 2018), others suggest that it may be related to radiative forcing (DiNezio et al., 2009, 2009; Seager et al., 2022). It is argued that the stronger upwelling in the central and eastern tropical Pacific works to oppose the radiatively forced temperature trends from the surface, while the western Pacific warm pool warms more effectively from radiative forcing due to weaker upwelling. This change is proposed to bolster the Bjerknes feedback and increase trade winds and the east-west SST temperature gradient (Seager et al., 2021). While many uncertainties related to our observational integrity, internal variability (Michel et al., 2020), and the presence of more uniform warming in global circulation models (Knutson & Manabe, 1998), it is still crucial to understand whether the observed SST trends will continue and how that may impact North American climate. Persistent and anomalously cool states of the central and eastern tropical Pacific have been associated with many of the severe droughts in the paleo record, motiving further analysis of these tropically induced drought regimes (Baek, Smerdon, et al., 2019; Baek, Steiger, et al., 2019; Cole et al., 2002).

There are also a lot of remaining questions regarding compounding continental extremes/anomalies in response to tropical teleconnections, extratropical variability, and anthropogenic climate change. The EP-NP and the NAWD patterns were commonly featured in this work, and while they are not strongly correlated enough to be analogues, their increasing importance on winter temperature, precipitation and extremes motivates

improved understanding. Notably, the EP-NP index exhibits a strong amplifying trend, and its relationship to western tropical Pacific SST anomalies suggests that it may also be an artifact of the strengthening zonal SST gradient in the tropics (Chapter 2, Schulte & Lee, 2017). With the emergence of the NAWD as the leading mode of winter atmospheric variability over North America (Chien et al., 2019), more work is needed to characterize these wave-trains which can enhance the climatological division between the east and west and drive opposing climate extremes on North America (S.-Y. Wang et al., 2015, 2017).

Chapter 1 is under its second stage of review at Climate Dynamics, Chapter 2 is published at the Journal of Geophysical Research: Atmospheres, and Chapter 3 is in preparation to be submitted to Geophysical Research Letters. Rights from these journals have been obtained for all work in this dissertation.

REFERENCES

Baek, S. H., Smerdon, J. E., Seager, R., Williams, A. P., & Cook, B. I. (2019). Pacific Ocean Forcing and Atmospheric Variability Are the Dominant Causes of Spatially Widespread Droughts in the Contiguous United States. Journal of Geophysical Research: Atmospheres, 124(5), 2507–2524. https://doi.org/10.1029/2018JD029219

Baek, S. H., Steiger, N. J., Smerdon, J. E., & Seager, R. (2019). Oceanic Drivers of Widespread Summer Droughts in the United States Over the Common Era. Geophysical Research Letters, 46(14), 8271–8280. https://doi.org/10.1029/2019GL082838

Chien, Y.-T., Wang, S.-Y. S., Chikamoto, Y., Voelker, S. L., Meyer, J. D. D., & Yoon, J.-H. (2019). North American Winter Dipole: Observed and Simulated Changes in Circulations. Atmosphere, 10(12), 793. https://doi.org/10.3390/atmos10120793

Cole, J. E., Overpeck, J. T., & Cook, E. R. (2002). Multiyear La Niña events and persistent drought in the contiguous United States. Geophysical Research Letters, 29(13), 25-1-25–4. https://doi.org/10.1029/2001GL013561

Coopersmith, E. J., Minsker, B. S., & Sivapalan, M. (2014). Patterns of regional hydroclimatic shifts: An analysis of changing hydrologic regimes. Water Resources Research, 50(3), 1960–1983. https://doi.org/10.1002/2012WR013320

DeFlorio, M. J., Waliser, D. E., Guan, B., Lavers, D. A., Ralph, F. M., & Vitart, F. (2018). Global Assessment of Atmospheric River Prediction Skill. Journal of Hydrometeorology, 19(2), 409–426. https://doi.org/10.1175/JHM-D-17-0135.1

DeFlorio, M. J., Waliser, D. E., Guan, B., Ralph, F. M., & Vitart, F. (2019). Global evaluation of atmospheric river subseasonal prediction skill. Climate Dynamics, 52(5), 3039–3060. https://doi.org/10.1007/s00382-018-4309-x

DeGaetano, A. T., Hirsch, M. E., & Colucci, S. J. (2002). Statistical Prediction of Seasonal East Coast Winter Storm Frequency. Journal of Climate, 15(10), 1101–1117. https://doi.org/10.1175/1520-0442(2002)015<1101:SPOSEC>2.0.CO;2

DiNezio, P. N., Clement, A. C., Vecchi, G. A., Soden, B. J., Kirtman, B. P., & Lee, S.-K. (2009). Climate Response of the Equatorial Pacific to Global Warming. Journal of Climate, 22(18), 4873–4892. https://doi.org/10.1175/2009JCLI2982.1

Fosu, B., He, J., & Liguori, G. (2020). Equatorial Pacific Warming Attenuated by SST Warming Patterns in the Tropical Atlantic and Indian Oceans. Geophysical Research Letters, 47(18), e2020GL088231. https://doi.org/10.1029/2020GL088231

Kestin, T. S., Karoly, D. J., Yano, J.-I., & Rayner, N. A. (1998). Time–Frequency Variability of ENSO and Stochastic Simulations. Journal of Climate, 11(9), 2258–2272. https://doi.org/10.1175/1520-0442(1998)011<2258:TFVOEA>2.0.CO;2

Knutson, T. R., & Manabe, S. (1998). Model Assessment of Decadal Variability and Trends in the Tropical Pacific Ocean. Journal of Climate, 11(9), 2273–2296. https://doi.org/10.1175/1520-0442(1998)011<2273:MAODVA>2.0.CO;2

Lee, S.-K., Wittenberg, A. T., Enfield, D. B., Weaver, S. J., Wang, C., & Atlas, R. (2016). US regional tornado outbreaks and their links to spring ENSO phases and North Atlantic SST variability. Environmental Research Letters, 11(4), 044008. https://doi.org/10.1088/1748-9326/11/4/044008

McCabe, G. J., & Dettinger, M. D. (1999). Decadal variations in the strength of ENSO teleconnections with precipitation in the western United States. International Journal of Climatology, 19(13), 1399–1410. https://doi.org/10.1002/(SICI)1097-0088(19991115)19:13<1399::AID-JOC457>3.0.CO;2-A

Michel, C., Li, C., Simpson, I. R., Bethke, I., King, M. P., & Sobolowski, S. (2020). The Change in the ENSO Teleconnection under a Low Global Warming Scenario and the Uncertainty due to Internal Variability. Journal of Climate, 33(11), 4871–4889. https://doi.org/10.1175/JCLI-D-19-0730.1

Miller, A. J., Cayan, D. R., Barnett, T. P., Graham, N. E., & Oberhuber, J. M. (1994). The 1976-77 Climate Shift of the Pacific Ocean. Oceanography, 7(1), 21–26.

Schulte, J. A., & Lee, S. (2017). Strengthening North Pacific Influences on United States Temperature Variability. Scientific Reports, 7(1). https://doi.org/10.1038/s41598-017-00175-y

Seager, R., Henderson, N., & Cane, M. (2022). Persistent discrepancies between observed and modeled trends in the tropical Pacific Ocean. Journal of Climate, 1(aop), 1–41. https://doi.org/10.1175/JCLI-D-21-0648.1

Seager, R., Henderson, N., Cane, M., Zhang, H., & Nakamura, J. (2021). Atmosphere-ocean dynamics of persistent cold states of the tropical Pacific Ocean. Journal of Climate, 1(aop), 1–44. https://doi.org/10.1175/JCLI-D-20-0694.1

Timmermann, A., An, S.-I., Kug, J.-S., Jin, F.-F., Cai, W., Capotondi, A., Cobb, K. M., Lengaigne, M., McPhaden, M. J., Stuecker, M. F., Stein, K., Wittenberg, A. T., Yun, K.-S., Bayr, T., Chen, H.-C., Chikamoto, Y., Dewitte, B., Dommenget, D., Grothe, P., … Zhang, X. (2018). El Niño–Southern Oscillation complexity. Nature, 559(7715), 535–545. https://doi.org/10.1038/s41586-018-0252-6

Wang, S.-Y. S., Huang, W.-R., & Yoon, J.-H. (2015). The North American winter 'dipole' and extremes activity: A CMIP5 assessment. Atmospheric Science Letters, 16(3), 338–345. https://doi.org/10.1002/asl2.565

Wang, S.-Y. S., Yoon, J.-H., Becker, E., & Gillies, R. (2017). California from drought to deluge. Nature Climate Change, 7, 465–468. https://doi.org/10.1038/nclimate3330

Yeh, S.-W., Kang, Y.-J., Noh, Y., & Miller, A. J. (2011). The North Pacific Climate Transitions of the Winters of 1976/77 and 1988/89. Journal of Climate, 24(4), 1170–1183. https://doi.org/10.1175/2010JCLI3325.1

Zhang, W., Hari, V., S-Y Wang, S., LaPlante, M. D., Garfin, G., Affram, G., & Kumar, R. (2022). Fewer Troughs, Not More Ridges, Have Led to a Drying Trend in the Western United States. Geophysical Research Letters, 49(1), e2021GL097089. https://doi.org/10.1029/2021GL097089

CURRICULUM VITAE
Jacob Stuivenvolt Allen

EDUCATION:

Ph.D. in Climate Science	Utah State University
08/2018 – 04/2022	Advisor: Shih-Yu Simon Wang
	Dissertation: *Impacts of the Changing Pacific on North American Drought, Atmospheric Rivers, and Explosive Cyclones*
B.S. in Environmental Science 08/2012 – 05/2016	Loyola Marymount University Focus on Earth Science, *Cum laude*

PUBLICATIONS:

In Preparation

Stuivenvolt-Allen, J., Chikamoto, Y., Wang, S.-Y. (2022). Emergence of decadal hydroclimate regime in the western United States. *Geophysical Research Letters.*

In Review

Pokharel, B., **Stuivenvolt-Allen, J.,** Wang, S.-Y. (Simon), Sharma, S., LaPlante, M., Gillies, R. R., Khanal, S., Wehner, M. F., Rhoades, A. M., Hamal, K., Liu, W.-Y., Mukherjee, S., & Aryal, D. (2021). Climate change and drought amplify the potential for uncontrollable fires in Nepal. *Environmental Monitoring and Assessment.*

Stuivenvolt-Allen, J., Wang, S.-Y., Chikamoto, Y., Meyer, J.D., Johnson, Z.F. and Deng, L. (2021). Growing Pacific linkage with the interannual variability of explosive cyclogenesis in the North Atlantic: *Climate Dynamics*. DOI: 10.21203/rs.3.rs-1157480/v1

Dalanhese, L., **Stuivenvolt-Allen, J.,** LaPlante, M., Wang, S.-Y. (2021). An inter-comparison of South American extratropical cyclogenesis using Brazilian Navy data and ERA5: *International Journal of Climatology.*

Stuivenvolt-Allen, J., Wang, S.-Y. (2021) North American fire weather catalyzed by the extratropical transition of tropical cyclones: *Climate Dynamics.*
https://doi.org/10.21203/rs.3.rs-740651/v1

Published

Stuivenvolt-Allen, J., Wang, S.-Y. S., Johnson, Z., & Chikamoto, Y. (2021). Atmospheric rivers impacting Northern California exhibit a quasi-decadal frequency. *Journal of Geophysical Research: Atmospheres,* 126, e2020JD034196. https://doi.org/10.1029/2020JD034196

Morgan, B., Spangler, K., **Stuivenvolt-Allen, J.,** Morrisett, C. N., Brunson, M. W., Wang, S.-Y. S., & Huntly, N. (2021). Water Availability for Cannabis in Northern

California: Intersections of Climate, Policy, and Public Discourse. *Water*, 13(1). https://doi.org/10.3390/w13010005

Stuivenvolt-Allen, J., Wang, S.-Y. S., LaPlante, M. D., & Yoon, J.-H. (2021). Three Western Pacific Typhoons Strengthened Fire Weather in the Recent Northwest U.S. Conflagration. *Geophysical Research Letters*, 48(3), e2020GL091430. https://doi.org/10.1029/2020GL091430

Stuivenvolt-Allen, J., & Wang, S.-Y. S. (2019). Data-mining climate variability as an indicator of U.S. natural gas: *Frontiers in Big Data: Integrating Big Data with Earth System Models of Natural and Human Systems*. https://doi.org/10.3389/fdata.2019.00020

PROFESSIONAL EXPERIENCE:

Graduate Research Assistant	Utah State University
08/2018 – 07/2022	See following section
Teacher's Assistant 01/2019 – 05/2021	Loyola Marymount University Meteorology, Climate and Climate Change
Research Intern 05/2019 – 06/2020	N.O.A.A. Climate Prediction Center Empirical prediction of wintertime teleconnections
Field Guide and Intern 06/2016 – 09/2016	Campanario Biological Station Tropical ecology guide and educator for student groups and tourists
Intern 06/2015 – 05/2016	Center for Urban Resilience Assisted in student projects researching insect biodiversity and behavioral crow studies
Intern 06/2015 – 05/2016	The Santa Monica Bay Foundation Aided in the construction of rain gardens to promote bioremediation and ground water infiltration

RESEARCH EXPERIENCE:

Hydroclimate	Atmospheric Rivers and Drought
	Low-frequency variability and dynamics of atmospheric rivers and multi-year droughts in the western US
Climate Dynamics	Ocean-atmosphere interactions Impacts of ENSO and tropical teleconnections on North American weather and climate

Fire Weather	Typhoons to fires Responses of North American fire weather to perturbations associated with western North Pacific tropical cyclones
Climate Prediction	Empirical prediction Prediction of winter teleconnections at 1-2 months lead time. Statistical prediction tools for Nepal fire occurrences from meteorological variables
Climate Modeling	Diagnostics with model data Use of partial assimilation experiments, the Community Earth System Model Large Ensemble, and CMIP6 models.

FELLOWSHIPS:

Southwest Climate Adaptation Science Fellowship 2020-2021	SW Climate Adaptation Science Center Research topic: Landscape regeneration in a changing climate after large and destructive fires.
Campbell Scientific Graduate Fellowship 2019 and 2020	AGRI Apogee Instruments Awarded to a student in the Plants, Soils, and Climate department for quality, hypothesis driven research.
Climate Adaptation Science Fellowship 2018-2020	NSF Research Traineeship Research topic: Intersections of Climate, Policy, and Public Discourse in Northern California

SOFTWARE PROGRAMMING AND TECHNOLOGY:

Python	Analysis: EOF, spherical harmonics, Fourier, Wavelet, statistics, regression modeling, composite, correlation, event tracking
	Packages: MetPy, Scipy/Numpy, Xarray, Matplotlib, eofs, windspharm, pyCWT, Sci-Kit Learn, Pandas,
GrADS	Analysis: Composite, correlation, event tracking
Climate Data Operators	Netcdf file management and manipulation
Linux/Unix	Netcdf file management, basic shell scripting
High Performance Computing	Experience working on Cheyenne, Casper and other Linux based HPCs

SERVICE AND OUTREACH:

Peer Review	Journals: Geophysical Research Letters, Frontiers in Earth Science
Scientific Journalism	The Butterfly and the Blaze – Eugene Weekly https://eugeneweekly.com/2020/12/10/the-butterfly-and-the-blaze/ Utah Water Issues https://Utahwaterissues.blogspot.com
Weather forecasting 2016-2020	Utah Public Radio
Ignatians Service Organization 2012-2016	Community Service in Los Angeles

CONFERENCES AND PRESENTATIONS:

Yosemite Hydroclimate Workshop	Oral: *Long-term cycles of water availability and atmospheric rivers in Northern California* Oral: *Connecting extremes: Typhoons catalyze fire weather in the western United States*
American Geophysical Union	Poster: *Water availability for cannabis in Northern California: Intersections of Climate, Policy, and Public Discourse*
American Meteorological Society Annual Meeting	Oral: *The modulation of natural gas through winter climate and cyclone variability*
Southeast Asian Paleo Environments Consortium	Oral: *Climate dynamics and climate data* Workshop: *Climate data analysis and stewardship*
NSF Research Traineeship Annual Meeting	Poster: *Partnerships to enable science that is useful and used*
Southern California Academy of Science	Poster: *Measuring runoff fecal indicator bacteria removal efficiency in the Ballona Creek rain garden*

AWARDS AND CERTIFCATIONS:

2022   Doctoral Researcher of the Year: Plants, Soils, and Climate Department

2021   Top Award for Science Writing from the American Society of Journalists and Authors: The Butterfly and the Blaze

2020   Graduate Enhancement Award

2019   Best Research Presentation: Plant, Soils and Climate Departmental Showcase

2017   Utah Master Naturalist: Wetlands Certification

2017   Utah Master Naturalist: Mountains Certification

2016   Sigma Xi National Research Honor Society Member